Relationship between Satellite-Derived Normalized Difference Vegetation Index (NDVI) and Surface Hydrology

by

Ana T. Pinheiro
Licenciatura in Environmental Engineering
New University of Lisbon, 1995

Submitted to the Department of Civil and Environmental Engineering in Partial Fulfillment of the Requirements for the Degree of

MASTER OF ENGINEERING
IN CIVIL AND ENVIRONMENTAL ENGINEERING

at the

MASSACHUSETTS INSTITUTE OF TECHNOLOGY
June 1998

Signature of the Author _____
(Ana T. Pinheiro
Department of Civil and Environmental Engineering
May 8, 1998

Certified by _____
Dara Entekhabi, Ph.D.
Assistant Professor of Civil and Environmental Engineering
Thesis Supervisor

Certified by _____
Professor Joseph Sussman
Chairman, Department Committee on Graduate Studies

Relationship between Satellite-Derived Normalized Difference Vegetation Index (NDVI) and Surface Hydrology

by

Ana T. Pinheiro

Submitted to the Department of Civil and Environmental Engineering on May 20, 1998

in partial fulfillment of the requirements for the degree of Master of Engineering

in Civil and Environmental Engineering

ABSTRACT

Recently, particular attention has been given to the study of seasonal to interannual global climate variability with the goal to obtain a predictive understanding of short-term climate fluctuations and be able to predict extreme environmental conditions such as droughts. Since vegetative processes are strongly dependent on water availability, large scale observations of vegetation allow monitoring of drought conditions. Due to the unique spectral properties of plant leaves, remote sensing has proven to be very useful in monitoring vegetation. The present study analyzes the spatial and temporal relationship between Normalized Difference Vegetation Index (NDVI), soil moisture and precipitation data, in Europe, for the period between 1982 and 1990. Five homogeneous areas are selected in order to evaluate, for different latitudes, the degree of correlation between the three different parameters. The results show higher correlations between NDVI and soil moisture than between NDVI and precipitation. In both cases higher magnitude, in positive correlations, were found in the south of Europe, since there water tends to be a strong limiting factor for vegetation growth. The study highlights the need for caution when extrapolating the results due to the limitations inherent to the datasets and parameters used.

Thesis Supervisor: Dara Entekhabi

Title: Career Development Associated Professor

ACKNOWLEDGMENTS

I would like to take the opportunity to thank all the people who made this thesis possible, and who helped me survive this last intensive year. First, I would like to thank two very special people, my parents who, although physically apart, where able to make me feel loved and supported all the time.

Next I would like to acknowledge Dara Entekhabi, my advisor, for his valuable guidance on this thesis work. I also thank him for being so supportive and for showing me the importance of finding our own path in science. Also related with the thesis work, I would like to thank my friend Karen Plaut for being extremely patient in helping me learn IDL in such a short period of time, and Tim Wuu for helping me with the FORTRAN code.

I would also like to thank all of my friends who, here and in Portugal, helped me go through the most stressful moments. Particularly I thank Amparo Flores, Charles Njendu, Vittorio Agnesi, Emilie Hung, Peter Israelsson, Ricardo Petroni, Conny Mitterhofer, and Ricardo Schiappa for the friendship and emotional support they gave to me over the past year. Thank you Amparo, companion of so many coffee-breaks, for being so patient with me and for always being there to talk to me.

I send a special thank you to Professor David Marks and to Professor Antonio Camara who always believed in me and in my abilities. They have shown to me how it is possible to be successful while still caring about people and relationships, keeping a good humor, and a smile on their face. I am really grateful for all their emotional support.

Next I would like to acknowledge Dr. Jim Collatz and Sietse Los, at the Goddard Space Flight Center/NASA, for their courtesy in allowing me to use the NDVI-FASIR dataset. I would also like to thank the PRAXIS program from the Portuguese Ministry of Science and Technology for providing the financial support that made my participation in the MENG program possible.

Finally, I would like to thank all my colleagues at the MENG program for their *esprit de corps*. I thank Jackie Donoghue, Muriel Frederick, Scott Hassell, Charles Helliwell and Bruce Jacobs for being always available for any necessary advice and support.

LIST OF CONTENTS

LIST OF FIGURES

LIST OF TABLES

LIST OF ACRONYMS

AVHRR	Advanced Very High Resolution Radiometer
BRDF	Biodirectional Reflectance Distribution Function
DAAC	Distributed Active Archive Center
DP	Difference Polarization
EOS	Earth Observing System
FASIR	Fourier-Adjusted, Solar zenith angle corrected, Interpolated and Reconstructed of NDVI data
FIFE	First ISLSCP Field Experiment
FPAR	fraction of PAR absorbed by the green portion of the vegetation canopy
GAV	Global Area Coverage
GCM	Global Circulation Model
GIMMS	Global Inventory, Monitoring and Modeling System
GSFC	Goddard Space Flight Center (NASA)
GVI	Global Vegetation Index
ISLSCP	International Satellite Land Surface Climatology Project
LAC	Local Area Coverage
LAI	Leaf Area Index
NASA	National Aeronautics and Space Administration
NDVI	Normalized Difference Vegetation Index

NIR	Near InfraRed
NOAA	National Oceanic and Atmospheric Administration
PAR	Photosynthetically Active Radiation
SR	Simple Ratio
SST	Sea Surface Temperature
TIROS-N	Television and InfraRed Observational Satellite

1.0. INTRODUCTION

Recently, there is an increasing awareness of and concern about the possible causes and consequences of climate fluctuations. As a consequence, particular attention has been given to the study of seasonal to interannual global climate variability, with the goal to obtain a predictive understanding of short-term climate fluctuations and apply these predictions to problems of social and economic development. Specific applications include helping farmers maintain their agricultural productivity, in spite of extreme climatic events such as droughts and floods; help water resource managers to ensure reliable water delivery, limit flood damage, and maintain optimal reservoir levels; and help foresters allocate resources effectively to safeguard forests (and the public) from major fires during droughts (GCRIO, 1998). Among these, preventing the effects of droughts is probably one of the most important tasks since droughts are considered to be the most damaging phenomena. From 1967 to 1991, 1.3 million of the 3.5 million people killed by disasters were due to the direct or indirect cause of drought (Kogan, 1997).

Climate and vegetation patterns are known to be strongly related. Detailed knowledge of the behavior and state of the land and the vegetative cover need to be advanced. Therefore, gaining a better understanding of the way that vegetation cover is evolving, seasonally and interannually, is a priority concern of the global change research community (Turner et al., 1993).

Observations of the global environment are critical for documenting global change and for providing the basis for how and why changes are occurring (Turner et al., 1993). In this context, remote sensing "...supplies publicly accessible information that matches the interconnectedness, diversity, and scale of global problems. Moreover, it maximizes diversity of information and area of coverage at minimal cost, and allows the interpreter to address several problems more rapidly than by any other method..." (Drury, 1990).

The present study analyzes the relationship between satellite-derived vegetation indices, particularly the Normalized Difference Vegetation Index (NDVI), and surface hydrology parameters, in order to gain a better understanding of the environmental constrains on vegetation growth. Since vegetation processes are strongly dependent on water availability, by monitoring vegetation it is possible to improve soil moisture estimates and ultimately allow the monitoring of

drought conditions. Several studies have been evaluating the relationship between precipitation data and NDVI. However, it is known that soil moisture more realistically represent an indicative of water availability for plants, and therefore it is expected to find higher correlations between NDVI and this parameter than with precipitation data. A limitation to this approach is due to the fact that observations of soil moisture on the large scale are scarce and consequently this study has to be carried out using modeled soil moisture data.

This report is organized in two main parts. The first is the main body of the text and it provides a brief overview of the current research in the field of vegetation monitoring using satellite-derived vegetation indices, and is the result of bibliographic review. This first part also includes the results of the study. The second part is an appendix consisting of a compilation of the main IDL (Interactive Data Language) routines used to process and display the data. A brief description of the different chapters follows.

Chapter 2 identifies some of the mechanisms linking climate and vegetation, focusing in the energy and water systems coupled through the evaporative component, in which vegetation plays a major role. Chapter 3 discusses the importance of water in plants metabolism and the main effects of water deficit in the photosynthetic process, and therefore in the production of biomass. The state of vegetation and a measure of its photosynthetic activity can be monitored with remote sensing techniques based on the unique spectral properties of vegetation. The main principles underlying this procedure, as well as some examples of previous studies, are discussed in Chapter 4. Chapter 5 describes the general and specific features of the satellite system most commonly used for remote sensing of vegetation purposes, the NOAA-AVHRR, highlighting some the limitations of the system. Chapter 6 consists of a description of commonly used satellite derived vegetation indices, focusing particular attention on the Normalized Difference Vegetation Index (NDVI), discussing some of the well established relationships between this index and biophysical parameters. Chapter 7 deals with the datasets used in this study, which include the NDVI, soil moisture and precipitation datasets, explaining the processes and methodologies underlying the acquisition, production and processing techniques used, and also its inherent limitations. Chapter 8 presents and discusses the results of this study concerning the evaluation of the relationship between NDVI and surface hydrology parameters.

2.0. LINKAGES BETWEEN CLIMATE AND VEGETATION

2.1. Introduction

Although more than two-thirds of the Earth is covered with oceans, continental surfaces provide much of the spatial and temporal variability that affect the weather and climate. To a larger extent, vegetation determines the physical characteristics of ice-free continental surfaces, and hence key climatic parameters such as albedo, and surface energy fluxes (Martin, 1988). Vegetation is also directly affected by climate. The distribution of global vegetation has traditionally been thought to be determined by local climatic factors, primarily precipitation, radiation, and temperature, and by soil properties, in particular water-holding capacity. Climate and vegetation coexist in a dynamic equilibrium that can be altered by large perturbations in either the two components. The equilibrium climate is determined by complex interactions among the dynamical processes in the atmosphere, and thermodynamic processes at the earth-atmosphere interface. Therefore, quantitatively estimating effects that large changes in terrestrial ecosystems can have on temperature, circulation, and rainfall has been a difficult task (Nobre et al., 1991).

Predictions of impact of climate change on the biosphere and of interactions of the biosphere with the climate (either due to natural factors or to human interference) can only be inferred from quantification and formalization of the mechanisms by which vegetation cover and ecosystems are functioning (TVP, 1997). In this context, surface parameters mapping is a basic requirement for climate and meteorological studies where boundary conditions have to be prescribed, as in the case of General Circulation Models and numerical weather forecasting models, discussed in Section 2.4..

Factors such as albedo, surface roughness, resistance to heat exchanges (sensible and latent) are important variables for these models and they can be either determined directly from the measurements, or inferred from identification of land cover. The seasonal and long-term variations of such variables are related to vegetation dynamics (TVP, 1997). Terrestrial vegetation is an important factor in the radiation balance and water balance of the

earth, and in numerous biogeochemical cycles related to climate maintenance and climate change (Matthews, 1983).

Locally the primary effect of vegetation is on surface hydrology, since the vegetation controls transpiration, determines interception losses, affects infiltration in the soil, and then greatly influences runoff. With regard to transpiration, which is vaporization at the leaf surface of water extracted from the soil by the plant, the physiological responses of the vegetation and its physical characteristics determine the partitioning between the sensible and latent heat at the surface of the earth. This, in turn, affects atmospheric motion and the water balance (Martin, 1988).

2.2. Energy and water balance

In its most general form, the total surface energy balance is partitioned between ground heat flux (*G*), sensible heat flux (*H*) and latent heat flux (λE), and is given by:

$$Rn + G = \lambda E + H \qquad (2.1)$$

in which:

Rn = net radiation, W m^{-2}

G = ground heat flux, W m^{-2}

λE = latent heat flux, W m^{-2}

H = sensible heat flux, W m^{-2}

The net radiation (Rn), is strongly dependent on surface albedo, which in turn is a function of the leaf area index, and the leaf and soil optical properties (Los, 1998; Sellers et al., 1996):

$$Rn = \int_{0}^{4\mu m} \int_{0}^{\pi/2} F_{\Lambda,\mu} \downarrow (1 - a_{\Lambda,\mu}) d\mu d\Lambda + \varepsilon (F_{T,d} \downarrow - \sigma T_s^4) d\mu d\Lambda \qquad (2.2.)$$

$F_{\Lambda,\mu}$ = incoming radiation flux, Wm^{-2}

Λ = (subscript) wavelength interval, μm

μ = (subscript) cosine of angle of incident radiation

$a_{\Lambda,\mu}$ = surface hemispheric reflectance

ε = emissivity (approximately 1)

$F_{T,d} \downarrow$ = incident thermal infrared radiation (TIR) (assumed to be all diffused), Wm^{-2}

T = (subscript) thermal wavelength interval

d = (subscript) diffuse radiation

σ = Stefan-Boltzman constant, $Wm^{-2}K^{-1}$

T_s = Surface temperature, K

In this parameterization process, the vegetation plays an important role since it directly affects the reflectances and albedo. Absolute errors or uncertainties in the albedo translate directly into errors in the calculation of net radiation and heat flux (Sellers et al., 1996).Albedo is a function of surface radioactive transfer properties which include the leaf spectral characteristics (live or dead) and the leaf angle distribution function. On the other hand, the total surface latent heat flux consists of a soil and a leaf component. Both the leaf and the soil latent heat components are split in a wet and dry fraction. According to Los (1998):

(a) The latent heat flux from the dry fraction of leaves (transpiration) can be calculated analogously to the Penman-Monteith equation and depends amongst other variables on the net radiation, aerodynamic resistance for heat and water vapor, and canopy resistance. The aerodynamic resistance is a function of roughness length and canopy resistance is inversely related to the stomatal conductance which is closely related to the assimilation rate.

(b) The latent heat flux from the wet fraction of leaves is a function of the canopy temperature and of the bulk canopy boundary layer resistance.

(c) The latent heat flux from the dry soil is a function of the ground temperature, soil water content, windspeed, and the incoming radiation. The incoming radiation for the soil is inversely related to the leaf area index.

(d) The latent heat flux from the wet soil is a function of the ground temperature and the aerodynamic resistance between the ground and the canopy air -space.

The sensible heat flux also consists of a soil and leaf component. The leaf sensible heat flux is related to the difference between the leaf and air temperature, and the soil sensible heat flux is related to the soil and air temperature (Los, 1998). The ground heat flux in the vertical soil column is given by:

$$G = -\kappa \frac{\partial T}{\partial z} \tag{2.3}$$

where κ is the thermal conductivity and it depends strongly on the soil moisture content. The latent heat component of the energy balance equations a weighted average of the evaporation forcing due to available energy $(R_n - G)$ and atmospheric vapor demand (δ_e / r_a) and can be obtained as following:

$$\lambda E =_a \frac{\Delta(R_n - G) + \rho c_p \delta_e / r_a}{\Delta + \gamma(r_c + r_a)/r_a} \tag{2.4}$$

where

Δ = Clausius-Clapeyron relation, Pa K^{-2}

ρ = psychrometric constant, Pa K^{-2}

δ_e = vapor pressure deficit at the depth of interest

r_a = aerodynamic resistance for heat and water vapor, s m^{-1}

r_c = stomatal and canopy resistance, s m^{-1}

Here, once again, vegetation plays an important role exerting control or resistance to evaporation. Since evaporation is also a component of the water balance equation:

$$\frac{d\omega}{dt} = P - Q - E \tag{2.5}$$

in which the change in water storage over time is a function of precipitation (P), runoff loss (Q) and evaporation (E), this last component works as a coupling factor between water and energy balance equations. Besides contributing to the evaporation, vegetation also affects the water balance of a system forced by precipitation.

Incoming precipitation is divided in a component intercepted by the canopy liquid water storage compartment and a throughfall component. Water intercepted by the canopy can either evaporate or, when the capacity of the canopy liquid water store is exceeded, contribute to throughfall. The throughfall component, the precipitation that fall through gaps in the canopy, is calculated as a function of leaf area index (LAI) and the fraction of vegetation cover in a grid cell (Los, 1998). The sum of the direct throughfall and the water dripping from the leaves reaching the ground is intercepted by the ground liquid water storage compartment. Water in the ground liquid store either evaporates, infiltrates into the surface layer when the capacity of the ground liquid water is exceeded, or contributes to the overland flow if the infiltration is in excess of the infiltration capacity of the soil. Overland flow contributes to the surface runoff. Water can either evaporate from the surface layer or infiltrate into the root zone. Water from the root zone can flow down into the deep soil, contribute to the runoff if the root zone saturates, or can be used by vegetation for transpiration. The root zone is the only layer that can be accesses by vegetation to fulfill its water demand (Los, 1998), and therefore the soil moisture content in that particular region is very important.

Soil moisture together with snow cover, is also the most important component of meteorological memory for the climate system over the land. The variation of soil moisture (as

opposed to fixed soil moisture) induces a redden spectrum in simulated climate by retaining the hydrological signature of anomalies for times scales longer than those of the atmosphere alone (Sellers et al., 1997). There are two distinct spatial scales of soil moisture variations. In the small scale, of the order of tens of meters, soil moisture can vary due to small scale variations of topography, soil type and texture, and vegetation. Superimposed on this small scale variability is a much larger scale of hundreds of kilometers that is due to the meteorological processes that influence soil moisture and that have this same scale on a monthly average, precipitation and evapotranspiration (Robock et al., 1997). Soil moisture variations from month to month are as well as large as the other terms in the hydrologic balance, namely precipitation, evaporation, and runoff, and correct simulation of these variations is necessary to correctly model the hydrological cycle.

The representation of soil moisture in land surface models is often strongly simplified. The difference in characteristics of soil moisture in models in nature is considerable (such as variations in depth, soil horizon dependency, multiple flow directions, flux divergence, liquid/vapor phase). According to Bastiaanssen et al. (1997), soil moisture in present land surface models is merely a model parameter and its physical meaning is somewhat vague. Soil moisture is considered an important factor in land surface evapotranspiration, which is also an important process in the weather and climate system of the Earth. By its influence on the vegetation structure, it also controls the reflected solar radiation, the albedo effect and the momentum flux at the surface (roughness effect) (Mintz and Serafini, 1992). Long-term water balance calculations, considering soil, vegetation and climate, with an accurate parameterization of soil moisture, may provide a quantitative approach to identify drought conditions.

2.3. Global Circulation Models (GCMs)

The most sophisticated tool with which to study global scale climate is the 3-D general circulation model (GCM). The accuracy of the climate generated by a GCM relies in part on the realistic representation of the land surface processes. The land surface model (LSM), in a GCM, plays the important roles of partitioning net incoming radiation into sensible and latent heat fluxes

and partitioning precipitation into runoff and storage (Scott et al., 1995). Prior to the work of Dickinson (1984) and Sellers et al. (1986) these land surface parametrizations were prescribed as independent boundary conditions, in which it was generally considered an unrealistic, and generally too low, specification of albedo, the use of constant values for the entire land surface of roughness length z_o and the water-holding capacity of the soil; and an unrealistic description of the evaporation process, leading to excessive estimates of the evaporation in humid regions (Los, 1998).

The Biosphere-Atmosphere Transfer Scheme (BATS) of Dickinson (1984) and the Simple Biosphere model (SiB) of Sellers et al (1986) were the first attempts of a biophysically realistic modeling approach for land surface parameters. In this models the emphasis is on modeling the soil-vegetation complex itself and thereby specify the surface attributes of albedo, roughness length and surface resistance as mutually consistent surface properties.

According to Los (1998), one of the first studies to investigate a feedback mechanism between the biosphere and climate with an atmospheric general circulation model, was a study by Charney et al. (1975,1977). They intended to study the effects of a decrease in vegetation cover on the albedo, for desert margins such as the Sahel, expecting to observe a decrease in that parameter since the landsurface would absorb less solar radiation and this would decrease the total energy (sum of latent and sensible heat) emitted by the land surface. The reduced radiation by the land surface cools the lower atmosphere and this would either enhance the sinking motion of air over deserts, or decrease the amount of convection. Precipitation rates would diminish leading to a decrease in the moisture availability for plant growth, thus enforcing or sustaining the initial decrease in vegetation. In some models, soil moisture also affects the surface albedo in a direct way, with wetter soil being darker, which also affects surface temperature (Robock et al., 1997).

Charney et al. (1975, 1977) also stated that the same logic should apply to the reversed situation, i.e. a situation in which an increase in vegetation would lead to an increase in precipitation which would sustain the increased vegetation. To test if the effects of the increased albedo would be sufficiently strong to affect large circulation patterns, e.g. monsoon circulation. Charney et al. (1975, 1977) compared two scenarios with a GCM, a high albedo scenario

representing conditions with low vegetation cover and a low albedo scenario representing conditions with high vegetation cover, both in the Sahel. Their GCM results predicted that induced changes in albedo, in the initial conditions, did result in a decrease of precipitation in the Sahel and an increase in precipitation over the tropical forest south of it (Los, 1998). The use of a biosphere model in the land surface parameterization revealed novel aspects in a feedback loop between vegetation and precipitation proposed by Charney et al. (1975, 1977). The current results indicate that transpiration by vegetation is a more important driver of convective precipitation than the overall changes in the energy balance. In addition, observations of the water balance showed that depletion of soil moisture produces a negative feedback on the increased vegetation leading to increased precipitation feedback loop, especially at low latitudes (Los, 1998). Mintz and Serafini (1992) also support these statements. They have demonstrated that the specification of albedo, roughness and, most importantly, the soil moisture have strong impacts in model-simulated climates. When soil moisture availability or surface albedo is changed regionally (or globally), changes in the precipitation, the temperature and the motion field of the atmosphere take place over the corresponding region (or over the globe), which are clearly above the level of the natural variability of the model simulated climates.

Several other studies have been conducted making use of general circulation model simulations to quantify the relative contributions of land surface variability to the variability in precipitation. They show that land surface processes contribute significantly to the variance of annual precipitation over continents (Koster and Suarez, 1995). The soil's ability to retain precipitated water can lead to a positive feedback that increases the duration of the hydrological state. Through soil moisture retention and anomalous large precipitation event can yield higher subsequent precipitation through local recycling. This feedback is implicit in the water budget model of Rodriguez-Iturbe et al. (1991) and Entekhabi et al. (1992), who showed that the nature of the coupled land/atmosphere systems can induce multiple stable climate states, including extended drought s and pluvial periods.

Scott et al. (1997) pointed out, however, that is not yet clear to what extent moisture anomalies are self-sustaining and what role they play in determining climate variability. The answer to these questions depend in part on the timescales of surface moisture retention, which describes how quickly the deposited precipitation is returned to the atmosphere. The timescale of moisture storage in the soil determines the timescale of evapotranspiration persistence and thus

the timescale of humidity persistence in the near-surface atmosphere. The anomalous soil moisture also affects the partitioning of available energy into latent and sensible heat flux, thereby affecting the temperature persistence.

Another elucidative example include the study of Xue and Shukla (1991) which investigated how changes in vegetation affected the climate in the Shael with a much improved land surface model, a simplified version of the SiN1, coupled to a GCM. They stated that a change in vegetation cover would not only affect the land surface albedo, but also parameters such as the roughness length, initial soil moisture conditions, leaf are index, soil depth, the hydraulic conductivity of the soil, and the fraction of vegetation cover (Los, 1998). As in the Charney et al. (1975, 1977) study, they found a decrease in the precipitation over the Sahel and an increase in the precipitation over the tropical forest. Xue and Shukla (1991) concluded however, that the major impact of vegetation changes on precipitation in desert margins was related to changes in the latent heat flux rather thanalbedo.

Nobre et al. (1991) studied the effect of large-scale deforestation of Amazonia on climate, using a coupled atmosphere-biosphere model. A significant result of this study is the simulated reduction in precipitation over Amazonia, which is larger than the corresponding regional reduction in evapotranspiration, implying that the dynamic convergence of moisture flux also decreased as a result of deforested case is associated with a longer dryer season.

With the inclusion of biosphere models into the GCMs, a need emerged for data sets from which the global distribution of biophysical parameters could be derived. The use of look-up tables, compiled from data sets to assigned biophysical parameters to the global land cover classifications, has some inherent problems. Los (1998) states that, in one hand, land cover classes typically contain only rudimentary information on within-class variations and vegetation seasonality. On the other hand, biophysical parameters reflect conditions at selected sites and these may not be representative for an entire class, e.g., if a classification distinguishes only one type of grassland, the parameters derived from grassland either C3 or C4 based photosynthesis cannot be properly assigned. Moreover, land cover data sets can be inaccurate.

At present-day, most of this studies rely on satellite data to produce vegetation indexes, such as NDVI and other derived indexes, to be incorporated in Global Circulation Models (GCM).

3.0. RESPONSES OF VEGETATION TO WATER STRESS CONDITIONS

3.1. Introduction

The factors governing vegetation structure and ecosystem processes vary considerably among biomes. In mesic forests, for example, a frequent constraint is availability of light. As a forest environment tends from mesic to xeric, or nutrient poor conditions, the effective constraint shifts from above- to below-ground factors (Shugart, 1988). Even within the same biome, the requirements vary considerably depending on the stage of the vegetation. Plants require a certain length of time to complete their life cycles; for example, trees require many years. Life cycles consist of several stages: the establishment of seedlings, the subsequent growth of established seedlings to reproductive maturity, and the production of healthy seeds which become available for establishment as seedlings. Each stage requires different environmental conditions. Some stages require moderate but constant soil moisture during several successive growing seasons. Others, such as in general mature trees, have less need for constant soil moisture than for nutrient-rich soils (Solomon and Cramer, 1988).

In global ecological studies, it is of particular importance the knowledge of the degree of dominance of particular causal factors at particular scales. The knowledge of which factors are important at a given scale is also involved in the determination of the 'rules' for modeling purposes. The relationship between form and function, or pattern and process, is a classical ecological theme. Bormann and Linkens (1979) pointed out the effects of changes in forests structure or processes such as productivity and nutrient cycling. Many ecologists recognize that patterns and process are mutually causal, with changes in ecosystem processes causing changes in pattern and modifications in ecosystem patterns changing processes. Although it is difficult to investigate directly the feedback between pattern and processes (Shugart, 1988), in the case of vegetation it is possible to predict patterns of vegetative response to limiting conditions such as water deficits in the soil.

The availability of water is usually measured based on the parameter of the 'soil water content', which is usually stated as the amount of water lost when the soil is dried at 105ºC, and expressed either as the weight of water per unit weight of soil, or as the volume of water per unit volume of soil, being the last one a better indicative of the water availability for plants. However, water content on a percentage basis tells little about the real amount of water available for plants, because, for example, a sand may be saturated at a water content that would be too dry for plant growth in a clay soil (Kramer, 1983). When water is applied to the soil surface, it infiltrates and drains downward through the larger soil pores by gravitational flows. Some is retained by capillary forces in the smaller pores (diameter less than 30-60 micromemters) and by absorption on the surfaces of the soil particles. These constitute of the matric forces that hold part of the soil water available to plants. However, a variable fraction of the matric water is held firmly and moves so slowly that it is treated as unavailable to plants. The availability of soil water for plants depends on the potential and on the hydraulic conductivity of the soil. The soil water potential measures the energy status of the soil water and therefore the amount of work required of the plant to absorb the water. According to Kramer (1983), the water readily available for plants occurs in the range between field capacity and permanent wilting percentage. Field capacity is the water content after drainage of gravitational water has become very slow and represents a water potential of -0.3 bar or less. Permanent wilting percentage is the water content at which plants become permanently wilted and corresponds to a water potential of -10 to -20 bars. The exact value varies with the kind of plant and the conditions under which wilting occurs.

Understanding the mechanisms that govern water availability for plants in the soil, is a vital component in the process of understanding water stress conditions for plants and water deficit related effects on vegetation.

3.2. Effects of water deficits

According to Kramer (1983), plant growth is reduced more often by water deficits than by any other factor. Water and nitrogen (N) supply have the greatest effect on the plant growth when availability of those resources is low, when other resources are nonlimiting, and for species with

high growth potential. Complications arise because drought reduces N availability and low N availability alters water use efficiency (Field et al.,1992).

Although the amount of water used directly in the biochemical reactions of photosynthesis is small compared with the transpired and stored by plants, plant water status strongly influences plant growth and biomass production (equivalent to the rate of photosynthesis) particularly through the effect on leaf and root expansion (Coombs et al., 1985). Water deficits affect practically every aspect of the plant growth, including the anatomy, morphology, physiology, and biochemistry. Plant size is reduced by a decrease in cell enlargement; photosynthesis by a decrease in leaf area, closure of stomata, and damage in the photosynthetic apparatus. Root expansion is also affected. Carbohydrate and protein metabolism are disturbed, often leading to accumulation of sugars and amino acids. Biochemical effects are attributed largely to damage to membrane structure of cells and changes in enzyme activity (Kramer, 1983),

Limiting flexibility of supply rates of water also tends to counteract environmental forcing factor-driven changes in production. Ecosystem-level water storage capacity is sensitive to rooting depth, and canopy interception of precipitation increases with the leaf area index, but the supply of precipitation is sensitive to ecosystem processes only over coarse spatial scales. Field et al. (1992) states that, in water-limiting ecosystems, increases in production caused by environmental forcing factors should be no greater than their effects on water use efficiency. For elevated CO2, increases in water use efficiency on the order of 30-40% can account for similar increases in production. Since any decrease in transpiration tends to prolong the moisture availability in water-limiting sites, environmental forcing factors that decrease photosynthesis or canopy development may result in longer growing seasons, and the increased season length will tend to offset the decrease in photosynthesis.

Moreover, the maintenance of plant turgor and transpiration from the crop canopy depends on the maintenance of water uptake by roots at the soil-root interface. The more extensive and dense the root system, the more efficiently will these demands be meet. As the soil dries shrinkage of both the soil and root decreases the soil-root contact. The ultimate effect will be a reduction in water uptake, stomatal closure and a decrease in photosynthesis and biomass production (Coombs et al., 1985).

For leaves to fix CO2 from the atmosphere they must lose water through their stomata if the leaf-to-air-vapor-pressure deficit (δ_1) is greater than zero. If this water is not replaced the leaf water potential (ψ_1) will fall, which will have adverse effects on photosynthesis and leaf growth. For leaves at the top of a tree to be supplied with water they must possess a sufficiently negative water potential to overcome the effects of gravity and stem resistance on water flow through the conducting vessels. However, a low ψ_1, can reduce a leaf's photosynthetic potential. Many of the components of the photosynthesis have been shown to be affected by ψ, particularly the Calvin cycle (Friend, 1988). As soil dries, the difference in ψ, between the root and the soil increases. This is due to the exponential increase in the resistance to flow of soil water with decreasing soil water content. The rate of this increase in soil resistance is dependent on soil type. In soil with small pore sizes and high water-retention capacities, such as clays, there is a greater increase in the resistance to flow for a given decrease in water content (Friend, 1988). Consequently, the water content at which wilting is thought to occur is higher than for more porous soils.

Under still drier conditions, and as a moderately long term effect, vegetation can respond to a natural selective process and change drastically its patterns of distribution (Shugart, 1988). For example, under still drier conditions, forest changes to grassland in which the principal constraint is below-ground, suggesting patterns in the influence of environmental constraints in structuring ecosystems across broad environmental gradients

3.3. Measurement of plant water stress

Since, in general, biomass production is directly proportional to the supply and use of water, measurements of the biomass production are an important part of understanding plant water status. The term biomass can be defined, according to Coombs et al. (1985), as the"... weight of living plant material contained above and below a unit of ground surface area at a given point in time".

Although the most evident effect of plant water stress is the decrease in productivity, native vegetation can respond in many different predictable ways to a variety of stresses. Depending on the intensity and duration of the stress, the response may be at the cellular

level, the morphological/macroscopic level, or the community level (Rock et al., 1988). Those changes at different levels have diagnostic spectral characteristics which can be detected by using various types of remote sensing systems. Because of the sensitivity of native vegetation to stress factors associated with environmental change (moisture levels, nutrient levels, temperature, anthropogenic factors, and other), the ability to remotely detect subtle levels of change (response to stress) in the vegetation may prove to be a very useful indicator of environmental change. Change at different scales in both vegetation kind (vegetation types, species associations, and other) and vegetation condition (state of the health, degree of deforestation, seasonal stage of growth, and others), can be accurately detected, quantified, mapped and monitored using various multispectral sensor systems and image processing techniques (Rock et al., 1988).

4.0. MONITORING VEGETATION WITH REMOTE SENSING

4.1. Introduction

The ultimate source of energy for photosynthesis and bioproductivity is solar energy. About 98 percent of the radiation emitted by the sun is in the wavelength from 0.3 to 3.0 micrometers (Figure 4.1).

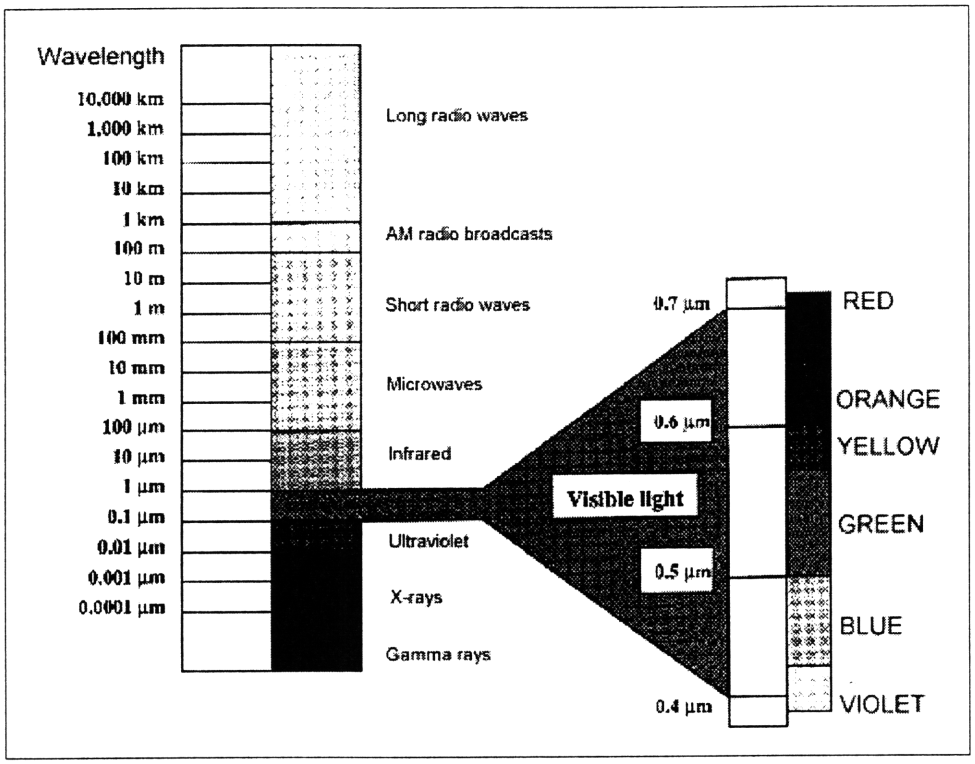

Source: *Conway, 1997*

Figure 4.1: The electromagnetic spectrum

Irradiance (I), or energy flux incident per surface area, is the correct radiometric term for 'light intensity'. Radiance, defined as irradiance per unit solid angle (Wallace and Hobbs, 1977),

can be described either as waves or as the number of photons. A simple graphical representation of radiance and irradiance is shown in Figure 4.2 .

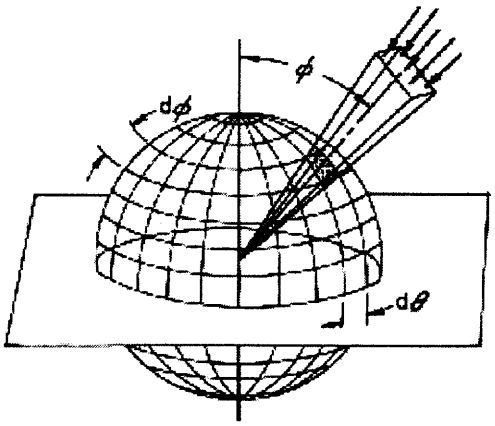

Source: *Wallace & Hobbs, 1977*

Figure 4.2: Relationship between radiance and irradiance. The radiation is impinging on a unit are in the "equatorial plane" of a sphere of unit radius (θ =azzimuth angle, ϕ =zenith angle)

The average irradiance of solar radiation (W_o: flux across unit area normal to the rays and at the top of the atmosphere) is 1353 Watts per square meter. The energy spectrum of this radiation, before it reaches the earth's atmosphere, peaks at 0.48 micrometers (Coombs et al., 1985), which is consistent with Planck's law for a blackbody with a temperature of 6000 °K (Figure 4.2). The amount incident at the top of the atmosphere over a location depends on inclination, season, latitude and solar altitude angle. Moreover, the solar beam is also attenuated by the atmosphere, and therefore, the solar radiation at the ground level, is significantly affected by the atmosphere including clouds.

Plants intercept the incident solar energy for photosynthesis but normally less than 5 percent is used in this process; the rest of this energy heats the plant and the surrounding

organism (Coombs et al., 1985). The component of solar radiation used in photosynthesis falls between

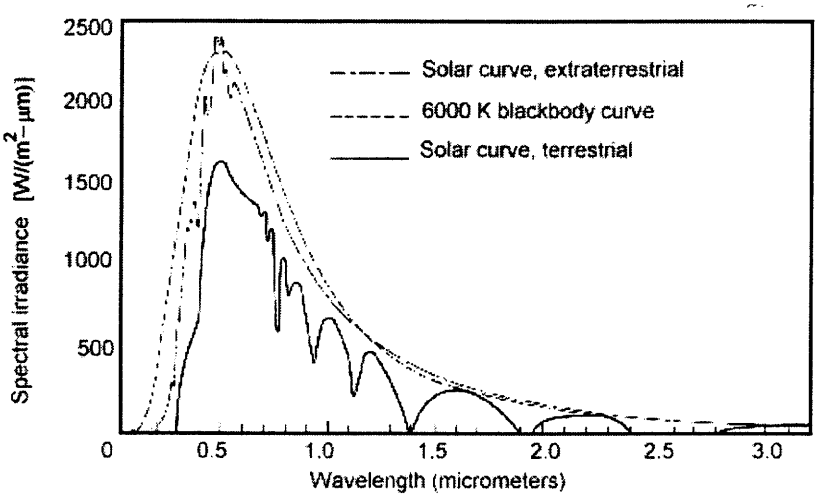

***Source:** Davis et al, 1978*

Figure 4.3 : Solar spectral irradiance

0.4 and 0.7 micrometers and is refereed to as the photosynthetically active radiation (PAR). Light quanta (photons) within this waveband are almost equally effective in driving the light reaction of photosynthesis.

Because of its unique spectral properties, plants are easily identified making use of remote sensing systems. Plant leaf responses dominate most signals that reach remote sensors. Even though plant appendages such as stems, branches, bracts and others affect the signals, their contribution is minor. Leaf characteristics such as pubescence and pigmentation, however, may have a major influence on the remote sensing signals (Gausman, 1985). Therefore, it is important to consider the optical properties of leaves in relation to observed or recorded sensor signals.

4.2. Spectral properties of vegetation

Radiation incident on a leaf or plant canopy can be absorbed, transmitted or reflected. When a leaf intersects incoming radiation at a critical angle, a portion of the light is absorbed. The amount of absorption depends on the energy (wavelength) of the photons involved; photons with a shorter wavelength are involved in photosynthesis and chlorophyll synthesis, whereas photons with the longest wavelength affect heating processes, evaporation, and transpiration. Consequently, changes in the concentration of leaf chloroplasts' pigments and tissue water content are largely responsible for inducing variability in plant tissue light absorption (Gausman, 1985). In the PAR region (0.4-0.7 micrometers) of the spectrum the leaf heavily absorbs the incident radiation. The absorption of PAR within the leaves is for the most part caused by the leaf pigments chlorophyll a, chlorophyll b, and carotenoids. The chlorophyll of green leaves usually absorbs 70 to 90 percent of the light in the blue (about 0.45 micrometers) or red (0.68 micrometers) of the spectrum (Gausman, 1985). Absorptance is smaller in the green-light region around the 0.55 micrometers wavelength.

A portion of the incoming photons are also reflected when they impinge on a leaf at a critical angle. Specular reflectance occurs at the leaf cuticle, whereas diffuse reflectance originates from light scattering (multiple reflection) mainly within the leaf mesophyll, due to the refractive index of the mesophyll structure (Coombs et al., 1985). Reflection of radiation occurs in the short-wave infra-red region (0.7 - 3.0 micrometers). The effect of this is to reduce the heat load from wavelengths which are not used in photosynthesis. However, in the far infra-red, leaves are good absorbers; thus (because good absorbers are also good emitters of radiation) they are able to dissipate excess heat very efficiently in the long-wave region of the spectrum. The reflection by leaves of near infrared radiation is due to differences in refractive indices between intercellular spaces, hydrated cells and the irregular facets of cell exteriors, and to a smaller extent to leaf material smaller than 1 micrometer (Los,1998). Approximately 50% of the near-infrared (NIR) energy is reflected by the leaf, although this value varies a lot for different species. Theories suggest that reflection takes place in the leaf at the transition of air and cellulose cell walls. It as also been suggested that reflection is determined by the number of cell walls parallel with the epidermis of the leaf and the orientation of the leaf in the vegetation. A reflectance peak

of usually less than 20 percent occurs from upper (adaxial) leaf surfaces. Light that is neither absorbed nor reflected is transmitted (Gausman, 1985).

Differences in the reflected light, not only in the green, may be originated from differences in the surface of foliage. Leaves may be covered with wax or have a hairy coat. These differences in light reflection can help in the identification of plant species. Another botanical characteristic is the structure of the vegetation, which causes differences in the reflection, for example, the position of the leaves and their distribution. In relation to the angle of incident radiation this may greatly influence the reflection. Also the growth stage or phonological stage of the plants has an influence on the reflection.

When compared with vegetation, soils show only a gradual increase in reflectivity across the spectrum (Figure 4.4). The reflectance of the soil in the infrared is only moderately higher than the reflectance in the visible. Although leaf spectra vary, the large differences between red and infrared reflectance occur for all photosynthetically active leaves, and this allows to distinguish leaves from other remotely sensed objects such as water, soils, and clouds (Los, 1998). The spectral characteristics captured will therefore change as vegetation develops over bare soil, being distinguished from other surfaces, and its changes can be related both to leaf area index and biomass (see Section 6.3.).

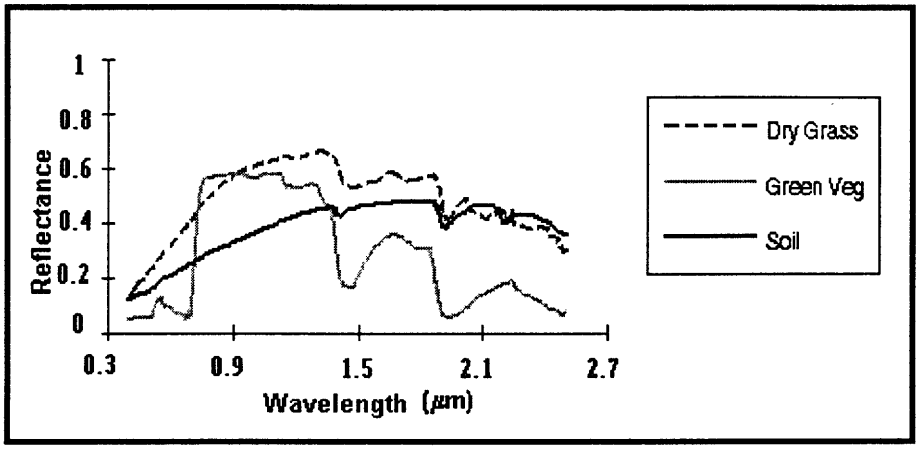

Figure 4.4: Reflectance of dry grass, green vegetation and soil at different wavelengths

Under certain circumstances, e.g. aging of plants, the yellow and red pigments present in the leafs show up clearly as the chlorophyll disintegrates. This is the case with deciduous trees, whose leaves becomes various colors just before they fall. This discoloring of leaves allows the identification of species in deciduous forests by remote sensing techniques based on the different spectral signature of the different species. The spectral signature is the characteristic of the reflection of an object with regard to the relationship of the wavelength and the reflectance.

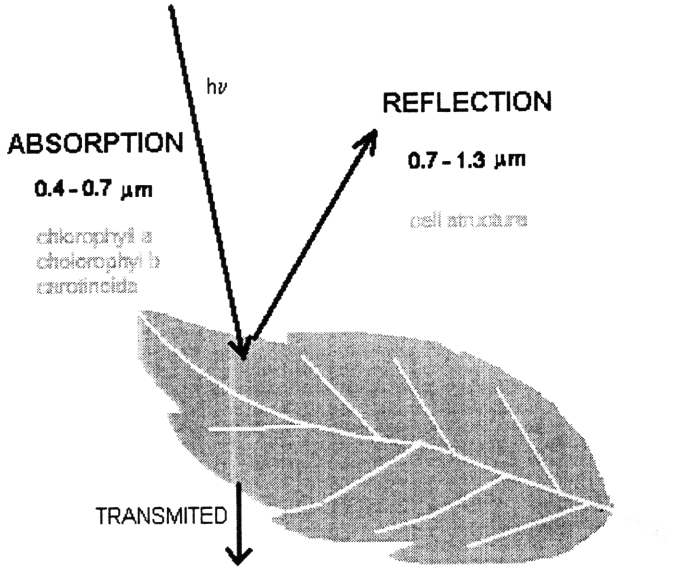

Figure 4.5: General spectral properties of leaves

In addition to the fact that biomass production can be monitored based on the optical characteristics of vegetation, several studies have been performed in order to monitor the general stress condition of the vegetation. In this context, reflectance measurements have been used to follow changes in leaf chlorophyll content. When physiological stresses affect the reflectance properties of leaves, the most pronounced initial changes often occur in the visible spectral region rather than in the near-infrared spectral region because of the absorptance of visible light by

chlorophyll. Sometimes, however, recognition of stress condition may be caused by the reduction in total leaf area rather than a change in leaf pigmentation or chlorophyll concentration (Gausman, 1985). On the other hand, it is known that healthy plants re-emit a small amount of absorbed radiant energy in the "far-red" (0.65 -0.70 micrometers) and near-infrared regions. This process of converting absorbed radiant energy at one wavelength to emitted radiation a longer wavelength without first converting the absorbed energy into thermal energy, is called fluorescence. In addition, a small emission of thermal radiation takes place at the longer wavelengths. Fluorescence increases when the process of photosynthesis does not operate optimally for reasons, and consequently measuring the fluorescence amount one can estimate stress conditions of the plant.

An understanding of the interaction of light with plant leaves of different moisture contents helps to predict their leaf water status from reflectance measurements. Leaf dehydration increases greatly the spectrophotometrically measured light reflectance over the 0.5 to 2.5 micrometers waveband (Figure 4.6). Gausman (1985) refers studies developed by Thomas et al. (1966) and Namken (1965) whose results show that reflectance increase, as relative turgidity decrease below values of 80 percent at selected 0.54, 0.85, 1.65, and 1.45 micrometers wavelength. Therefore, relative turgidity is used to measure plant water stress. Relative turgidity is the actual leaf water content expressed as a percentage of the turgid or saturation water content. In general, the linear correlation of leaf water content with reflectance is strongest in the near-infrared region. Johannsen (1969) supported those results showing water absorption centered at the 1.45 and 1.95 micrometers wavelengths were inversely related to leaf moisture, when evaluating the response of corn and soybean leaves to different soil moisture content. Sinclair (1968) explains this behavior relying on the fact that tissue of dehydrated leaves collapses in such a manner that the number of air voids increase in the cell mesophyll, and consequently, infrared reflectance increases. Johannsen' s results suggest that the green color and chlorophyll absorption responses (0.53 and 0.64 micrometer, respectively) also showed a high negative linear correlation with the leaf moisture. This indicated that changes in the leaf moisture content quickly affected the leaf spectral responses to pigment concentrations.

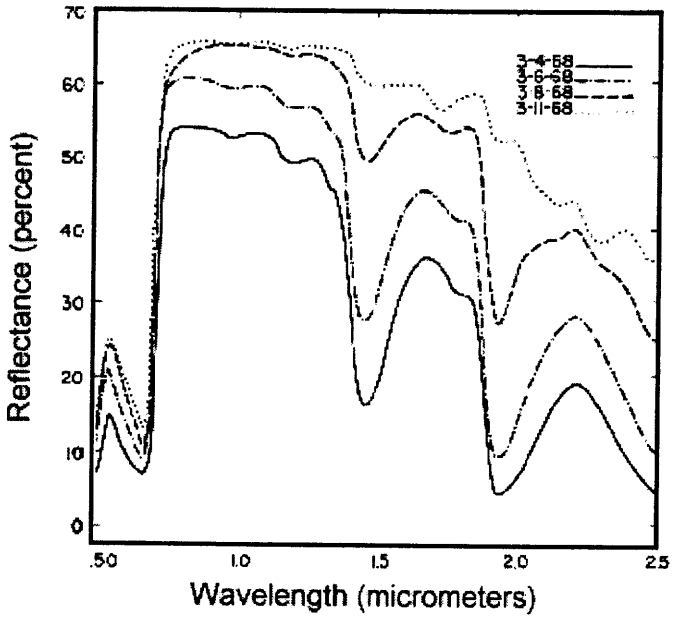

Source: *Gausman, 1985*

Figure 4.6: The effects of leaf dehydration (water loss) on increasing reflectance over the 0.5 to 2.5 micrometer waveband of the upper surface of cotton (*Gossypium hirsutum*) leaves.

Generally, stressed plant leaves have a lower near-infrared light reflectance that do nonstresses leaves. However, spectrophotometric measurements often show that diseased leaves have higher thermal-infrared light reflectance than "normal" leaves (Gausman, 1985). Plant temperatures increase with decreasing availability of soil moisture. For example, Gausman (1985) refers that plant canopy differences up to 6 °C were observed between the most and the lest water-stressed cotton fields. Those differences can be easily detected using remote sensing instruments in the thermal infrared spectral region.

4.3. Previous studies

Several studies have been conducted using remote sense techniques and using different platforms and sensors, with the goal to acquire data to produce vegetation indices and ultimately monitor vegetation changes. The two most common spectral bands detected by the satellites,

one in VIS-red part of the spectrum (0.68 micrometers) and one in the NIR (0.7-1.3 micrometers), have been used to successfully map green leaf area or intercepted photosynthetically active radiation (Tucker, 1979). By analyzing data collected over the past several years by these satellites, estimates have been obtained of the rates of clearing in Africa (Tucker et al., 1985a).

Landsat Thematic Mapper (TM) data have been proven to be useful to detect, quantify, and map areas of forest-decline in the northeastern U.S.. A damage ratio was developed by using the TM5/TM4 ratio to assess damage levels (the higher the ratio, the higher the damage). In addition to using satellite datasets to assessing forest damage across a region (spatial patterns of change), the long-term datasets provided by the Landsat satellite series (acquired continuously since 1972) allow for assessment of temporal patterns of change. According to Rock et al. (1988), advanced sensor systems known as imaging spectrometers have been shown to provide more detailed spectral information than broad-band sensors such as the Landsat TM. This additional spectral information may prove useful and diagnostic regarding specific type of damage and canopy.

Tucker et al. (1985a) used the advanced very high resolution radiometer (AVHRR) that is carried on the National Oceanic and Atmospheric Administration's (NOAA) weather satellites to map the greenness of vegetation at the continental and global scale. AVHRR observations have been used for various applications such as crop yield modeling, vegetation monitoring for famine early warming systems, detection of vegetation conditions favorable for locust breeding, land cover classification for large areas (Tucker et al., 1985a), studies of relationships between rainfall and vegetation growth (Nicholson et al, 1990), monitoring the desert expansion and contraction (Tucker et al., 1991, 1994). NDVI data were also used to estimate the global net primary production of vegetation and to study the effects of interannual climate variations in sea surface temperatures and precipitation on vegetation. Of all the sensors available, the AVHRR onboard the NOAA series of satellites is considered the one giving the most reliable and most easily handled vegetation information for the whole planet (Drury, 1990), The results of the initial AVHRR-based vegetation studies were based on empirical relationships between NDVI and biophysical parameters such as the above-ground biomass, leaf area index and fraction of vegetation cover. Physically-based models

and field measurements of light transport in a vegetation canopy revealed similar relationships and thus provided a physical explanation for the correlations between biomass and AVHRR observations (Los, 1998).

The use of longer wavelengths, such as those in the microwave part of the spectrum, have been revealing high usefulness in assessing to vegetation change, based upon the difference of vertically and horizontally polarized brightness temperature (ΔT). An example includes the 37-GHz (wavelength about 8 mm) channel of the scanning multi-channel microwave radiometer (SMMR) onboard the Nimbus-7 satellite. The basic physical priciples underlying this technique are fully supported by experimental results. Field studies and radiance transfer modeling for agricultural crops have shown that ΔT is affected by soil wetness, soil surface, soil surface roughness, and vegetation water content. ΔT values range between 25 to 30 K over dry bare soils, and this value increases to about 35 K when the soil gets moderately wet. With increasing vegetation, the ΔT value decreases due to scattering and absorption of microwave radiation emitted from the soil and also because vegetation emits largely depolarized radiation (Rock et al., 1988). Field studies show that ΔT over dense agricultural crops is about 3 K. Thus the temporal pattern ofΔT would reflect the temporal pattern of vegetation growth and decay if the effect of temporal variations of soil moisture on ΔT could be minimized.

5.0. NOAA-AVHRR

5.1. Introduction

The use of NOAA-AVHRR data for vegetation monitoring began in the early 1980s, when the potential of AVHRR data for vegetation monitoring was indicated by Tucker and co-workers (Los, 1998). They concluded that, at that time, the AVHHR was the only sensor system in operation suitable to estimate vegetation primary production from space with a vegetation index approach. A study was initiated to estimate crop production in the Nile delta with NOAA-AVHRR data and thus determine the potential of the instrument for vegetation monitoring. Seasonal sums of NDVI were calculated from cloud free 1.1 km AVHRR data and compared with annually accumulated above ground biomass and crop yield. The relationships between these variables were similar to relationships found in earlier studies where the vegetation index was determined from ground studies with hand held radiometers.

The NOAA-AVHRR collects data over the entire globe at 4 km resolution twice daily, once during day time, and once during night time. The frequent global coverage makes AVHRR data suitable for applications that require high temporal resolution and coverage over large areas. Those applications include for example, the comparison of vegetation density between years, monitoring of snow cover extent, and observation of weather systems and cloud patterns (Los, 1998).

5.2. NOAA-AVHRR characteristics

The NOAA, under the Department of Commerce, operates the civil polar-orbiting and geo-stationary NOAA satellites, which are numbered after they are placed in orbit. The primary set of sensors on board the NOAA polar orbiting satellites in known as the Advanced Very High Resolution Radiometer (AVHRR).

The AVHRR is an imager used for primarily remotely determining cloud cover and surface temperature. AVHRR has five spectral bands (see Table 5.1) in the visible (VIS) (channel 1), near-infrared (NIR) (channel 2), mid-infrared (MIR) (channel 3), and thermal infrared (TIR) (channel 4 and 5) regions of the electromagnetic spectrum. Channels 1 and 2 monitors energy in the red and near-infrared portion of the electromagnetic spectrum to observe vegetation, clouds, lakes, shorelines, snow, and ice. Channel 1 of AVHRR (Figure X) coincides with the spectral region of maximum leaf absorption (red) and channel 2 with a spectral region of maximum leaf reflectance (near infrared) (Los,1998). The other three channels operate entirely within the infrared band to detect the heat radiation from, and hence the temperature of land, water, and sea surfaces and the cloud above them (USDOC, 1998).

Table 5.1: Summary of channels on the AVHRR

CHANNEL	SPECTRAL BANDWITH	TYPES OF DATA PROVIDED
1 (Visible)	0.58 - 0.68 μm	Daytime cloud cover, snow cover, ice studies, mapping, pollution
2 (Near Infrared)	0.73 - 1.10 μm	Daytime cloud cover, surface water, vegetation/agricultural assessment
3 (Thermal Infrared)	3.55 - 3.93 μm	Black body temperatures, nighttime cloud cover, sea surface temperatures, forest fire and volcano monitoring
4 (Thermal Infrared)	10.50 - 11.50 μm (NOAA 6,8, 10) 10.30 - 11.30 μm (NOAA 7, 9, 11, 12)	Daytime/nighttime cloud cover, land and sea temperature patterns
5 (Thermal Infrared)	11.50 - 12.50 μm (NOAA 7, 9, 11 and 12 only)*	Water vapor correction when paired with channel 4, daytime/nighttime cloud cover, land and sea temperature patterns

* On NOAA 6, 8, and 10, channel 5 is a repeat of channel 4

Source: *Conway, 1997*

The AVHRR is onboard the NOAA polar-orbiting sun-synchronous satellites and scans the earth in a cross-track mode with a maximum scan angle of 55.4 degrees. The field of view

degrades from a circle with 1.1 km diameter at nadir to an ellipse (2.5 km x 6.8 km in size) at the largest scanning angle (Los et al., 1994). Each satellite will pass within radio range of a ground station once a day, traveling from north to south, known as descending node, and once a day

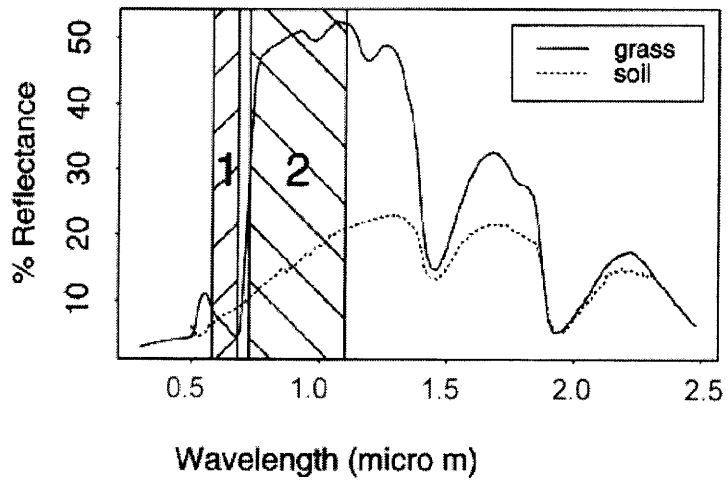

Source: *Los, 1998*

Figure 5.1: Spectral bandwidths of NOAA-AVHRR channel 1 and channel 2, and plot of leaf reflectance.

traveling from south to north, known as ascending node. The descending and ascending passes are approximately 12 hours apart for one satellite (Conway, 1997). The two polar orbiting satellites are in such orbits that one satellite (NOAA 10 or NOAA 12) will make a descending pass in the morning, while the second satellite (NOAA 9, NOAA 11 or NOAA 14) will make an ascending pass in the afternoon, approximately 6 hours later. The two satellites will then cross approximately the same point going in the opposite direction 12 hours later. This allows a ground station to receive images of the local area at least every 6 hours.

5.2.1. *Measurements in the visible part of the spectrum*

Visible (VIS) imagery indicates de amount of solar radiation reflected from the Earth. A visible image is an approximation of the Earth's albedo, that is the percentage of incoming sunlight reflected by a surface. In satellite VIS imagery, light tones represent areas of high reflectivity and darker tones represent areas of low reflectivity. Features on the surface of the Earth or of the atmosphere vary in their reflectivity and can therefore be discerned on a VIS image (Table 5.2). The land, characterized by albedos that depend on the nature of the surface, appears as various shades of gray (Conway, 1997).

Table 5.2: Approximate albedos for various features in visible (VIS) satellite imagery

SURFACE	ALBEDO	SURFACE	ALBEDO
Ocean, Pacific	7	Savanna, dry season	25-30
Snow, freshly fallen	75-90	Crops	15-25
Sand dune, dry	35-45	Savanna, wet season	15-20
Soil, dry clay or gray	20-35	Tundra	15-20
Concrete, dry	17-20	Chaparral	15-20
Soil, dark	5-15	Meadows, green	10-20
Road, blacktop	5-10	Forest, deciduous	10-20
Desert	25-30	Forest, coniferous	5-15

Source: *Conway, 1997*

The angle of illumination by the sun affects brightness in VIS imagery. Midday VIS images will be brightest, while images with low sun angles will be less bright. The location of sunlight depends on the location of the satellite point, the point directly below the spacecraft, and the solar subpoint (the point where the sun's most direct rays strike the Earth. In NOAA polar orbiter imagery, sunlight often appears as an elongated region that is oriented approximately north-south, parallel to the path of the satellite. The sunlight appears to the east of the satellite subpoint

track on local morning passes and to the west of the sub-point track during local afternoon passes. (Conway, 1997).

Many terrain features can be seen on satellite visible imagery. Heavily vegetated and wooded areas have a very low reflectivity and therefore appear darker in VIS imagery. Mountain ranges are often identified on imagery by the patterns created by wooded slopes (which appear dark in an image) and farmland in the valleys (which appear lighter). Sparsely vegetated soils of desert regions also appear bright in VIS images due the very high reflectivity of the light-colored sands and soils.

5.2.2. *Measurements in the NIR part of the spectrum*

Within the infrared part of the spectrum, the near-infrared (NIR) wavebands are particularly important when trying to map vegetative cover characteristics of the Earth's surface. In fact, electromagnetic radiation, with wavelengths in the range of about 0.75 to 1.1 micrometers, is sensitive to the mesophyll structure of leaves, as described in Section 4.0 and in conjunction with VIS imagery allows the production of vegetation indexes.

5.3. Sensor degradation

When multi-year NOAA-AVHRR data sets became available, several shortcomings were noticed. Los (1998) states that these shortcomings are caused by changes in the sensitivity of the visible and infrared sensors, scattering and absorption by atmospheric constituents, soil background effects, cloud contamination, and errors in navigation of the satellite. In particular, the change in the data receiving protocol from one NOAA platform to the next revealed large discontinuities in the AVHRR data.

Sensor degradation results in gradual changes in the observed reflectance over the lifetime of the sensor and leads to discontinuities between successive instruments. NOAA provides a preflight calibration for the visible and near-infrared channels, which relates the signal received by the satellite by the satellite to a pre-launched standard. This preflight calibration is not

updated during the operation of the AVHRR, hence it does not take sensor degradation into account. Correction of AVHRR data for sensor degradation is important to do meaningful interannual comparisons. Several coefficients have been estimated for historic AVHRR data. Currently, these coefficients are not available for real time applications. However, According to Los (1998), a technique exists to derive calibration coefficients from the NDVI data over desert targets, which can be used to obtain a good approximation of the rate of sensor degradation in near-real time in cases that channel 1 and 2 data components are not available.

With the availability of longer, multi-year NOAA-AVHRR data records, it became possible to study the effects of interannual variations in climate on vegetation. Successful studies have been carried analyzing the occurrence of anomalies in NDVI during and El Nino for South America (Myneni et al., 1995; Anyamba and Eastman, 1996)

5.4. NOAA-AVHRR data

Data from the NOAA polar orbiting satellite sensors are transmitted continually and can be received by any properly equipped ground station within radio range. The kind of service is known as direct readout. To received data from the AVHRR there are two categories of direct readout services: High-Resolution Picture Transmission (HRPT) and Automatic Picture Transmission (APT) (Conway, 1997). The APT signal from the U.S. polar orbiting satellites is broadcast at 137.50 or 137.62 megahertz (MHz) in analog transmission at 120 lines per minute. The ground stations required to receive APT use little more than FM antenna and a radio receiver tuned to the proper frequency. The radio signal is converted to a digital image, which can be displayed on a personal computer. The relatively simple and inexpensive equipment needed to capture this imagery makes APT the most commonly used form of direct readout. APT transmits data from two channels of the AVHRR at a reduced resolution of 4 km. The reduced resolution allows a larger area of view than the HRPT data, although smaller features may not show up. During the day, both a VIS and IR channel are used, while nighttime transmissions usually consist of two different IR channels. The images are received simultaneously, resulting in a side-by-side double image. Comparisons between the two different channels can help an investigator

to infer various characteristics of the clouds, oceans, and land surfaces that could not be determined with data from only one channel .

The HRPT signals from U.S. polar orbiting satellites is broadcast at 1698.0 MHz. The receiving stations for HRPT are more complex and expensive than those designed for receiving APT; therefore HRPT imagery can be more difficult to obtain. However, Advances in receiver technology and innovations in building advanced receiving stations are bringing HRPT close to an affordable level for use by many. Additionally, organizations equipped with HRPT direct readout systems often make imagery available to the public through various electronic bulletin boards. An HRPT transmission consists of data from all five channels of the AVHRR. While the resolution of the HRPT image is very high, the area covered in each image is smaller. This often makes HRPT imagery more useful when studying smaller-scale features such as individual storms or surface characteristics of the land and oceans (Conway, 1997).

The average instantaneous field-of-view (IFOV) of the NOAA-AVHRR (1.4 milliradians) yields a ground resolution of approximately 1.1 km at the satellite nadir from the nominal orbit altitude of 833 km. The GAC (Global Coverage Area) data are derived from an on board sample averaging of full resolution AVHRR data. Four, out of five, samples along the scan line are used to compute one average value and the data from every third scan line are processed, yielding 1.1 by 4 km resolution at nadir.

6.0. NDVI - NORMALIZED DIFFERENCE VEGETATION INDEX

6.1. Introduction

Because the spectral properties of the leaf are unique, combinations of reflected radiances from the visible (VIS) and near infrared (NIR) spectral regions are directly related to the photosynthetic capacity and have been used to estimate green leaf biomass of plant canopies. (Fung et al., 1987). Monteith (1972) showed that for a given photosynthetic crop types (C_3 and C_4), the efficiency (ε) of conversion of intercepted radiation into biomass is remarkably constant. Based on the knowledge, solar radiation in the VIS and NIR wavebands, reflected by the Earth's surface and collected by a remote sensing device, have been combined into spectral vegetation indices. Two commonly used vegetation indices are the Simple Ratio Vegetation Index (SRVI), and the Normalized Difference Vegetation Index (NDVI).

The SRVI, defined the ratio $\frac{NIR}{R}$, in which R designate the energy reflected in the red portion of the visible spectrum, has shown to be particularly valuable in remote sensing. This index has been used to determine biomass in natural communities and ground cover by crops (Coombs et al., 1985). Kumar and Monteith (1981) showed on theoretical grounds that the SRVI was linearly related to the fraction of available light intercepted by vegetation. A limitation of this ratio is that is not bounded and therefore does not allow relative comparison of biomass for different locations.

To overcome this limitation, a recently developed satellite methodology has been used, also based on the differential reflection of green vegetation in the visible (red portion) and infrared portions of the spectrum. The Normalized Difference Vegetation Index (NDVI) is defined as:

$$NDVI = \frac{(NIR - VIS)}{(NIR + VIS)} \tag{6.1}$$

and is therefore a measure of the slope around 0.7 micrometers, indicative of the photosynthetically active leaves. Since, the red reflectance is inversely related to the chlorophyll density, and the near infrared reflectance is directly related to scattering within individual leaves and between leaves in the canopy, the combination of these two adjacent spectral regions in an index provides a first order correction for differences in irradiance, and gives and estimate of the intercepted fraction of the photosynthetically active radiation absorbed by vegetation (Los, 1998).

The NDVI equation produces values in the range of -0.1 to 1.0, where increasing positive values indicate increasing green vegetation, and negative values indicate nonvegetated surface features such as water, barren, ice, and snow or clouds (Eidenshink and Faundeen, 1997). NDVI assumes values between -0.2 and 0.05 for snow, inland water bodies, deserts and exposed soils, and increases from about 0.05 to 0.7 for progressively increasing amounts of green vegetation (Myneni et al., 1997). The distribution of NDVI represents green-leaf vegetation rather than the distribution of vegetation *per se* (Townshend et al., 1993), and therefore, an NDVI profile throughout an annual cycle helps to determine whether the land cover at a particular location is broadleaf evergreen forest or broadleaf deciduous forest or grassland, or some other kind of biome.

In the specific case of the NOAA-AVHRR, an initial and simple index should also be mentioned, which is the Global Vegetation Index (GVI). The GVI is a specific AVHRR application that uses global area coverage (GAC) data to produce NDVI. GAC data are processed daily and then composited on a weekly basis to produce a global map portraying vegetation vigor. The NDVI produced by the AVHRR data is obtained as following:

$$NDVI = \frac{(Ch2 - Ch1)}{(Ch2 + Ch)} \tag{6.2}$$

where Ch1 and Ch 2 are the reflectances in the visible (0.58 to 0.68 μm) and near-infrared channels (0.725 to 1.1 μm), respectively.

6.2. Compositing techniques

An ideal vegetation index is able to simultaneously retain maximum sensitivity to vegetative cover characteristics, and be relatively unaffected by solar angle, atmospheric turbidity, topography and viewing direction (Walter-Shea et al., 1997). The daily satellite derived images generally show large areas where data are missing. These areas result from gaps between mapped orbits and from data elimination during the various stages of processing. The amount of useful data is further reduced by the effects of clouds, atmosphere, and viewing and illumination geometry.

To achieve more accurate NDVI values is recommended to apply temporal compositing processes. One of the recommend method consists in the maximum compositing NDVI in which the NDVI values are examined, pixel by pixel, for each observation during the compositing period to determine the maximum value. This procedure allows to obtain almost complete cover of the land surface and to reduce the impact of the described effects. Because most of the cloud, atmosphere and viewing effects decrease the NDVI, compositing will result in monthly NDVI values that for the main part are selected from data collected at near-nadir viewing angles under cloud-free, clear atmospheric conditions. However, changes in NDVI values as a result of sensor degradation, solar zenith angle and soil background cannot be accounted for by compositing (Los, 1994).

In the procedure of forming composite images the first factor to consider is the length of the compositing period. Compositing periods of 7, 10, and 14 days have been used most commonly. The choice of the period is usually based on the length of time necessary to obtain a composite with minimal cloud contamination and the amount of time necessary to observe meaningful changes in surface characteristics. The compositing period that is recommended for the prototype products is approximately 10 days created by month. Thus January has three composites of 10, 10 and 11 days; February has 10, 10 and 9 or 8 depending on whether it is a leap year, and so on. This procedure has the advantage of creating calendar month composites, which is a common reporting period for agronomic and biophysical characteristics (Eidenshink and Faundeen, 1997).

6.3. Relationship between NDVI and biophysical parameters

Underlying the relationships between NDVI and various biophysical parameters are the unique reflective properties of green leaves described in Chapter 4.0.. Ultimately the NDVI is determined by the degree of absorption by chlorophyll in the red wavelengths, which is proportional to leaf chlorophyll density, and by the reflectance of near infrared radiation, which is proportional to green leaf biomass, leaf area index (LAI), total dry matter accumulation and annual net primary productivity. However, this index most directly represents the absorption of photosynthetically active radiation (PAR) and hence is physiologically a measure of the photosynthetic capacity of the vegetation (Nicholson et al., 1990). Privette et al. (1996) highlighted the fact that those relationships can be site-sampling-condition-dependent, and therefore one should carefully take that fact into consideration, when extrapolating the results.

The fraction of the photosynthetically active radiation absorbed by the green canopy is denominated as FPAR. NDVI data are strongly correlated with the fraction ofphotosynthetically active radiation absorbed by vegetation (Myneni et al., 1997). For longer time scales, several factors enhance the usefulness of the relation between accumulated, absorbed PAR and productivity. First, a correlation usually exists between radiation and other environmental factors that affect productivity, such as temperature. Second, this productivity-light relation is quite conservative because plants adapt to their environment by changing the duration of their various growth periods. Finally, plant productivity per unit of leaf area is relatively stable, so that the accumulated effect of many factors on productivity tends to be reflected in the amount of leaf area, given that the plant has sufficient time to respond (usually weeks to months) and thus maintain some sort of equilibrium with its environment. The effect of nutrient status is implicitly accommodated in the strong feedback between nutrient availability and leaf area (NASA, 1989). Moreover, much of the long-term effect on the productivity of temperature, water availability and nutrient availability is accommodated in the relation between productivity and absorbed PAR through leaf-area effects.

Model results and field experiments for several broadleaf land cover types have shown a consistent relationship between FPAR and NDVI. Los (1998) argues that this relationship is dependent only, to a minor extent, on model formulation and leaf properties. However, Walter-Shea et al., (1997) states that the relation have been shown to be sensitive to a variety of factors such as the viewing geometry. According to Walter-Shea et al. (1997) the linear relation between nadir-derived NDVI and FPAR varied by 10-15% over a range of solar zenith angles and plant canopy geometry. The same authors also refer that off-nadir vegetation indices can also be nonlinearly related to FPAR. This throws some uncertainty to the assumption of Sellers et al. (1992) who states that, since the relationships between NDVI, FPAR and photosynthesis are approximately linear, they should be largely scale invariant. Several authors have investigated the relationship between the fraction of photosybnthetically active radiation (FPAR) absorbed by vegetation and NDVI, or functionally equivalent vegetation indices. Relations between vegetation indices and FPAR can be linear (Kumar and Monteith,1981), non linear (Asrar et al., 1984), including exponential (Steven et al, 1983) and quadratic (Gallo et al., 1985). Most of those relationships are evaluated for measured or simulated data viewed at nadir as limited solid angle or hemispherically.

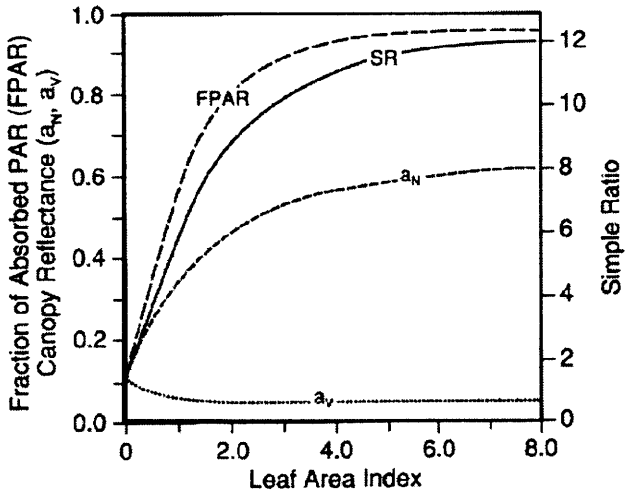

Source: Sellers et al, 1996

Figure 6.1: Relations between FPAR, LAI and Simple Ration

The studies show that the relationship between productivity, NDVI, and incident solar radiation depends on plant type, for several reasons. First, the relation between NDVI and absorbed PAR depends on leaf orientation and spatial foliage distributions; to some extent this effect is accommodated by the NDVI. Second, plant type can affect the conversion factor relating productivity to intercepted PAR and how this factor changes with water availability, temperature, or nutrient status. Third, the amount of fixed carbon used to maintain respiration depends on plant type. This is specially true for perential forests, where the old trees may respire away a large fraction of the carbon fixed in photosynthesis to maintain their bulk. Fourth, the presence of senescent leaves can affect the dependence of dry matter productivity on absorbed PAR and NDVI. Fifth, the rooting depth depends on plant type, so that the size of the reservoir of stored soil water may be related to plant type (NASA, 1989).

In addition to FPAR, leaf area index (LAI) can be estimates from satellite data. Leaf Area Index (LAI) can be expressed as :

$$LAI = \frac{s_i}{\mathrm{P}} \tag{6.3}$$

where s_i is the functional (green) leaf area of the crop canopy standing on ground area *P*. Both variables, s_i and *P* are normally measured in m^2; LAI is dimensionless. s_i can refer to the total surface area of the leaves, i. e., both the upper and lower surface, the area of a single surface, or the projected area where leaves are other than flat, e.g. conifers. Coombs et al. (1985) highlight the importance of taking into account this variability in the definition of LAI when making comparisons between different studies.

The relationship between NDVI and leaf area index is not a strong as the relationship between FPAR and NDVI and depends on several factors such as the canopy structure and leaf optical properties (Los, 1998). Sellers et al. (1992) showed that relationships between NDVI and total leaf area index (green and dead leaves plus branches and stems) vary widely between

vegetation morphologies, but that the relationships among vegetation indices, FPAR, photosynthesis and albedo are more consistent.

The relation between NDVI and LAI has been showed to be more nonlinear than between SRVI and LAI (Holben et al., 1980). Walter-Shea et al., (1997) present graphical relations (Figure 6.2) between LAI and SRVI and NDVI, for different view zenith angles (θ_v) and solar zenith angles (θ_s). General trends in the data are shown with smoothed data lines from data measured at the specific θ_v and θ_s and indicate the bounds of the data set.

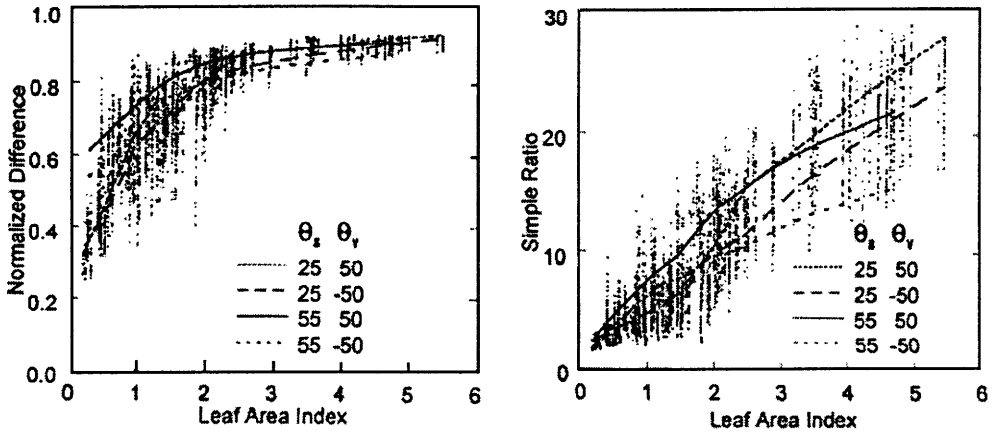

Source: *Walter-Shea et al., 1997*

Figure 6.2: Vegetation indices derived from canopy bidirectional reflectance factors (BDRFs) over a developing alfalfa canopy over the measurement period characterized as functions of LAI.

Walter-Shea et al. (1997) results show that careful selection of view geometries can greatly affect the success of vegetation indices, and suggest that NDVI and SRVI in the near-nadir or backscatter direction gives the highest correlation yet not the highest sensitivity. Those authors also argue that, because of existing NDVI composing methods (Section 6.2.) to choose viewing angles close to nadir, relatively favorable NDVI-FPAR relations are probably being acquired.

6.4. Linkages between NDVI and climate

Several studies have been performed trying to correlate climate and variations in surface cover using satellite derived observations. Most of them have been focusing in the Sahel zone of Africa due to the fact that this region experiences long-term droughts and changes in the land use patterns. For this area particular attention have been given to the study of correlations between NDVI and precipitation. The relationship between rainfall and vegetation growth can help to determine the sensitivity of various vegetation formations to climate variability and to establish the climatological limits in which NDVI is a useful indicator of vegetation growth. Tucker et al. (1985a) used AVHRR data to estimate biomass production for the period 1981-1984, and found that these production values are consistent with the expected from the observed rainfall patterns. Also for the same region, a study performed by Nicholson et al. (1990), which compared the vegetation response in the Sahel and East Africa using NOAA-AVHRR derived NDVI, shown that: (1) the spatial patterns of annually-integrated NDVI closely reflect mean annual rainfall; (2) there is a good relationship between rainfall variations and NDVI on seasonal and interannual time scales for areas where mean annual rainfall ranges from approximately 200 to 1200 mm; (3) Mean annually-integrated NDVI is linearly related to mean annual rainfall in the Shael. In East Africa the relationship is approximately log-linear; above some threshold value of rainfall, NDVI values level off and vary minimally with rainfall.

Los (1998) conducted a study, also trying to achieve an understanding of the degree of correlation between NDVI patterns and climatological parameters, using global NDVI data from the GIMMS with a resolution of 1° x 1°. His results show that positive correlations between NDVI and precipitation anomalies dominate over mid and high latitudes areas in the Northern Hemisphere, and positive correlations between precipitation and NDVI anomalies dominated at low latitudes and tend to be localized in semi-arid regions. For the mid and high latitude areas where water is not a limiting factor (e.g. Western Europe, and the boreal forests of North America and Asia), negative NDVI anomalies were associated with decreased ocean and land surface temperatures and shorter growing seasons. The effects are widespread and affect land surface vegetation over a large part of the Northern Hemisphere. For low latitudes, alternating patterns of warming and cooling in the oceans are

observed that have been associated with changes in convection, and rainfall and because of increased drought or wetness, with changes in NDVI. According to Los (1998), the anomalies in rainfall and NDVI at low latitudes have been associated with changes in convection and SSTs: increased SSTs lead to increased convection, rainfall and vegetation greenness and decreased SSTs lead to decreased convection, rainfall and vegetation greenness. Los (1998) used the same data set to explore correlations between SSTs and NDVI and precipitation and NDVI and concluded that the data suggests a similar positive linkage at mid and high latitudes between anomalies in SSTs and vegetation greenness but driven by land surface air temperature anomalies instead of precipitation anomalies. Los (1998) argues that the positive correlations between NDVI and land surface temperature may be an artifact resulting from a relationship between increased temperature, decreased cloudiness and as a result increased NDVI because of a clearer, less cloud atmosphere.

Nicholson et al. (1990) claims that the NDVI-rainfall relationship has not yet been investigated in enough depth and little is known about the timing of NDVI response to rainfall. On the other hand, it remains to established whether and under what conditions NDVI is a sensitive indicator of the interannual variability of rainfall and what hydrological variables, such as soil moisture, are more closely linked with NDVI.

7.0. DATASETS

7.1. NDVI

7.1.1. Introduction

The basis of this dataset is the normalized difference vegetation index (NDVI) dataset calculated by Los et al. (1994), Los et al. (1994) used a multi-year, 1982-1990, monthly composited global vegetation data set 1° by 1° resolution derived from observations by the Advanced Very High Resolution Radiometer (AVHRR), on board of the National Oceanic Atmospheric Administration (NOAA) series of meteorological satellites. NOAA-AVHRR channel 1 and 2 data were converted monthly continental NDVI datasets with a resolution of 5-8 km and processed and archived by the Global Inventory Monitoring and Modelling Studies (GIMMS) group at NASA/Goddard Space Flight Center. The continental GIMMS NDVI datasets were calculated from Global Area Coverage (GAC) data collected at daily intervals by the AVHRR onboard the NOAA-7, -9 and -11 satellites.

Based on NDVI dataset another global NDVI dataset, with a higher resolution of 1° x 1°, was produced to estimate land surface parameters for use within general circulation models of the atmosphere (Los, 1998). Several algorithms for error correction were applied to the data-set producing a new one: the FASIR-NDVI dataset. As a courtesy of Dr. Jim Collatz and Sietse Los, at the Goddard Space Flight Center (GSFC)/NASA, a subset of the FASIR-NDVI dataset, for the period between 1982 and 1990, and for the European region (latitude ranging from 30.5N to 89.5 N; longitude ranging from 14.5 W to 59.5E), was made available for this study.

7.1.2. FASIR-NDVI

In order to obtain consistent global land surface parameters from NOAA-AVHRR NDVI data, the data needed to be corrected for the various interferences: sensor degradation, cloud contamination, absorption, and scattering by atmospheric constituents, variations in solar zenith angle, and missing data. Therefore, the GIMMS monthly continental

NDVI data from 1982-1990 was subjected to sensor correction, which included a correction for the period 1982-1984 to take into account the aerosols induced in the atmosphere by the eruption of El Chichon in April 1982 located in Chiapas, Mexico (Los, 1998)

Figure 7.1 shows a sequence of several corrections applied to the global 1° x 1° NDVI data, collectively referred to as FASIR, which stands for Fourier Adjustment, Solar zenith angle correction, Interpolation of missing data, and reconstruction of NDVI values over tropical rain forests which have almost continuous cloud cover.

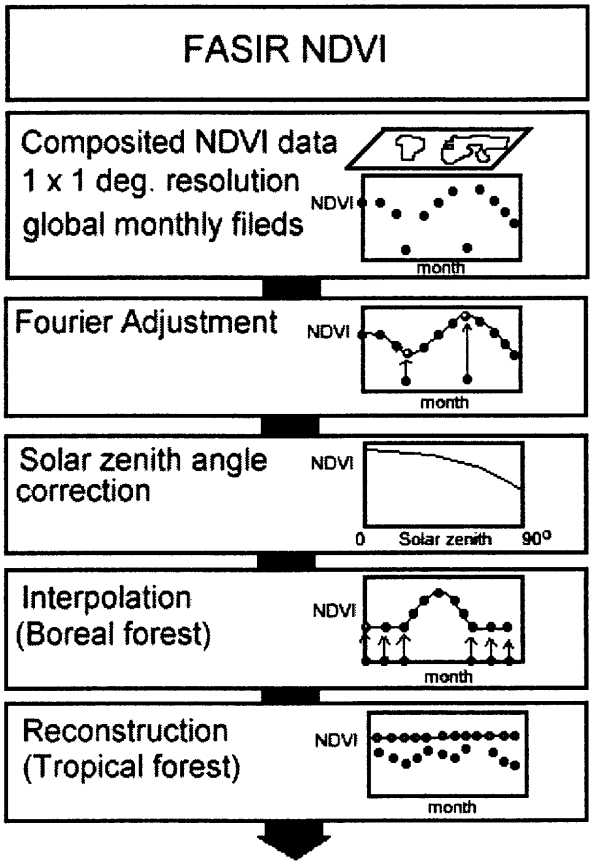

Source: *Los, 1998*

Figure 7.1: Outline of FASIR corrections

7.1.2.1. Fourier Adjustment

The Fourier-based adjustment technique (FA of FASIR) was developed to remove cloud interferences and atmospheric effects of outliers in the NDVI time-series and is based on two assumptions (Sellers et al, 1996; Los, 1998): (1) NDVI varies smoothly over time, which implies that outliers in the NDVI time-series are the result of either cloud-contamination or sudden changes in the amount of atmospheric constituents; (2) most sources of errors decrease the value of the NDVI, which justifies the calculation of monthly maximum value composites.

The FA provides a conservative correction to the data, i.e. suspected values are adjusted relative to the position of more reliable data. According to Los (1998), the procedure may lead to some small overestimation in specific cases, e.g., when a large, sudden change in the amount of vegetation occurs, such as a climate with large seasonality. For these biomes, overestimation could be a problem at the start and end of the growing season.

7.1.2.2. Solar Zenith Angle Correction

The NDVI varies with solar zenith angle as a result of increased atmospheric path length and surface bidirectional reflectance distribution function (BDRF) effects. Lacking of calibrated, physically based model, a simple empirical procedure was used to account for solar zenith angle effects. The solar zenith angle correction adjusts NDVI values for effects related to variations in time of overpass of the NOAA satellite. Validation of the solar zenith angle adjustment (S of FSAIR) is complicated because it depends of several factors, such as the landsurface (BRDF), the composition of the atmosphere and the viewing angle (Los, 1998). The effect of solar zenith angle on the global NDVI data is estimated from a statistical analysis of NDVI distributions. The solar zenith angle effect was established for two situations where interannual variation in NDVI is low: land covers with dense vegetation and bare soils.

More detailed information on the methodology applied for this purpose is described in Sellers et al.(1996) and Los (1998).

7.1.2.3.Interpolation

The original NDVI dataset of Los et al. (1994) contains data missing values whenever the surface radiative temperature falls below 273 °K (288 K in Africa). These missing values represent a significant problem at high latitudes during the Northern Hemisphere winter, specially for modeling purposes. To overcome this problem of several successive missing NDVI values, a best guess is made about the "effective winter" NDVI values or evergreen neadleleaf vegetation by selecting a value at the end of the growing season, when the only remaining green component is assumed to be evergreen. In this particular dataset, the NDVI value of October is used to replace missing values in areas covered with neadleleaf evergreen vegetation during winter. A similar procedure, with a six-month phase shift, was followed for missing winter values in the Southern Hemisphere (Sellers et al., 1996).

7.1.2.4. Reconstruction

The Fourier adjusted NDVI time series over the tropics show strong evidence of serious cloud contamination, e.g. low NDVI values coinciding with the climatological occurrence of rainfall and cloud cover. To avoid low values in evergreen broadleaf land cover types, the maximum NDVI values over the year is selected for each pixel to represent the annual time-series. The FASIR corrected NDVI data are taken to be indicative of the amount of green leaves in the vegetation canopy (Los, 1998). The Fourier-adjustment NDVI time-series over the tropics show incontrovertible evidence of serious cloud contamination (Sellers et al., 1996). A temporary solution for this problem is the raise of NDVI values for evergreen broadleaf vegetation pixels to the maximum observed for that pixel for that pixel during the year.

7.1.3. Discussion

Some limitations have been found in NDVI products. The most important is the absence of on-board calibration for channel 1 and channel 2, since these were originally designed purely for imaging. Also AVHRR sensors on different platforms have different gains and offsets. Consequently, interannual comparisons must be carried out with considerable care (Townshend et al., 1993).

Problems also arise because of the limitations of the NDVI index itself. A single average of NDVI may provide a poor representation of the cell, since areas of approximately 10000 km^2 can include a wide range of vegetation types and conditions. This is particularly the case in areas of rugged relief or those areas exhibiting a strong climate gradient. Los et al. (1994) argues that, If one wishes to monitor such areas in the context of climate change studies, then clearly it is advisable to do so at a much higher spatial resolution than 1° x 1°. However, previous research has demonstrated that at 1° x 1° degree spatial resolution it is possible to capture the broad patterns of global vegetation and that at this scale climate appears to be the major factor in vegetation patterns. Moreover, the coarse resolution of the data sets in itself poses problems because of the difficulties of accurate ground location and high physical variability of many land areas of the Earth. For example, soils can have a substantial influence on the index, especially where vegetation cover.

In order to overcome some of these limitations, modifications of the index have been proposed (e.g. Huete, 1987), which help reduce, but do not eliminate the effects of the soil background. According to Crist and Cicone (1984) the use of other spectral bands could possibly help to reduce soil effects to a greater extent, but currently there are no data sets with such spectral bands available at a global scale.

7.2. Soil wetness and precipitation

7.2.1. Introduction

The hydrology parameters used in this study include precipitation and soil wetness, defined as the ratio of soil moisture to the maximum moisture allowed. The underlying dataset comes from the Data Assimilation Office (DAO) of the Goddard Space Flight Center Laboratory for Atmospheres (GLA) (available at: ftp://hera.gsfc nasa.gov/pub/ verification /Station_obs/surface/tpgev/tpgev.b1979.e1992.doc).

Although the original data period is 14 years from January 1979 to December 1992, in this study only data for the period of January 1992 to December 1990 was used in order to be consistent with the NDVI dataset. The global fields are gridded in a 2° latitude x 2.5°. longitude resolution and the grid point (1,1) corresponds to the point at -180 ° longitude and the South Pole. The first index indicates points eastward out to 177.5 ° and the second index points northward up to the North Pole. From the global area available, it was extracted the data corresponding to the European area, with latitude ranging from 30.5°N and 89.5°N, and longitude ranging from 14.5°W to 59.5°E.

Soil moisture was derived using the procedure proposed by Thornthwaite (1948) to compute soil moisture from observed monthly mean precipitation, and estimated potential evapotranspiration using surface air temperature. The procedure has been tested in many field studies (Mintz and Serafini, 1984), and shown to give, in general, a reasonable approximation to local measurements of the soil moisture and evapotranspiration. Mintz and Serafini (1992) adopted this procedure to generate gridded climatological soil moisture distributions which have been used as part of the Global Circulation Models (GCMs) boundary conditions. This was also the procedure used, although with some alterations, to generate soil moisture fields for each month of the period of this study.

More detailed description on the dataset is included in a NASA Tech. Memorandum publication (Schemm et al., 1992).

7.2.2. Soil moisture estimates

In the methodology to compute the soil moisture estimates, the equation for the soil moisture, ω, can be written as (Schemm et al., 1992).

$$\frac{\partial \omega}{\partial t} = P - E \qquad , \omega_{ax} = \omega_s \tag{7.1}$$

where

$$E = E_p \beta(\omega, \omega_s) \tag{7.2.}$$

and P denotes de precipitation rate, E the rate of evapotranspiration, ω_s the maximum soil moisture available for evapotranspiration which is defined as the difference between the moisture storage capacity of soil and soil moisture at the wilting point of plants, E_p the potential evapotranspiration, and β the evapotranspiration coefficient. The magnitude of ω_s is fixed at 150 mm as in Mintz and Serafini, and any amount greater than ω_s is treated as runoff (Schemm et al., 1992).

Following Thornthwaite (1948), the potential evapotranspiration for a month is estimated as a function of the monthly mean surface air temperature and duration of daylight.

$$\begin{aligned} E_p &= 0, && T_A < 0^o C \\ E_p &= 16L(10T_A / I)^a, && 0 \le T_A \le 26.5^o C \\ E_p &= -415.85 + 32.35T_A - 0.43T_A{}^2, && T_A > 26.5^o C \end{aligned} \tag{7.3}$$

where, E_p *is in mm/day and*

$$I = \sum_{m=1}^{12} (T_{Am} / 5)^{1.514} \tag{7.4}$$

$$a = (6.75x10^{-7} I^3) - (7.71x10^{-5} I^2) + (1.79x10^{-2} I) + 0.49 \tag{7.5}$$

$$L = (D / 30)(h / 12) \tag{7.6}$$

where D is the number of days in the month, h the number of hours of daylight, and T_{Am} the monthly mean surface air temperature (°C) in each month of the year (Schemm et al., 1992).

The evapotranspiration coefficient, β, is given as

$$\beta = 1 - \exp[-6.8(\omega / \omega_s)]. \tag{7.7}$$

This relationship is based on the analysis of field measurements by Nappo (1975) as adopted by Mintz and Serafini (1984), and represents the curve of best fit to (E/E_p) plotted against the volumetric soil moisture content. Although this procedure has shown to give reasonable results, according to Sellers (1965), in some cases, it is known to underestimate the potential evapotranspiration.

Schemm et al. (1992) highlights the fact that the described procedure does not account for frozen ground and ice formation. Since there is no transpiration when the air

temperature is below the freezing point, the precipitation is simply accumulated as soil moisture. This might overestimate the soil moisture during the winter season.

In order to generate data suitable for GCM boundary conditions, the station values of soil moisture were interpolated to a 2° x 2.5° latitude/longitude grid. The interpolation was performed by averaging station values within a 300 km radius of each grid point. The averaging weights are proportional to the inverse of the square of the distance of stations from the grid point. The value at a grid point with no station data within the 300 km radius was denoted as undefined (Schemm et al., 1992).

For the purposes of the present study, and to have some consistency between the different datasets used, it was necessary to re-sample the pixels of the precipitation and soil wetness data using bilinear interpolation methods to obtain a spatial resolution of 1° x 1°.

7.2.3. Discussion

Under the context of the Atmospheric Model Circulation Project (AMIP), Robock et al. (1997) conducted simulations with different atmospheric circulation models forced by observed sea surface temperatures for the 10-year period, 1979-1988. Their intention was to compared the parameterizations, and evaluate their simulations of soil moisture by comparing them with actual observations of soil moisture, from 150 stations in the former Soviet Union for 1979-1985 and Illinois for 1981-present. The spatial patterns, mean annual cycles, and interannual variations were compared to plant-available soil moisture in the upper 1 m of soil.

Among the several different models evaluated and compared, Robock et al. (1997) compared the dataset used in this study, obtained by the Schemm's et al. (1992) procedure, described above, and the original dataset Mintz and Serafini (1984). The datasets were compared at a 2° x 2.5° degree grid base and the results showed that they are quite different from each other, even though they use the same method. Moreover, the study shows that both are much drier than the observations for most of the area Russia. Therefore, any GCMs that use

these models-based 'data-sets' as fixed surface or subsurface conditions will be biased toward a particular soil moisture distribution that is different from what is observed (Robock et al., 1997).

More conclusions were taken concerning the Schemm et al. (1992) dataset and those include the fact that, since models with 15-cm field capacity do not capture the large high latitudes values of soil moisture, this model may add substantial errors to the dataset. In addition, the model does not simulate properly the winter soil moisture variations in high latitudes, keeping soil moisture constant, while observations show that soil moisture varies in the winter as much as in other seasons. The observed interannual variations of soil moisture were not captured by the model (Rocket et al., 1997). However, the conclusions of the study performed by Robock et al. (1997) show that there is no evidence that more complicated models produce better simulations, and that models with multiple levels, or explicitly considered vegetation, or explicitly considered immediate or subsurface runoff did not produce better simulations of soil moisture than the bucket models.

8.0. RELATIONSHIP BETWEEN NDVI AND SURFACE HYDROLOGY IN EUROPE

8.1. Introduction

In order to assess the viability of using satellite-derived vegetation indices for monitoring drought conditions, this study analyzes the three datasets described in the previous chapter, which includes NDVI, soil moisture and precipitation data for the period between 1982 and 1990, and for the European region (latitude ranging from 30.5 N to 89.5 N; longitude ranging from 14.5W to 59.5E). With the intent to evaluate to which extent the relationship between NDVI and surface hydrology vary with latitude, five homogeneous regions were identified (Figure 8.1) and will be referred in this report as 'South Portugal', 'South Spain', 'North Spain', 'South England' and 'Ireland'. The criteria used for this purpose considered climatological characteristics and patterns of vegetative cover (making use of vegetation classification maps). It should be mentioned that, due to the low resolution of the dataset (1°x1°), the delimitation may have not been completely precise.

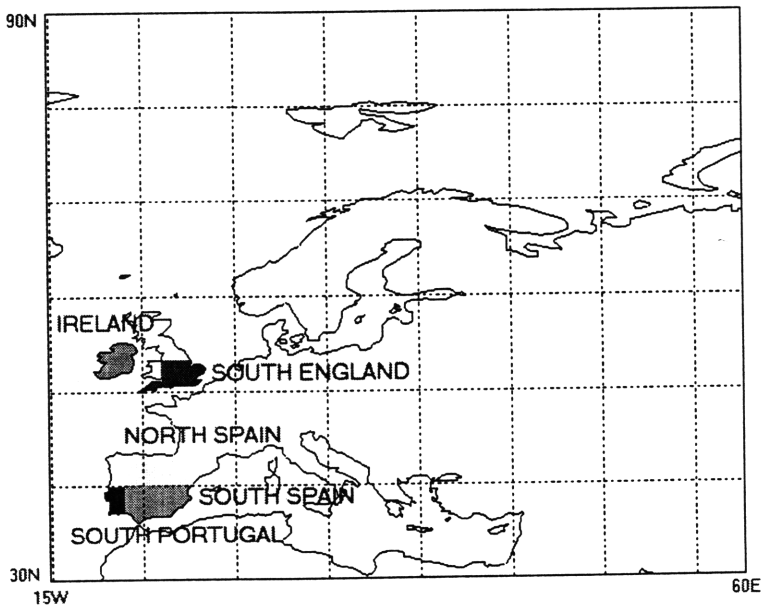

Figure 8.1: Homogeneous areas in Europe (isotropic map) used in the study

Due to the inconsistency of the spatial resolution of the different datsets, it was necessary to re-grid the soil wetness and precipitation data. This procedure, as well as all the processing and visualization procedures, were handled in IDL (Interactive Data Language), version 5 (Appendix). Bilinear interpolation was applied to the 2^{o}x2.5^{o} data in order to produce soil wetness and precipitation data with a spatial resolution of 1^{o}x1^{o}. The seasonality as well as the spatial variability of the data was plotted and analyzed.

8.2. Spatial and temporal distribution of NDVI, soil wetness and precipitation

The NDVI dataset used in this study shows a high spatial variability, increased when comparing inland and coastal areas. In general, the regions of greatest increase in NDVI are inland from the oceans (Figure 8.2), except the very high latitudes where, in general, not much variation is observed seasonally. On the other hand, higher temporal variability occurs at the lowest latitudes, which according to Soloman and Cramer (1988) can be explained with the fact that the sensitivity of plants and plant communities to interannual variations is inversely related to latitude, with plants at higher latitudes, which experience the greatest climatic variation, being the most plastic in their environmental requirements, and hence more insensitive to weather and climate extremes. This occurs because, in general, at the lower latitudes there is always enough warmth for routine growth, and hence precipitation and soil moisture are critical as limiting factors.

In Figure 8.2 is represented the spatial distribution of NDVI, over Europe, for the months of January and August of 1988. This was a particularly dry year and that is reflected in the vegetation distribution and in the NDVI index. Note that in the South of Europe even during the driest period (summer) high values in NDVI are observed, as in the Iberian Peninsula, and in some areas this index seems to increase in comparison with the values registered in January. This is most probably the result of the bright reflectivity of sands and soils in sparsely vegetated regions, that show up due to the arid conditions. This situation highlights one of the limitations of the normalized difference vegetation index, which results from high contamination of the index by soil background signal.

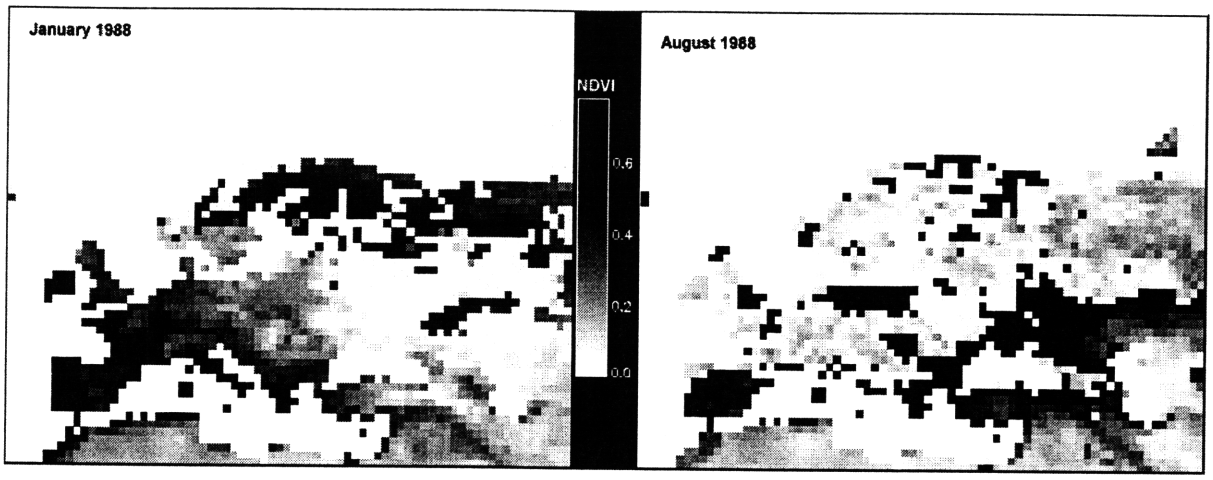

Figure 8.2: Example of NDVI data over Europe: January 1988 and August 1988

As observed by Los (1998), who analyzed the same NDVI dataset used in this study, the decrease in NDVI values between May and October in southern Europe is smaller than the increase in NDVI values in the northern Europe for those months, reflecting a smaller seasonality of vegetation in the southern Europe. Several areas show higher values in winter than in summer, specially in southern Portugal and southern Spain. These areas have climates with moderate to high temperatures throughout the year and receive most of their rainfall during winter.

The space-temporal relationship between NDVI and soil wetness, and between NDVI and precipitation, seem not to show any particular trend for the most part of the year. However, in the warmer months, such as June, July, August, and September, it is possible to observe a rapid increase of NDVI, responding to small increases of soil wetness until a threshold value of water availability is achieved. In fact, NDVI seems to exhibit a 'saturation' response to soil wetness, leveling as soil wetness increases and being relatively constant after a certain threshold value of soil wetness is reached. This relationship is also observed for rainfall, although in a less pronounced way. According to Nicholson et al. (1990), the most likely reason for this is found in the relationship between NDVI and vegetation growth, which is also exponential, NDVI, which is strongly related with the physiological capacity of plant canopy increases in proportion to leaf area index until some threshold value of NDVI (and canopy density) is reached. Above that, NDVI is relatively constant because the maximum photosynthetic capacity is attained even though

growth may continue. In fact, as the canopy density increases, additional growth contributes progressively less to the photosynthetic process because leaves that are lower in the canopy receive a continually diminishing amount of PAR. A point of saturation is reached such that PAR absorption, and therefore vegetation index, are constant while leaf are index increases. Nicholson et al. (1990) argues that, consequently, NDVI might be a sensitive indicator of rainfall of rainfall in drier regions but not humid ones and might potentially serve as an indicator of abnormally dry conditions but not wet ones. Studies have suggested that, for rainfall, the values above which NDVI is insensitive to rainfall fluctuations, for arid regions such as the Sahel, appear to lie at approximately 1000-1100 mm per year. However, the slope of association between NDVI and vegetation varies with plant formation as a consequence of differences in the rate of growth, or primary productivity, per unit rainfall.

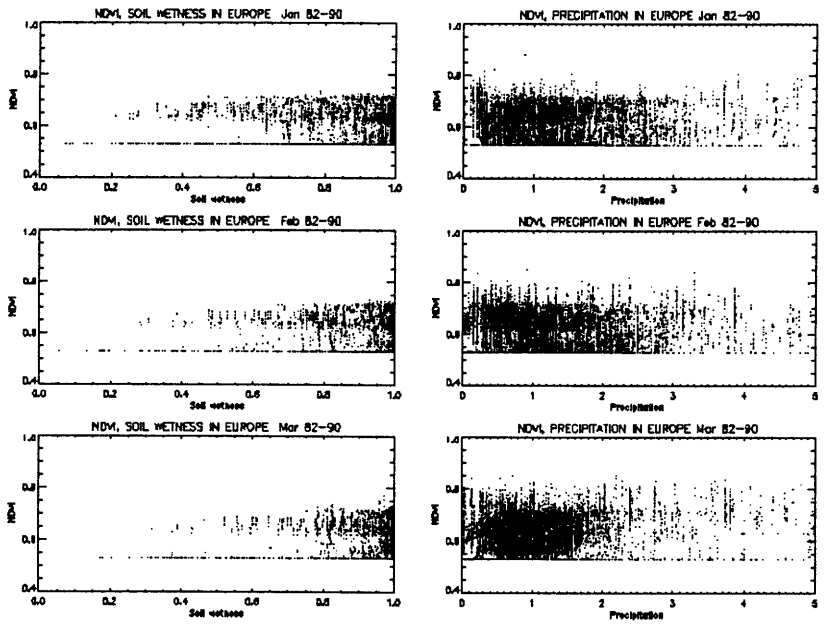

Figure 8.3a: Relation between NDVI and soil wetness, and NDVI and precipitation for the first three months of the period 1982-1990.

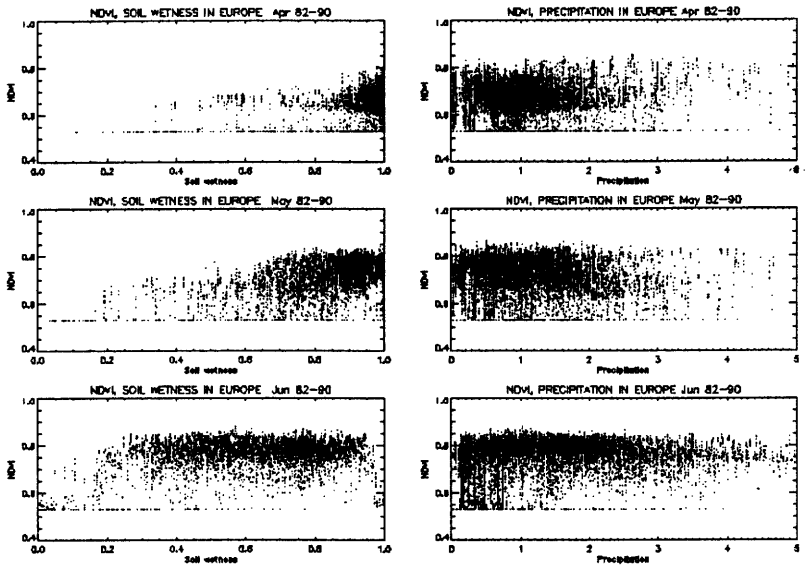

Figure 8.3b: Relation between NDVI and soil wetness, and NDVI and precipitation for the second three months of the period 1982-1990.

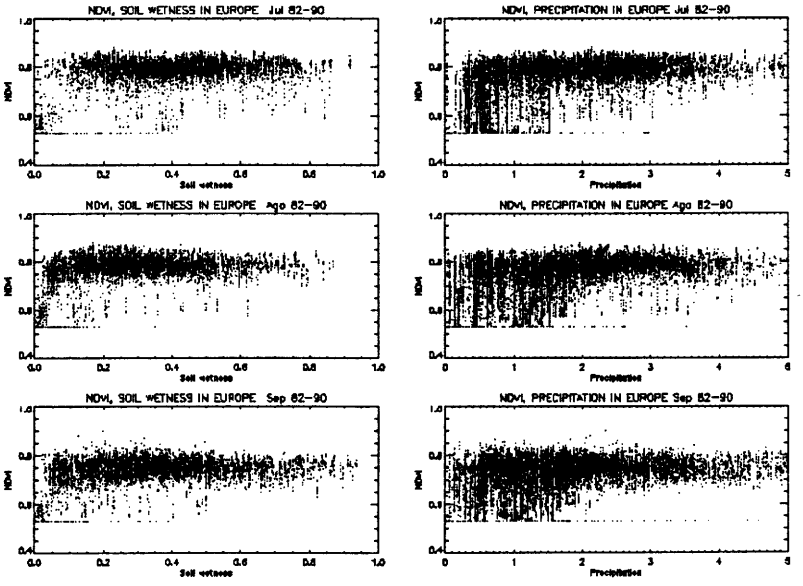

Figure 8.3c: Relation between NDVI and soil wetness, and NDVI and precipitation for the third three months of the period 1982-1990.

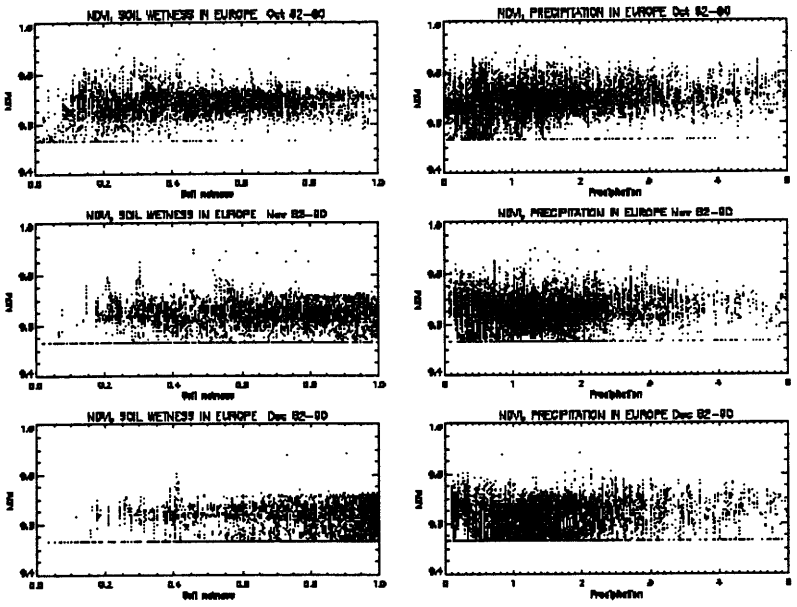

Figure 8.3d: Relation between NDVI and soil wetness, and NDVI and precipitation for the fourth three months of period between 1982-1990.

The NDVI, soil wetness and precipitation data were averaged over the growing season, i.e. from May to October, and plotted (NDVI *versus* soil wetness, and NDVI *versus* precipitation). The results (Figure 8.4) better illustrate the threshold value behavior explained before. One could say that, in this case, the soil moisture threshold lies somewhere between 0.2 and 0.3, and for precipitation around 1 mm/day. The maximum signal capture by the remote sensing system produces values of NDVI not superior to 0.7, which corresponds to heavily vegetated surfaces, and the lower values lie slightly above 0.4.

Concerning the soil moisture and precipitation data, the average in mostly clustered, in the first case, between 0.3 and 0.5, and in the second case between 1.0 and 2.5 mm/day.

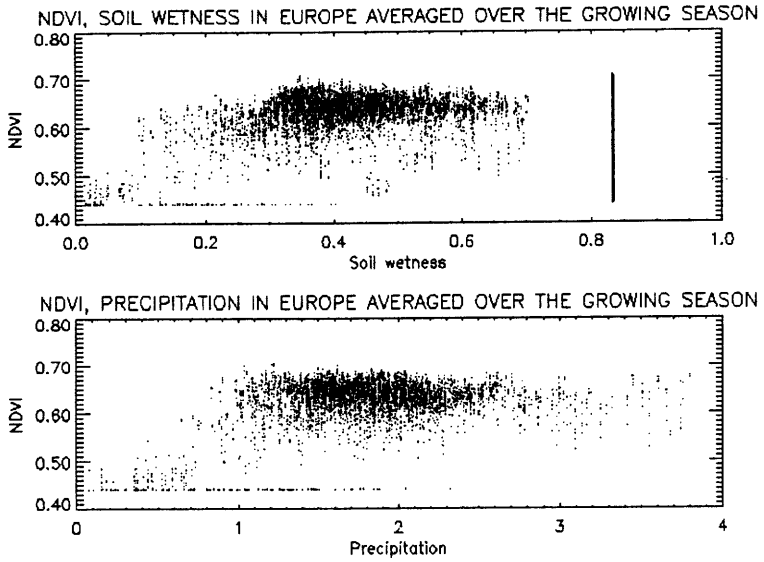

Figure 8.4: NDVI, soil wetness and precipitation averaged over the growing season (May to October) in Europe

The result of the analysis, for each of the five homogeneous areas, shows clear differences in the seasonal amplitude, for different latitudes, of the NDVI data, as well as for soil moisture and precipitation data. In South Portugal and South Spain the oscillation in the NDVI lies in a short interval between 0.65 and 0.75 for the all period between 1982 and 1990. In both cases NDVI seems to follow from close the behavior of the soil moisture, more than precipitation. Note however that, in years where it is observed an abnormal increase of on precipitation and an increase of water available in the soil, the NDVI does not drop out of its normal amplitude of its oscillation, which suggests that water at that point is not a limitation for the photosynthetic activity. At such latitudes, availability of water varies significantly from saturated conditions (soil wetness=1.0) to null soil wetness values. Such huge seasonal amplitude, observed in Figure 8.5 and Figure 8.6, would make us expect to observe also variations in NDVI with a similar amplitude, which is not the case. This can be, in part, explained by the presence of bare soils which reflectance may interfere in the capture of the signal, misleading the interpretation of the results and the final NDVI value.

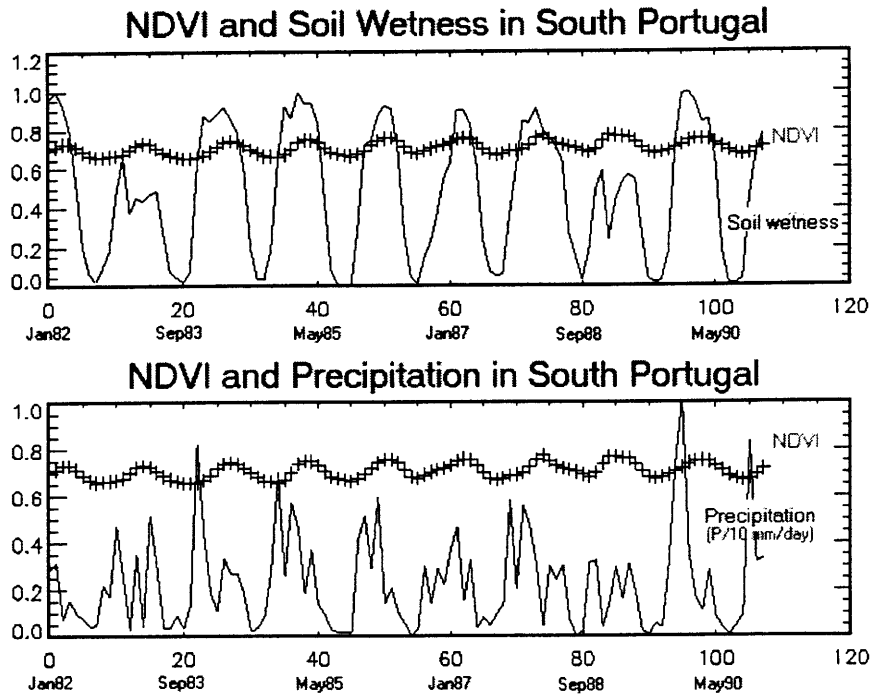

Figure 8.5: Seasonality of NDVI, soil wetness and precipitation in the South of Portugal

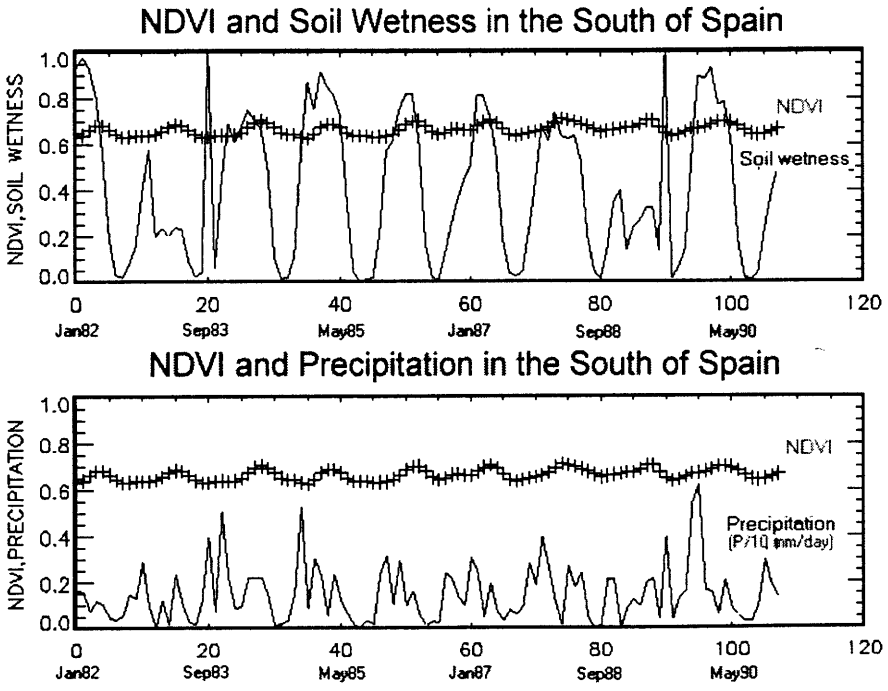

Figure 8.6: Seasonality of NDVI, soil wetness and precipitation in the South of Spain

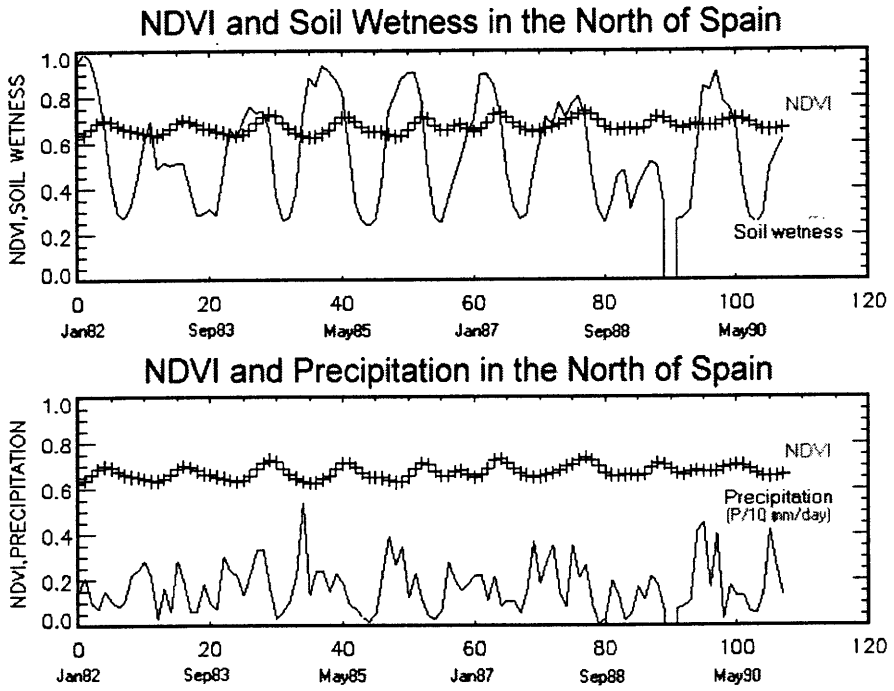

Figure 8.7: Seasonality of NDVI, soil wetness and precipitation in the North of Spain

In North Spain, NDVI seasonality shows a short amplitude, as in the cases described before, although in this case NDVI values are, in general, lower than 0.7. Figure 8.7 suggests a decrease in the amplitude of that oscillation in the most recent years of the study, which is also observed in the South England plot (Figure 8.8), and Ireland plot (Figure 8.9). In the former case it is simultaneously observed an increase in the temporal amplitude of the seasonal cycle. This may denote a change in photosynthetic activity, and eventually changes in the length of the active growing season (period during which photosynthesis actually occurs). Myneti et al. (1997) argue that there is evidence, from satellite data, that photosynthetic activity of terrestrial vegetation increased from 1981 to 1991 in a manner that is suggestive of an increase in plant growth associated with a lengthening of the active growing season. They also mention that the regions exhibiting the greatest increase lie between 45° and 75°N where marked warming has occurred in the spring time due to an early disappearance of snow. The satellite data are concordant with the increase in amplitude of seasonal cycle of atmospheric carbon dioxide exceeding 20% since the early 1970s, and an advance of up to seven days in the timing of the drawdown of CO_2 in

spring and early summer. However, due to the short period of time considered in this study, it is not advisable to conclude about any possible trend in this respect.

The soil moisture dataset shows, in general, some perturbations in its regular cycle and amplitude around the years of 1987 and 1988, with abnormally low values been observed (computed, in the case of soil wetness). This is consistent with the conditions of less precipitation and drought observed in 1988. According to Zhang and Randall (1997), both the summer average and the annual mean show dry soil for 1988, being the drought more intensive during the summer.

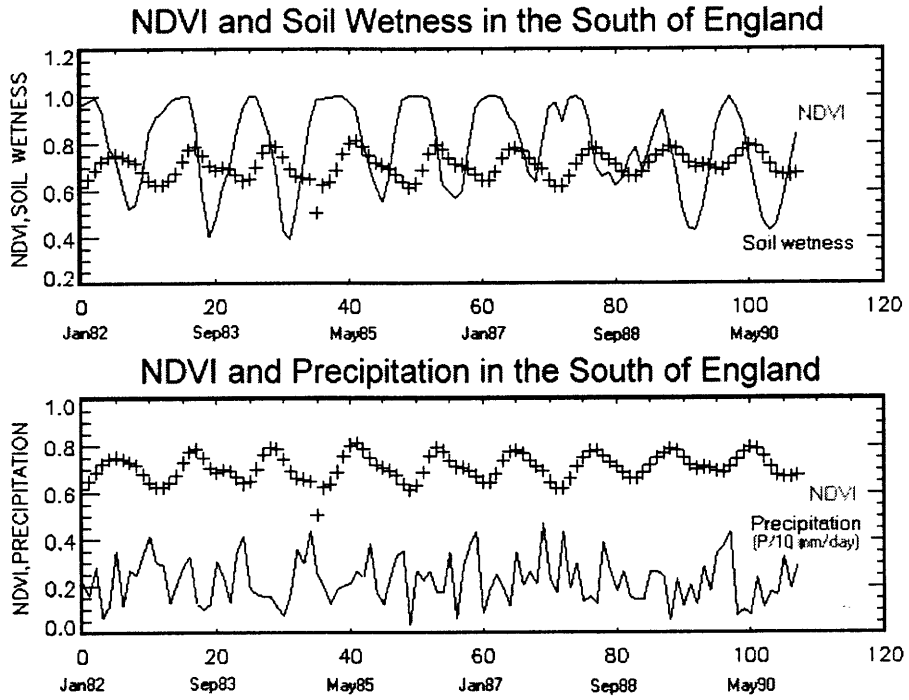

Figure 8.8: Seasonality of NDVI, soil wetness and precipitation in the South of England

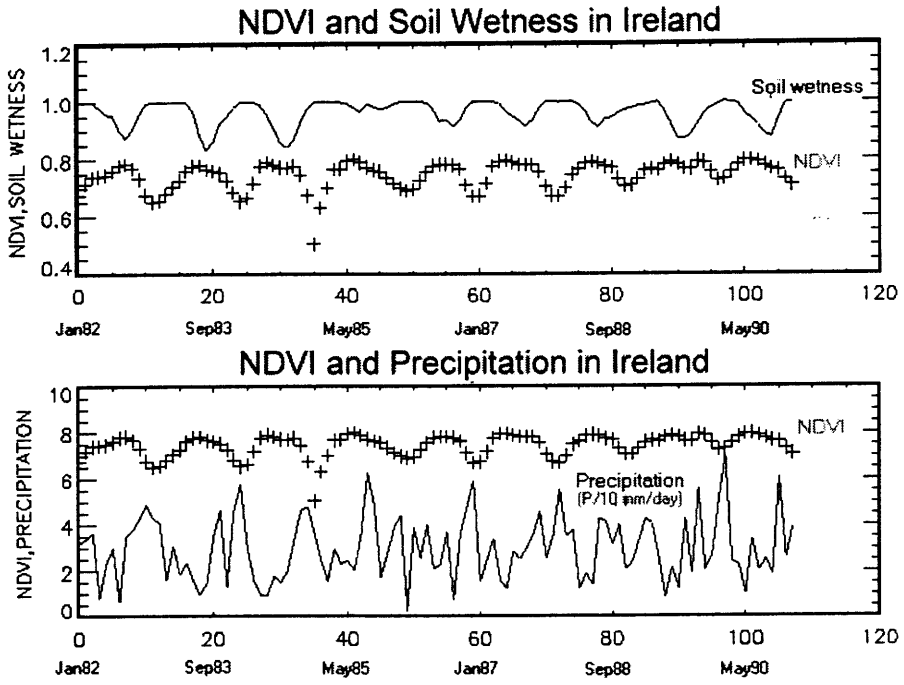

Figure 8.9: Seasonality of NDVI, soil wetness and precipitation in Ireland

In the Ireland plotted dataset, probably the most notable feature is the low amplitude of soil moisture seasonal variation. In fact, in the period between the end of 1984 and mid 1986 Figure 8.9 shows almost no variation at all in the plotted data. In general, the values are constrained between an upper boundary, at the saturation level (soil wetness equals one), and approximately 0.85. This may be the result of limitations in the computational procedure of soil moisture. As mentioned before, the model used has shown not to be able to simulate properly the winter soil moisture variations at higher latitudes, keeping soil moisture approximately constant. Consequently, the model does not capture the full range of interannual variations of hydrology observed in the field.

In South England, the same upper saturated limit, in soil moisture variation, is frequently observed along the time series considered in this study. However, the amplitude of the oscillation is much higher than in Ireland, and values in he soil moisture can be as low as 0.4. From 1985 to 1989 it is observed a decrease in this oscillation more evident around 1988, which probably

reflects the drought conditions of 1988. The precipitation data, in these two areas, seems to have a similar seasonal pattern, although the amplitude of the oscillation in Ireland is higher.

8.3. Looking at anomalies in NDVI, soil wetness and precipitation

The deterministic seasonality of the three datasets was removed by calculating the anomalies, for each month, for the whole region (Europe) and the five considered homogeneous areas. The anomalies were calculated by subtracting from each value (for each dataset) the correspondent mean for that month in the nine years (1982-1990) of that dataset, and dividing the difference by the standard deviation of the sample (σ_{month}) for that month. This procedure can be formulated as follows:

$$Anomalies = \frac{X_{month,year} - \overline{X}_{month}}{\sigma_{month}} \qquad (8.1)$$

The anomalies dataset allows, in a better way, to correlate the patterns, if any, of covariance of the different parameters. In general, it is observed that NDVI and soil moisture vary along more closely than NDVI and precipitation. In the last relationship it is observed a lag in the response of NDVI, which appears to be related to the fact that vegetation does not respond directly to rainfall, but rather to soil moisture, which is a multi-month integral of rainfall. Another general feature of the data is the decrease of NDVI to negative values in areas where moisture is a limiting factor and when it is observed a reduction in rainfall.

Figure 8.10 presents the covariance of NDVI, soil wetness and precipitation anomalies in South of Portugal and it shows that for the most part of the time series from 1982 to 1990, soil moisture and NDVI anomalies have a quite similar pattern of variation, being the similarities intensified from 1986 to 1988. Around 1988, however, it is observed that NDVI goes in the opposite direction of soil moisture, as well as precipitation, which, as explained before, results most likely from the fact that soil background shows through canopy andalbedo is affected by the exposed soil in very dry years. This phenomena is also observed in all the other areas of study.

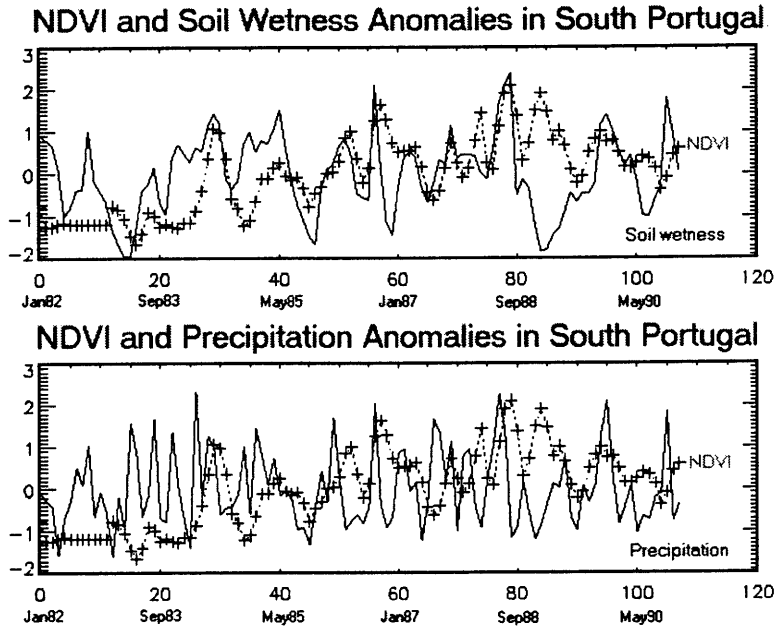

Figure 8.10: NDVI, soil moisture and precipitation anomalies in South Portugal

It is also observed that, in general, the boundaries of the oscillation of the anomalies, for the three parameters considered, are quite similar for the five areas. As mentioned before, NDVI anomalies tend to respond to precipitation anomalies with some lag, and that behavior can also be observed in all five areas studied.

Figure 8.10 through Figure 8.14 suggest a general positive trend in the NDVI anomalies, with higher magnitudes in the NDVI anomaly values being observed in the most recent years of the dataset timeseries. The plots of the data suggest that this apparent trend does not appear to occur in the other parameters. Particularly in the case of precipitation anomalies, it seems that the upper and lower limits of distribution of this data remains quite uniform along the period studied, although in South Spain there is an increase in this oscillation between 1988 and 1990.

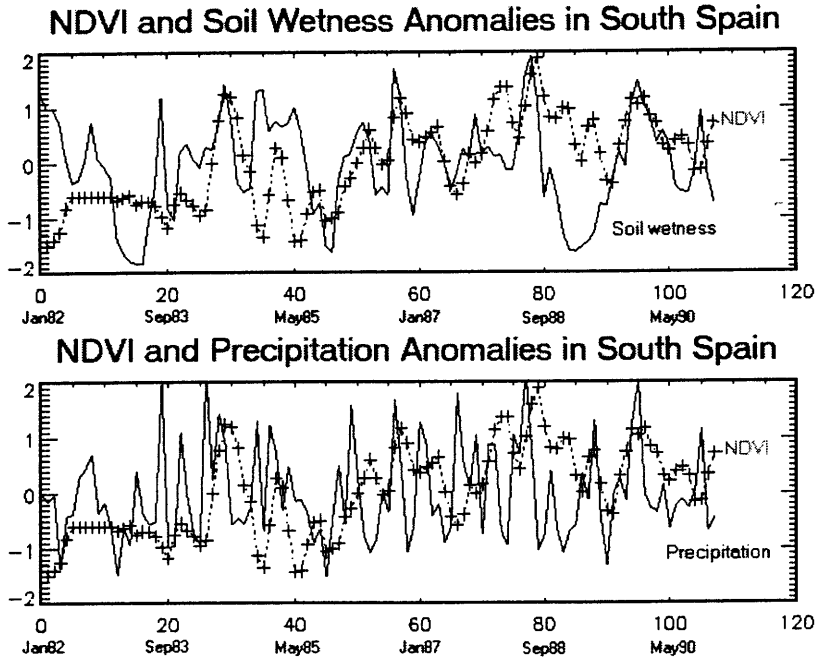

Figure 8.11: NDVI, soil moisture and precipitation anomalies in South Spain

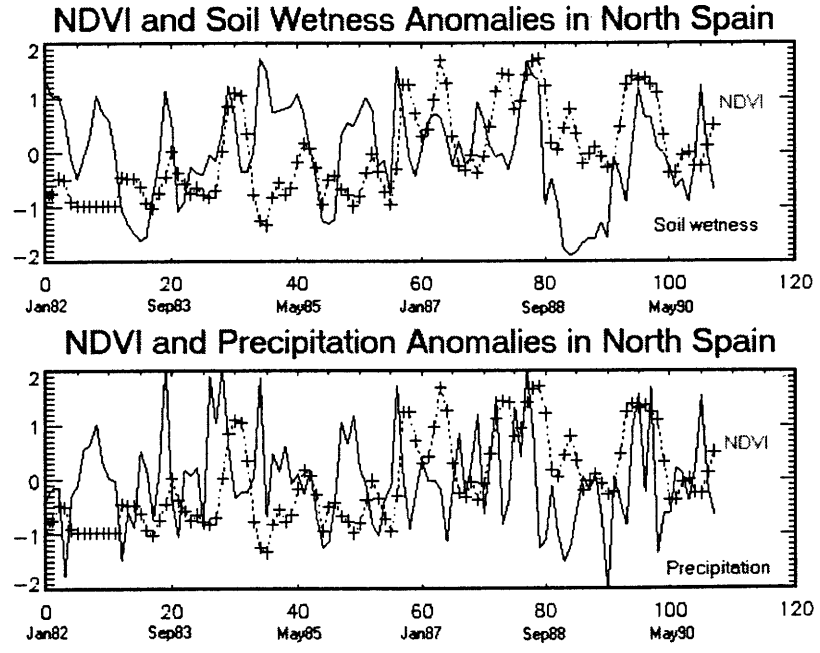

Figure 8.12: NDVI, soil moisture and precipitation anomalies in North Spain

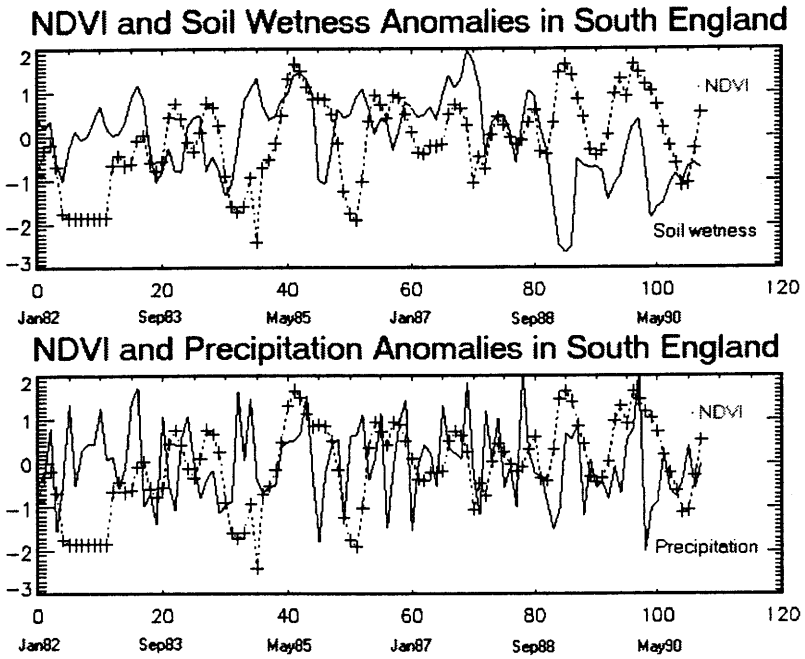

Figure 8.13: NDVI, soil moisture and precipitation anomalies in South England

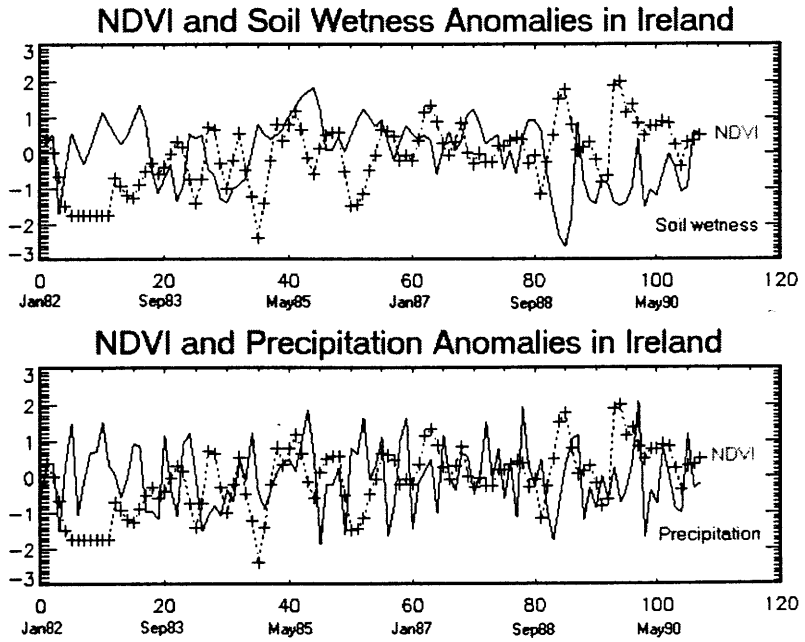

Figure 8.14: NDVI, soil moisture and precipitation anomalies in Ireland

8.4. Correlation between NDVI, soil moisture and precipitation

For the area of Europe (including the five homogeneous areas) the linear correlation between monthly NDVI and soil moisture, and NDVI and precipitation, was calculated. The correlation was assessed for concurrent monthly values of soil wetness, NDVI and precipitation, and for one-, two-, three-, four- and five-previous months. The routine

Table 8.1: Correlation coefficients between NDVI, soil wetness and precipitation data

CORRELATION COEFFICIENT (r)					
NDVI and soil wetness					
Area	**South Spain**	**North Spain**	**South Portugal**	**South England**	**Ireland**
0 month	0.1432	0.0737	0.2124	-0.1619	-0.3483
1 month	0.1514	0.0788	0.2126	-0.1580	-0.3528
2 month	0.1528	0.0788	0.2089	-0.1596	-0.3570
3 month	0.1552	0.0832	0.2140	-0.1681	-0.3549
4 month	0.1550	0.0828	0.2132	-0.1821	-0.3609
5 month	0.1578	0.0836	0.2147	-0.1883	-0.3599
NDVI and soil precipitation					
Area	**South Spain**	**North Spain**	**South Portugal**	**South England**	**Ireland**
0 month	0.1039	-0.0697	-0.0047	-0.0154	-0.0889
1 month	0.1088	-0.0654	-0.0024	-0.0152	-0.0889
2 month	0.1125	-0.0651	0.0016	-0.0169	-0.0863
3 month	0.1154	-0.0613	0.0030	-0.0155	-0.0923
4 month	0.1155	-0.0607	0.0026	-0.0189	-0.0961
5 month	0.1168	-0.0606	0.0029	-0.0230	-0.0933

CORRELATION, used in IDL, calculates the Pearson correlation coefficient, assuming that the two variables are independent, i.e., knowledge of the value of one variable provides no information about the value of another variable. The correlation between two variables reflects the degree to which the variables are related, and in the Perason's coefficient of correlation (r) reflects the degree of linear relationship between those variables. It ranges from -01 and +1. A correlation of +1 means that there is a perfect positive linear relationship between the two

variables. Considering that the sample contain 108 monthly values, correlations higher than 0.19 are associated with a level of significance of 0.05, and correlations with a magnitude higher than 0.16 have a statistical significance of 90%.

The coefficients of correlation show that the correlation is higher between NDVI data and soil wetness data than between NDVI data and precipitation data. The magnitude of the correlation between NDVI and soil moisture seems not to increase with lag (Figure 8.15), which supports the idea that vegetation responds immediately to that parameter. Higher positive correlations between NDVI and soil moisture are observed at lower latitudes, such as in south Portugal and south Spain, as expected, since there water tends to be a limiting factor for plant growth. In South Portugal the statistical significance of the correlation found is of 95%. At higher latitudes correlations tend to be lower. However, for Ireland a negative correlation with high magnitude was observed, intuitively not expected, and which may reflect errors in the dataset.

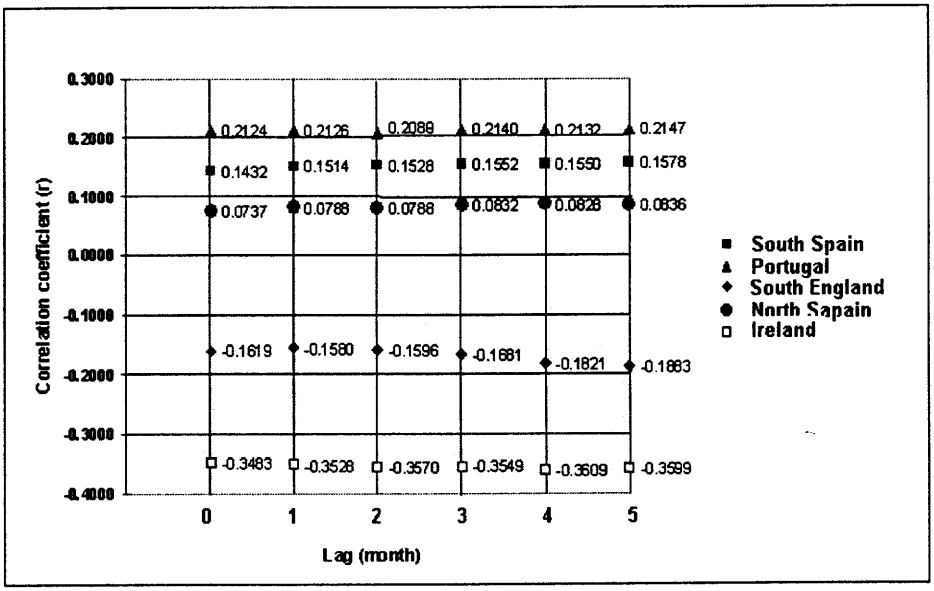

Figure 8.15: Coefficients of correlation between NDVI and soil wetness anomalies

The magnitude of the correlations between NDVI and precipitation, for the different homogeneous areas, tend to increase with lag in time. However, all correlations observed show a low significance. Higher correlation coefficients are registered in South Spain.

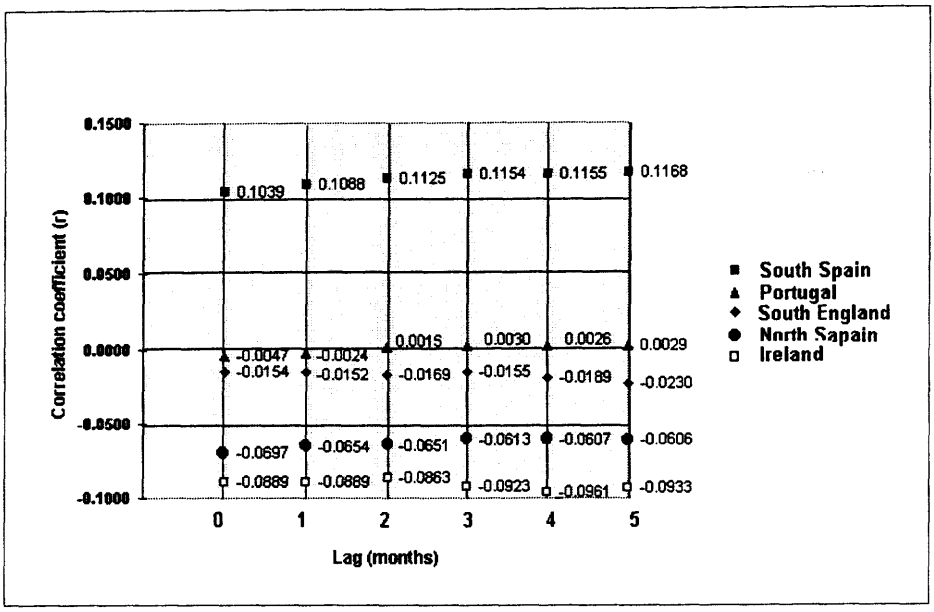

Figure 8.16: Coefficients of correlation between NDVI and precipitation anomalies

Correlation coefficients were also calculated for the global area of study, i.e. Europe, in a pixel-by-pixel basis, between NDVI and soil wetness anomalies, and between NDVI and precipitation anomalies, averaged over the growing season (from May to October). The results are graphically displayed in Figure 8.17 and are consistent with what was inferred based on the study of the five individual areas, supporting the hypothesis of higher correlation between NDVI and surface hydrology parameters, being found at lower latitudes, where water more than light, tends to be a limiting factor for biomass production an photosynthesis. Moreover, the upper limit of the magnitude of the correlations between NDVI and soil wetness (r=0.984), for the all area, is higher than the correlation coefficient obtained for NDVi and precipitation (r=0.910). However, Figure 8.17 suggests that, in the vicinities of the Black Sea, particularly in the northern part, NDVI and precipitation seem to be more correlated (in a positive way) than NDVI and soil moisture.

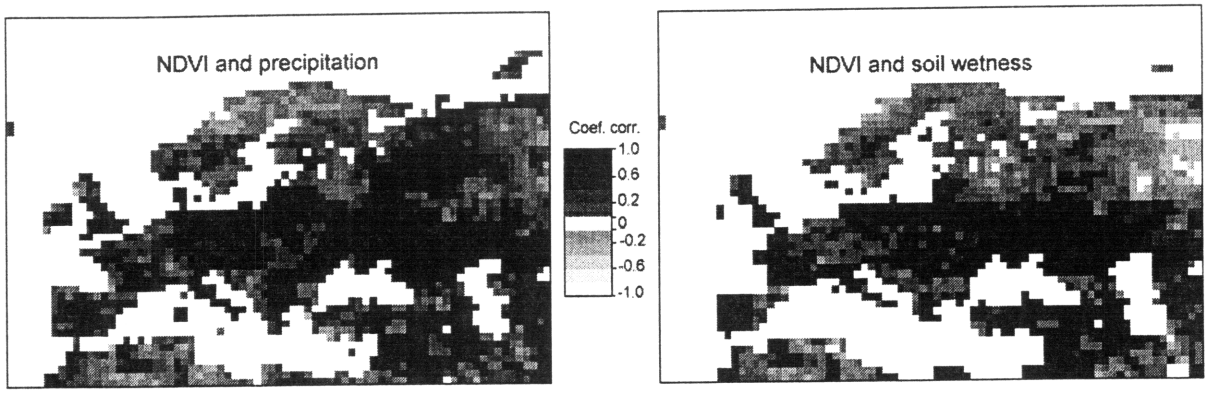

Figure 8.17: Pixel-by-pixel correlation between NDVI, precipitation, and soil moisture anomalies averaged over the growing season

Since data was averaged over the growing season, the correlation coefficient was calculated based on a sample with a size of nine observations. Therefore, the statistical significance of the correlation is of 95% in the cases were correlation coefficients are higher than 0.66, which can be observed over large areas in the Mediterranean Europe

9.0. CONCLUSIONS

Five areas, considered homogeneous in terms of climatological and vegetative patterns, were identified in Europe in order to study the relationship between NDVI and surface hydrology parameters at different latitudes. Correlations were assessed for concurrent monthly values of soil moisture and NDVI, and NDVI and precipitation, and for one-, two-, three-, four- and five-previous months values. The results suggest some consistency, being the correlations found higher for areas at lower latitudes, either when comparing NDVI and soil moisture data, as in the case of the study of the correlation between NDVI and precipitation data. The study demonstrated that there is no significant statistical association between precipitation and NDVI for the datasets used. However, the mean spatial patterns of NDVI and soil moisture variables are quite similar. This behavior is evident in South Portugal where soil wetness and NDVI anomalies covariation follows similar patterns. However, around 1988, it is observed that NDVI goes in the opposite direction of soil moisture, as well as precipitation, which, results most likely from the fact that soil background shows through very dry canopy and albedo is affected by the exposed soil, consequently misleading the calculation of the NDVI value. This phenomena is also observed in all the other areas of study and reflects a limitation of the NDVI index itself.

The magnitude of the correlation between NDVI and precipitation anomalies tends to increase when plotted with some months of lag, and higher values are observed, in general, with 3 to 5 months lag. That appears to relate to the fact that the vegetation does not respond directly to rainfall, but rather to soil moisture, which is a multi-month integral of rainfall

The anomalies of NDVI and soil wetness indices are significantly correlated over South Portugal (>95% confidence) and South Spain (>90% confidence) regions. In Ireland a negative correlation with high magnitude was observed, intuitively not expected, and which may reflect errors in the soil moisture dataset.

One should be cautious in extrapolating the results of this study due to the limitations inherent to the datasets used, particularly with the soil moisture data. In fact, several handicaps have been identified in the model used to compute the soil moisture, and

therefore soil wetness. It has been shown that the model is not capable to capture variations in soil moisture at high latitudes, specially under winter conditions. Moreover, the NDVI index still have to deal with some misleading factors. Additionally, cumulative errors are expected to have occurred in the processes of interpolation and re-grid of the soil wetness and precipitation data, inhibiting a correct parameterization of the real surface hydrologic conditions of the areas.

Therefore, it is suggested the need for future studies making use of more reliable data, and eventually, higher spatial and temporal resolution in order to evaluate the extent of influence of the scale effects. The new instruments, such as the EOS instrumentation, namely the Moderate-resolution Imaging Spectroradiometer (MODIS), whose high spatial resolution products will be available in the very near future, are expected to play an important role in the better understanding of the linkages between biosphere and hydrology, and consequently in the prediction of extreme climatological events such as drought conditions. Moreover, although NDVI has demonstrated to play a valuable role in the monitoring of vegetation, at the global scale, its use as an indicator of drought conditions is still constrain by limitations inherent to the index itself. The main limitation is due to soil background signal contamination inhibiting the correct monitoring of stressful conditions for plants, which suggests the need to improve algorithms capable of correcting the soil interference.

REFERENCES

Anyamba, A., and Eastman, R. (1996). Interannual variability of NDVI over Africa and its relation to El Nino/Southern Oscillation. *Int. J. Remote Sens*, **17**, 2533-2548 (Cited in Los, 1998).

Asrar, G., Fuchs, M., Kanemasu, E.T., and Hatfield, J.L. (1984). Estimating absorbed photosynthetic radiation and leaf area index from spectral reflectance in wheat. *Agron. J.*, **76**, 300-306. (Cited in Walter-Shea et al., 1997).

Bastiaanssen, W.G.M., van der Hurk, B.J.J.M., and Pelgrum, H. (1997). A new approach for updating soil moisture in meteorological models by surface energy partitioning indicators. In: *Proc. 13th Conference on Hydrology.* American Meteorological Society. Long Beach, California, February 2-7.

Bormann, G.B., and Likens, G.E. (1979). *Pattern and process in a forested ecosystem.* New York, Springler-Verlag (Cited in Shugart, 1988).

Charney, J., Stone, P.H., and Quirk, W.J. (1975). Drought in the Sahara: A biogeophysical feedback mechanism. *Science.* **187**, 434-435 (Cited in Los, 1998).

Charney, J., Quirk, W.J., Chow, S.H., and Kornfield, J. (1977). A comparative study of the effects of albedo change on drought in semi-arid regions. *J. Atmos. Sci*, **34**, 1366-1385 (Cited in Los, 1998).

Conway, E.D. (1997). *An Introduction to Satellite Image Interpretation* The Maryland Space Grant Consortium, John Hopkins University Press.

Coombs, J., Hall, D.O., Long, S.P., and Scurlock, J.M.O. (Eds.) (1985). *Techniques in Bioproductivity and Photosynthesis.* Pergamon Press, Oxford, 298 pp.

Crist, E.P., and Cicone, R.C. (1984). A physically-based transformation of ThematicMapper data - the TM tasseled cap. *IEEE Trans.*, **GE-22**, 256-263 (Cited in Towshend et al, 1993).

Davis, S., Landgrebe, D, Phillips, T., Swain, P., Hoffer, R., Lindenlaub, J., and Silva, L. (1978). *Remote Sensing: the quantitative approach.* Philip H. Swain and Shirley M. Davis (Eds.) McGraw-Hill, 396 pp.

Dickinson, R.E. (1984). Modeling evapotranspiration for three-dimensional global climate models. *Climate Processes and Climate Sensitivity, geophysical monograph,* **29**, J.E. Hansen and T. Takahashi (Eds). Amer. Geophys. Union, Washington DC, 58-72 (Cited in Los, 1998).

Drury, S.A. (1990). *A Guide to Remote Sensin : Interpreting images of the Earth.* Oxford University Press, Oxford.

Eidenshink, J.C.,and Faundeen, J.L. (1997). The 1-km AVHRR Global Land Data Set: First Stages in Implementation. Available at the URL: http://edcwww.cr.usgs.gov/landdaac/1km/paper.html#bands1.

Entekhabi, D., Rodriguez-Iturbe, I., and Bras, R.L. (1992). Variability in large-scale water balance with land surface-atmosphere interaction. *J. Clim.*, **5**, 798-813.

Field, C.B., Stuart Chapin III, F., Matson, P.A., and Mooney, H.A. (1992). Responses of terrestrial ecosystems to changing atmosphere. *Ann. Rev. Ecol.Syst.*, **23**, 201-235.

Friend, A.D. (1988). The prediction and physiological significance of tree height. In: *Vegetation dynamics and globalcChange*. Allen M. Soloman and H. H. Shugart (Eds). Chapman&Hall, NY, 338 pp.

Fung, I.Y., Tucker, C.J. and Prentice, K.C. (1987). Application of Advanced Very High Resolution Radiometer Vegetation Index to study atmosphere-biosphere exchange of CO_2. *J. of Geophys. Res.*, **92**, NO.D3, 2999-3015.

Gallo, K.P.,Daughtry, C.S.T., and Bauer, M.E. (1985). Spectral estimation of absorbed photosynthetically active radiation in corn canopies. *Remote Sens. Environ.*, **17**, 221-232 (Cited in Walter-Shea et al., 1997).

Gausman, H.W. (1985). *Plant leaf optical properties in visible and near-infrared light.* Texas Tech University. Graduate studies No. 29. 78 pp.

GCRIO (1998). Our changing planet FY 1998. Available at the URL: http://www.gcrio.org/ocp98/ch2.html#seasonal.

Holben, B.N., Tucker, C.J., and Fan, C. (1980). Spectral assessment of soybean leaf area and leaf biomass. *Photogramm. Eng. Rem. Sens.*, **46**, 651-656 (Cited in Walter-Shea et al., 1997).

Huete, A.R. (1987). Soil-dependent spectral response in the developing plant canopy. *Agron. J.*, **79**, 61-68.

Johannsen, G.J. (1969). *The detection of available soil moisture by remote sensing techniques.* Ph.D. Thesis, Purdue Univeristy. 266 pp (Cited in Gausman, 1985).

Kogan, F.N. (1997). Global drought watch from space. *Bulletin of American Meteorological Society*, **78**, NO.4, 621-636.

Koster, R.D. and Suarez (1995). Relative contributions of land and ocean processes to precipitation variability. *J. of Geophys. Res.*, **100**, NO.D&, 13775-13790.

Kramer, P.J. (1983). *Water Relations of Plants*. Academic Press. NY, 489 pp.

Los, S., Justice, C., and Tucker, C.J. (1994). A 1° x 1° global NDVI data set for climate studies derived from the GIMMS continental NDVI data. *Int. J. Remote Sen.*, **15**, 3493-3518.

Los, S.O. (1998). *Linkages between global vegetation and climate: An analysis based on NOAA Advanced Very High Resolution Radiometer data*. Ph.D. Dissertation Vrije

Universiteit Amsterdam. NASA-CASI, Hanover, 7121 Standard Drive, Maryland 21076-1320, NASA Report GSFC/CR-1998-206852, ISBN 0-16-049527-X, 199 pp.

Martin, P. (1988). Coupling of the atmosphere with vegetation. In*: Vegetation dynamics and global change*. Allen M Soloman and Herman H. Shugart (Eds.). Chapman&Hall, NY, 338 pp.

Matthews, E. (1983). Global vegetation and land use: new high-resolution data bases for climate studies. *J. of Clim. and Appl. Meteor.* , **22**, 475-487.

Mintz, Y. and Serafini, Y. (1984). Global fields of monthly normal soil moisture as derived from observed precipitation and an estimated potential evapotranspiration. Final scientific report under NASA grant NAS 5-26, Part V, Dept. Of Meteorology, University of Maryland. College park, MD (Cited in Schemm et al., 1992).

Mintz, Y. and Serafini, Y. (1992). A global monthly climatology of soil moisture and water balance. *Climate Dynamics*, **8**, 13-27.

Monteith, J.L. (1972). *Survey of Instruments for micrometeorology*. IBP Handbook No.22. Blackwell Scientific Publications, Oxford (Cited in Coombs et al., 1985).

Myneni, R.B., Los, S.O., and Tucker, J.C (1995). Satellite-based identification of linked vegetation index and sea surface temperature anomaly areas from 1982-1990 for Africa, Australia and South America. *Geophys. Res. Let.,* **23**, 729-732.

Myneni, R.B., Keeling, C.D., Tucker, J.C.,Asrar, G. , and Nemani, R.R. (1997). Increased plant growth in the northern high latitudes from 1981 to 1991.*Nature*, **368**, 698-702.

Namken, L.N. (1965). Relative turgidity technique for scheduling cotton (*Gossypium hirsutum*) irrigation. *Agron. J*, .**57**,38-41 (Cited in Gausman, 1985).

Nappo, C.J. (1975). Parameterization of surface soil moisture and evaporation rate in a planetary boundary layer model. *J. Applied Meteor.*, **14**, 289-296 (Cited in Schemm et al., 1992).

NASA (1989). *From pattern to process: the strategy of the Earth Observing System*. National Aeronautics and Space Administration, Volume II, 140 pp.

Nicholson, S.E., Davenport, M.L. and Malo, A.R. (1990). A comparison of the vegetation response to rainfall in the Sahel and East Africa, using normalized difference vegetation index from NOAA AVHRR. *Climatic Change*, **17**, 209-241.

Nobre, C. Sellers, J., and Shukla, J. (1991). Amazonian deforestation and regional climate change. *Journal of Climate*, **4**, 957-988.

Privette, J.L., Emery, W.J., and Schimel, D.S. (1986). Inversion of a Vegetation reflectance model with NOAA AVHRR data. *Remote Sen. Environm.*, **58**, 187-200.

Robock, Alan, Schlosser, A., Vinikov, K., Speranskaya, N., and Entin, K. (1997). Evaluation of AMIP soil moisture simulations. Submitted to Global and Planetary Change. Available at the URL: http:metosrv2.umd.edu/~alan/amipsm#table1.

Rock, B.N., Skole, D.L., and Choudhury, B.J.(1988). Monitoring vegetation change using satellite data. In: *Vegetation Dynamics and Global Change*. Allen M Soloman and Herman H. Shugart (Eds.). Chapman &Hall, NY, 338 pp.

Rodriguez-Iturbe, I., Entekhabi, D. , and Bras, R.L. (1991). Nonlinear dynamics of soil moisture at climate scales, 1, Stochastic analysis. *Water Resour. Res.,* **27**, 1899-1906.

Schemm, J., Schubert, S. , Terry, J., and Bloom, S. (1992*). Estimates of monthly mean soil moisture for 1979-1989*. NASA Technical Memorandum 104571. National Aeronautics and Space Administration. Goddard Space Flight Center. Greenbelt, Maryland. October 1992.

Scott, R., Koster, R., Entekhabi, D., and Suarez, M. (1995). Effect of canopy interception reservoir on hydrological persistence in General Circulation Model. *Journal of Climate*, **8** , No7, 1917-1922

Scott, R., Entekhabi, D., Koster, R., and Suarez, M (1997). Timescales of land surface evapotranspiration response. *J. of Climate*, **10** , No4, 559-566.

Sellers, W.D. (1965). *Physical Climatology*. The University of Chicago Press. 272 pp. (Cited in Schemm et al., 1992).

Sellers, P.J., Mintz, Y., Sud, Y.C., and Dalcher, A. (1986). A simple biosphere model (SiB) for use with general circulation models. *J. Atmos. Sci.*, **43**, 505-531 (Cited in Los, 1998).

Sellers, P.J., and Hall, F.G. (1992). FIFE in 1992: Results, scientific gains, and future research directions. *J. Geophys. Res.*, **97**, 19091-19109.

Sellers, P.J., Los, S., Tucker, C.J., Justice, C., Dazlich, D., Collatz, G.J., and Randall, D. (1996). A revised land surface parametrization (SiB2) for atmospheric GCMs. Part II: The generation of global fields of terrestrial biophysiscal parameters from satellite data. *Journal of Climate*, **9**, No. 4, 705-737.

Sellers, P.J., Dickinson, R.E., Randall, D.A., Betts, A.K., Hall, F.G., Berry, J.A., Collatz, G.J., Denning, A.S., Mooney, H.A., Nobre, C.A., Sato, N., Field, C.B., and Henderson-Sellers, A. (1997a). Modeling the exchange of energy, water, and carbon between continents and the atmosphere. *Science*, **275**, 502-509 (Cited in Robock et al., 1997).

Sinclair, T.R. (1968). *Pathway of solar radiation through leaves.* M.S. Thesis. Purdue University, Lafayette, Indiana. 179 pp. (Cited in Gausman, 1985).

Shugart, H.H. (1988). Global change. In: *Vegetation dynamics and global change*. Allen M. Soloman and Herman H. Shugart (Eds.). Chapman&Hall, NY, 338 pp.

Soloman, A.M., and Cramer, W. (1988). Biospheric implications of global environmental change. In: *Vegetation dynamics and global change.* Allen M. Soloman and Herman H. Shugart (Eds.). Chapman &Hall, NY, 338 pp.

Steven, M.D., Biscoe, P.V., and Jaggard, K.W. (1983). Estimation of sugar beet productivity from reflection in the red and infrared spectral bands. *Int. J. Remote Sens.,***4**, 325-246.

Thomas, J.R., Myers, V.I., Heilman, M.D., and Wiegand, C.L. (1966). Factors affecting light reflectance in cotton. *Proc. 4th Symp. Remote Sensing Environ.*, Inst. of Sci. and Tech., Univ. Michigan. Ann Arbor, Michigan, 305-312 (Cited in Gausman, 1985).

Thornthwaite, C.W. (1948). An approach toward a rational classification of climate. *Geophisical Review.* **38**, 55-94 (Cited in Schemm et al., 1992).

Townshend, J. R. G., Tucker, C.J. and Goward, S.N. (1993). Global vegetation mapping *In: Atlas of the satellite observations related to global change* R.J. Curney, J.L. Foster, and C.L. Parkinson (Eds.), Cambridge Press.

Tucker, C.J. (1979). Red and infrared linear combinations for monitoring vegetation. *Remote Sensing Environment.*, **8**, 127-150.

Tucker, C.J., Townshend, and Golf, T.E. (1985a). African land-cover classification using satellite data. *Science.* **227**. 369-375.

Tucker, J.C. , Townshend, J.R.G., and Goff, T.E. (1985b). African land-cover classification using satellite data. *Science,* **227**, 369-375.

Tucker, C.J., Fung, I., Keeling, C. and Gammon, R. (1986). Relationship between atmospheric CO_2 variations and satellite-derived vegetation index. *Nature,* **319**, 195-199.

Tucker, C.J., Dregne, H.E., and Newcomb, S.D. (1991). Expansion and contraction of the Sahara desert from 1980 to 1990. *Science*, **253**, 299-301 (Cited in Los, 1998).

Tucker, C.J., Dregne. H.E., and Newcomb, W.W. (1994). AVHRR data sets for determination of desert spatial extent. *Int. J. Remote Sens.*, **15**, 3547-3565.

Turner B. L., R. H. Moss, and D.L. Skole (Eds.) (1993). *Relating land use and global land-cover change: A proposal for an IGBP-HDP core project. Report from the IGBP-HDP Working Group on Land-use/Land-cover Change.* Joint publication of the International Geosphere-Biosphere Program (Report No. 24) and Human Dimensions of Global Environmental Change Program (Report No. 5). Available at URL: http://www.ciesin.org/docs/002-105/002-105.html).

TVP (1997). The Vegetation Programme. Available at the URL: www-vegetation.cst.cnes.fr:8050/overview/intro.html.

USDOC, (1998). *NOAA Operational Environmental Satellites*. Available at the URL: http://pegasus.nesdis.noaa.gov/avhrr.html

Wallace, J. and Hobbs, P. V. (1977). *Atmospheric science: an introductory survey.* Academic Press. 467 pp.

Walter-Shea, E.A., Privette, J., Cornell, D., Mesarch, M.A., and Hays, C.J. (1997). Relations between directional spectral vegetation Radiation in Alfalfa. *Remote Sensing of the Environment.* **61**,162-177.

Xue, Y., and Shukla (1991). The influence of land properties on Sahel climate. Part I: Desertification. *J. Climate*, **6**, 2232-2245 (Cited in Los, 1998).

Zhang, C., and Randall, D.A. (1997). The simulated soil moisture budget and its sensitivity to variations of land vegetation parameters. *Proc. 13th Conference on Hydrology.* American Meteorological Society. Long Beach, California, February 2-7.

APPENDIX: IDL routines

For more information contact:

Ana Pinheiro
GASA/DCEA/FCT-UNL
2825 Monte da Caparica
Portugal

acp@mail.fct.unl.pt

- **IDL routine to transpose and rotate NDVI original array, and save it as a new file.**

Note: Similar routine was applied to all the years and months.

```
PRO correctNDVI

temp =fltarr(75,60)
alfa=fltarr(75,60)

ndvi1=fltarr(75,60)
ndvi2=fltarr(75,60)
ndvi3=fltarr(75,60)

anom1=fltarr(75,60)
anom2=fltarr(75,60)
anom3=fltarr(75,60)

loadct, 38

openr, 1, '/pamenar/u1/anap/NDVI/IDL/NDVI_anomjan82_correct'
readf, 1, temp
openr, 2, '/pamenar/u1/anap/NDVI/GSFC/fasir_eur82_1.img'
readf,2, alfa

anom1= rotate(temp, 3)
anom2=transpose(anom1)
anom3=rotate(anom2,2)

ndvi1= rotate(alfa, 3)
ndvi2=transpose(ndvi1)
ndvi3=rotate(ndvi2,2)

openw,3, '/pamenar/u1/anap/NDVI/GSFC/right_fasir_eur82_1'
printf,3, ndvi3

openw,4, '/pamenar/u1/anap/NDVI/IDL/right_NDVI_anomjan82_c'
printf,3, anom3

tv, ndvi3
tv, anom3

close, 1
close, 2
close, 3
close, 4

end
```

- **IDL routine to calculate NDVI anomalies in Europe**

Note: Similar routine was applied to soil wetness and precipitation data.

```
PRO NDVI_anomalies

temp=fltarr(75,60,9)
mean=fltarr(75,60)
stdv=fltarr(75,60)
anomalies=fltarr(75,60)

openr, 1, '/pamenar/u1/anap/NDVI/IDL/NDVI_nov82_90'
readf, 1, temp
openr, 2, '/pamenar/u1/anap/NDVI/IDL/mean_nov82_90'
readf,2,mean
openr, 3, '/pamenar/u1/anap/NDVI/IDL/stdv_nov82_90'
readf,3,stdv

FOR i=0,74 do begin
        FOR j=0,59 do begin
                anomalies[i,j]=(temp[i,j,8]-mean[i,j])/stdv[i,j]
        ENDFOR
ENDFOR
close, 1
close, 2
close, 3
print, anomalies

openw, 1, '/pamenar/u1/anap/NDVI/IDL/NDVI_anomnov90'
printf, 1, anomalies
close, 1

end
```

- **IDL routine to convert 'NaN' strings to '200'**

Note1: Similar routine was applied to soil wetness and precipitation data.
Note2: Similar routine was applied to all months and years.

```
PRO NDVI_conv_val

temp=fltarr(75,59)

openr, 1, '/pamenar/u1/anap/ /NDVI/IDL/NDVI_anomnov90'

readf, 1, temp
close, 1

FOR i=0,74 do FOR j=0,59 do begin

                IF (temp[i,j] GT 0) OR (temp[i,j] LE 0) OR (temp[i,j] EQ 0) THEN begin temp[i,j]=temp[i,j]
                ENDIF ELSE begin
```

```
            temp[i,j]=200
            ENDELSE

ENDFOR

openw,1, '/pamenar/u1/anap/ /NDVI/final/right_NDVI_anomnov90_c'

printf, 1, temp
close, 1

print, temp

end
```

- **IDL routine to average NDVI anomalies data in Ireland.**

Note1: Same routine was applied to soil wetness and precipitation anomalies.
Note2: Same routine was applied to South Portugal [50:60,60:80], South Spain [80:110,60:80], North Spain[80:120,80:100], and South England [90:127,170:180]
Note3: Similar routine was applied to NDVI, soil wetness and precipitation data.

```
PRO irelandANOMndvi

alfa=fltarr(75,60)
gama=fltarr(600,480)
beta=fltarr(4,3)
mean=fltarr(1,1)

final=fltarr(9,1)
final_t=fltarr(108,1)

openr,1, '/pamenar/u1/anap/NDVI/final/right_NDVI_anomjan82_c'
readf,1, alfa

gama=congrid(alfa,600,480)
beta=gama[50:70,180:200]

tv, beta

FOR i=0,2 do begin
  FOR j=0,2 do begin
      result=moment(beta)
      mean=result[0]
   ENDFOR
ENDFOR

final[0,0]=mean
final_t[0,0]=mean

close,1

openr,1, '/pamenar/u1/anap/NDVI/final/right_NDVI_anomjan83_c
```

```
readf,1, alfa

gama=congrid(alfa,600,480)
beta=gama[50:70,180:200]

tv, beta

FOR i=0,2 do begin
  FOR j=0,2 do begin
      result=moment(beta)
      mean=result[0]
   ENDFOR
ENDFOR

final[1,0]=mean
final_t[12,0]=mean

close,1
openr,1, '/pamenar/u1/anap/NDVI/final/right_NDVI_anomjan84_c
readf,1, alfa

gama=congrid(alfa,600,480)
beta=gama[50:70,180:200]

tv, beta

FOR i=0,2 do begin
  FOR j=0,2 do begin
      result=moment(beta)
      mean=result[0]
   ENDFOR
ENDFOR

final[2,0]=mean
final_t[24,0]=mean

close,1

openr,1, '/pamenar/u1/anap/NDVI/final/right_NDVI_anomjan85_c
readf,1, alfa

gama=congrid(alfa,600,480)
beta=gama[50:70,180:200]

tv, beta

FOR i=0,2 do begin
  FOR j=0,2 do begin
      result=moment(beta)
      mean=result[0]
   ENDFOR
ENDFOR

final[3,0]=mean
final_t[36,0]=mean

close,1
```

```
openr,1, '/pamenar/u1/anap/NDVI/final/right_NDVI_anomjan86_c
readf,1, alfa

gama=congrid(alfa,600,480)
beta=gama[50:70,180:200]

tv, beta

FOR i=0,2 do begin
  FOR j=0,2 do begin
      result=moment(beta)
      mean=result[0]
   ENDFOR
ENDFOR

final[4,0]=mean
final_t[48,0]=mean

close,1

openr,1, '/pamenar/u1/anap/NDVI/final/right_NDVI_anomjan87_c
readf,1, alfa

gama=congrid(alfa,600,480)
beta=gama[50:70,180:200]

tv, beta

FOR i=0,2 do begin
  FOR j=0,2 do begin
      result=moment(beta)
      mean=result[0]
   ENDFOR
ENDFOR

final[5,0]=mean
final_t[60,0]=mean

close,1

openr,1, '/pamenar/u1/anap/NDVI/final/right_NDVI_anomjan88_c
readf,1, alfa

gama=congrid(alfa,600,480)
beta=gama[50:70,180:200]

tv, beta

FOR i=0,2 do begin
  FOR j=0,2 do begin
      result=moment(beta)
      mean=result[0]
   ENDFOR
ENDFOR

final[6,0]=mean
final_t[72,0]=mean
```

```
close,1

openr,1, '/pamenar/u1/anap/NDVI/final/right_NDVI_anomjan89_c
readf,1, alfa

gama=congrid(alfa,600,480)
beta=gama[50:70,180:200]

tv, beta

FOR i=0,2 do begin
  FOR j=0,2 do begin
      result=moment(beta)
      mean=result[0]
   ENDFOR
ENDFOR

final[7,0]=mean
final_t[84,0]=mean

close,1

openr,1, '/pamenar/u1/anap/NDVI/final/right_NDVI_anomjan90_c
readf,1, alfa

gama=congrid(alfa,600,480)
beta=gama[50:70,180:200]

tv, beta

FOR i=0,2 do begin
  FOR j=0,2 do begin
      result=moment(beta)
      mean=result[0]
   ENDFOR
ENDFOR

final[8,0]=mean
final_t[96,0]=mean

print, final

close,1

openw,1, '/pamenar/u1/anap/NDVI/plots/ireland/NDVI_ANOM_jan'
printf,1, final

close, 1

openr,1, '/pamenar/u1/gamap/NDVI/final/right_NDVI_anomfev82_c
readf,1, alfa

gama=congrid(alfa,600,480)
beta=gama[50:70,180:200]

tv, beta

FOR i=0,2 do begin
```

```
 FOR j=0,2 do begin
     result=moment(beta)
     mean=result[0]
  ENDFOR
ENDFOR

final[0,0]=mean
final_t[1,0]=mean

close,1

openr,1, '/pamenar/u1/anap/NDVI/final/right_NDVI_anomfev83_c
readf,1, alfa

gama=congrid(alfa,600,480)
beta=gama[50:70,180:200]

tv, beta

FOR i=0,2 do begin
 FOR j=0,2 do begin
     result=moment(beta)
     mean=result[0]
  ENDFOR
ENDFOR

final[1,0]=mean
final_t[13,0]=mean

close,1

openr,1, '/pamenar/u1/anap/NDVI/final/right_NDVI_anomfev84_c
readf,1, alfa

gama=congrid(alfa,600,480)
beta=gama[50:70,180:200]

tv, beta

FOR i=0,2 do begin
 FOR j=0,2 do begin
     result=moment(beta)
     mean=result[0]
  ENDFOR
ENDFOR

final[2,0]=mean
final_t[25,0]=mean

close,1

openr,1, '/pamenar/u1/anap/NDVI/final/right_NDVI_anomfev85_c
readf,1, alfa

gama=congrid(alfa,600,480)
beta=gama[50:70,180:200]

tv, beta
```

```
FOR i=0,2 do begin
  FOR j=0,2 do begin
      result=moment(beta)
      mean=result[0]
   ENDFOR
ENDFOR

final[3,0]=mean

final_t[37,0]=mean

close,1

openr,1, '/pamenar/u1/anap/NDVI/final/right_NDVI_anomfev86_c
readf,1, alfa

gama=congrid(alfa,600,480)
beta=gama[50:70,180:200]

tv, beta

FOR i=0,2 do begin
  FOR j=0,2 do begin
      result=moment(beta)
      mean=result[0]
   ENDFOR
ENDFOR

final[4,0]=mean
final_t[49,0]=mean

close,1

openr,1, '/pamenar/u1/anap/NDVI/final/right_NDVI_anomfev87_c
readf,1, alfa

gama=congrid(alfa,600,480)
beta=gama[50:70,180:200]

tv, beta

FOR i=0,2 do begin
  FOR j=0,2 do begin
      result=moment(beta)
      mean=result[0]
   ENDFOR
ENDFOR

final[5,0]=mean
final_t[61,0]=mean

close,1


openr,1, '/pamenar/u1/anap/NDVI/final/right_NDVI_anomfev88_c
readf,1, alfa
```

```
gama=congrid(alfa,600,480)

beta=gama[50:70,180:200]

tv, beta

FOR i=0,2 do begin
  FOR j=0,2 do begin
      result=moment(beta)
      mean=result[0]
   ENDFOR
ENDFOR

final[6,0]=mean
final_t[73,0]=mean

close,1

openr,1, '/pamenar/u1/anap/NDVI/final/right_NDVI_anomfev89_c
readf,1, alfa

gama=congrid(alfa,600,480)
beta=gama[50:70,180:200]

tv, beta

FOR i=0,2 do begin
  FOR j=0,2 do begin
      result=moment(beta)
      mean=result[0]
   ENDFOR
ENDFOR

final[7,0]=mean
final_t[85,0]=mean

close,1

openr,1, '/pamenar/u1/anap/NDVI/final/right_NDVI_anomfev90_c
readf,1, alfa

gama=congrid(alfa,600,480)
beta=gama[50:70,180:200]

tv, beta

FOR i=0,2 do begin
  FOR j=0,2 do begin
      result=moment(beta)
      mean=result[0]
   ENDFOR
ENDFOR

final[8,0]=mean
final_t[97,0]=mean

print, final
```

```
close,1

openw,1, '/pamenar/u1/anap/NDVI/plots/ireland/NDVI_ANOM_fev'
printf,1, final

close, 1

openr,1, '/pamenar/u1/anap/NDVI/final/right_NDVI_anommar82_c
readf,1, alfa

gama=congrid(alfa,600,480)
beta=gama[50:70,180:200]

tv, beta

FOR i=0,2 do begin
  FOR j=0,2 do begin
      result=moment(beta)
      mean=result[0]
  ENDFOR
ENDFOR

final[0,0]=mean
final_t[2,0]=mean

close,1

openr,1, '/pamenar/u1/anap/NDVI/final/right_NDVI_anommar83_c
readf,1, alfa

gama=congrid(alfa,600,480)
beta=gama[50:70,180:200]

tv, beta

FOR i=0,2 do begin
  FOR j=0,2 do begin
      result=moment(beta)
      mean=result[0]
  ENDFOR
ENDFOR

final[1,0]=mean
final_t[14,0]=mean

close,1

openr,1, '/pamenar/u1/anap/NDVI/final/right_NDVI_anommar84_c
readf,1, alfa

gama=congrid(alfa,600,480)
beta=gama[50:70,180:200]

tv, beta

FOR i=0,2 do begin
  FOR j=0,2 do begin
```

```
      result=moment(beta)
      mean=result[0]
  ENDFOR
ENDFOR

final[2,0]=mean
final_t[26,0]=mean

close,1

openr,1, '/pamenar/u1/anap/NDVI/final/right_NDVI_anommar85_c
readf,1, alfa

gama=congrid(alfa,600,480)
beta=gama[50:70,180:200]

tv, beta

FOR i=0,2 do begin
  FOR j=0,2 do begin
      result=moment(beta)
      mean=result[0]
  ENDFOR
ENDFOR

final[3,0]=mean
final_t[38,0]=mean

close,1

openr,1, '/pamenar/u1/anap/NDVI/final/right_NDVI_anommar86_c
readf,1, alfa

gama=congrid(alfa,600,480)
beta=gama[50:70,180:200]

tv, beta

FOR i=0,2 do begin
  FOR j=0,2 do begin
      result=moment(beta)
      mean=result[0]
  ENDFOR
ENDFOR

final[4,0]=mean
final_t[50,0]=mean

close,1

openr,1, '/pamenar/u1/anap/NDVI/final/right_NDVI_anommar87_c
readf,1, alfa

gama=congrid(alfa,600,480)
beta=gama[50:70,180:200]

tv, beta
```

```
FOR i=0,2 do begin
  FOR j=0,2 do begin
      result=moment(beta)
      mean=result[0]
   ENDFOR
ENDFOR

final[5,0]=mean
final_t[62,0]=mean

close,1

openr,1, '/pamenar/u1/anap/NDVI/final/right_NDVI_anommar88_c
readf,1, alfa

gama=congrid(alfa,600,480)
beta=gama[50:70,180:200]

tv, beta

FOR i=0,2 do begin
  FOR j=0,2 do begin
      result=moment(beta)
      mean=result[0]
   ENDFOR
ENDFOR

final[6,0]=mean
final_t[74,0]=mean

close,1

openr,1, '/pamenar/u1/anap/NDVI/final/right_NDVI_anommar89_c
readf,1, alfa

gama=congrid(alfa,600,480)
beta=gama[50:70,180:200]

tv, beta

FOR i=0,2 do begin
  FOR j=0,2 do begin
      result=moment(beta)
      mean=result[0]
   ENDFOR
ENDFOR

final[7,0]=mean
final_t[86,0]=mean

close,1

openr,1, '/pamenar/u1/anap/NDVI/final/right_NDVI_anommar90_c
readf,1, alfa

gama=congrid(alfa,600,480)
beta=gama[50:70,180:200]
```

```
tv, beta

FOR i=0,2 do begin
  FOR j=0,2 do begin
      result=moment(beta)
      mean=result[0]
  ENDFOR
ENDFOR

final[8,0]=mean
final_t[98,0]=mean

print, final

close,1

openw,1, '/pamenar/u1/anap/NDVI/plots/ireland/NDVI_ANOM_mar'
printf,1, final
close, 1

openr,1, '/pamenar/u1/anap/NDVI/final/right_NDVI_anomapr82_c
readf,1, alfa

gama=congrid(alfa,600,480)
beta=gama[50:70,180:200]

tv, beta

FOR i=0,2 do begin
  FOR j=0,2 do begin
      result=moment(beta)
      mean=result[0]
  ENDFOR
ENDFOR

final[0,0]=mean
final_t[3,0]=mean

close,1

openr,1, '/pamenar/u1/anap/NDVI/final/right_NDVI_anomapr83_c
readf,1, alfa

gama=congrid(alfa,600,480)
beta=gama[50:70,180:200]

tv, beta

FOR i=0,2 do begin
  FOR j=0,2 do begin
      result=moment(beta)
      mean=result[0]
  ENDFOR
ENDFOR

final[1,0]=mean
final_t[15,0]=mean
```

```
close,1

openr,1, '/pamenar/u1/anap/NDVI/final/right_NDVI_anomapr84_c
readf,1, alfa

gama=congrid(alfa,600,480)
beta=gama[50:70,180:200]

tv, beta

FOR i=0,2 do begin
 FOR j=0,2 do begin
     result=moment(beta)
     mean=result[0]
  ENDFOR
ENDFOR

final[2,0]=mean
final_t[27,0]=mean

close,1

openr,1, '/pamenar/u1/anap/NDVI/final/right_NDVI_anomapr85_c
readf,1, alfa

gama=congrid(alfa,600,480)
beta=gama[50:70,180:200]

tv, beta

FOR i=0,2 do begin
 FOR j=0,2 do begin
     result=moment(beta)
     mean=result[0]
  ENDFOR
ENDFOR

final[3,0]=mean
final_t[39,0]=mean

close,1

openr,1, '/pamenar/u1/anap/NDVI/final/right_NDVI_anomapr86_c
readf,1, alfa

gama=congrid(alfa,600,480)
beta=gama[50:70,180:200]

tv, beta

FOR i=0,2 do begin
 FOR j=0,2 do begin
     result=moment(beta)
     mean=result[0]
  ENDFOR
ENDFOR

final[4,0]=mean
```

```
final_t[51,0]=mean

close,1

openr,1, '/pamenar/u1/anap/NDVI/final/right_NDVI_anomapr87_c
readf,1, alfa

gama=congrid(alfa,600,480)
beta=gama[50:70,180:200]

tv, beta

FOR i=0,2 do begin
 FOR j=0,2 do begin
     result=moment(beta)
     mean=result[0]
  ENDFOR
ENDFOR

final[5,0]=mean
final_t[63,0]=mean

close,1

openr,1, '/pamenar/u1/anap/NDVI/final/right_NDVI_anomapr88_c
readf,1, alfa

gama=congrid(alfa,600,480)
beta=gama[50:70,180:200]

tv, beta

FOR i=0,2 do begin
 FOR j=0,2 do begin
     result=moment(beta)
     mean=result[0]
  ENDFOR
ENDFOR

final[6,0]=mean
final_t[75,0]=mean

close,1

openr,1, '/pamenar/u1/anap/NDVI/final/right_NDVI_anomapr89_c
readf,1, alfa

gama=congrid(alfa,600,480)
beta=gama[50:70,180:200]

tv, beta

FOR i=0,2 do begin
 FOR j=0,2 do begin
     result=moment(beta)
     mean=result[0]
  ENDFOR
ENDFOR
```

```
final[7,0]=mean
final_t[87,0]=mean

close,1

openr,1, '/pamenar/u1/anap/NDVI/final/right_NDVI_anomapr90_c
readf,1, alfa

gama=congrid(alfa,600,480)
beta=gama[50:70,180:200]

tv, beta

FOR i=0,2 do begin
  FOR j=0,2 do begin
      result=moment(beta)
      mean=result[0]
  ENDFOR
ENDFOR

final[8,0]=mean
final_t[99,0]=mean

print, final

close,1

openw,1, '/pamenar/u1/anap/NDVI/plots/ireland/NDVI_ANOM_apr'
printf,1, final
close, 1

openr,1, '/pamenar/u1/anap/NDVI/final/right_NDVI_anommai82_c
readf,1, alfa

gama=congrid(alfa,600,480)
beta=gama[50:70,180:200]

tv, beta

FOR i=0,2 do begin
  FOR j=0,2 do begin
      result=moment(beta)
      mean=result[0]
  ENDFOR
ENDFOR

final[0,0]=mean
final_t[4,0]=mean

close,1

openr,1, '/pamenar/u1/anap/NDVI/final/right_NDVI_anommai83_c
readf,1, alfa

gama=congrid(alfa,600,480)
beta=gama[50:70,180:200]
```

```
tv, beta

FOR i=0,2 do begin
  FOR j=0,2 do begin
      result=moment(beta)
      mean=result[0]
   ENDFOR
ENDFOR

final[1,0]=mean
final_t[16,0]=mean

close,1

openr,1, '/pamenar/u1/anap/NDVI/final/right_NDVI_anommai84_c
readf,1, alfa

gama=congrid(alfa,600,480)
beta=gama[50:70,180:200]

tv, beta

FOR i=0,2 do begin
  FOR j=0,2 do begin
      result=moment(beta)
      mean=result[0]
   ENDFOR
ENDFOR

final[2,0]=mean
final_t[28,0]=mean

close,1

openr,1, '/pamenar/u1/anap/NDVI/final/right_NDVI_anommai85_c
readf,1, alfa

gama=congrid(alfa,600,480)
beta=gama[50:70,180:200]

tv, beta

FOR i=0,2 do begin
  FOR j=0,2 do begin
      result=moment(beta)
      mean=result[0]
   ENDFOR
ENDFOR

final[3,0]=mean
final_t[40,0]=mean

close,1

openr,1, '/pamenar/u1/anap/NDVI/final/right_NDVI_anommai86_c
readf,1, alfa

gama=congrid(alfa,600,480)
```

```
beta=gama[50:70,180:200]

tv, beta

FOR i=0,2 do begin
  FOR j=0,2 do begin
      result=moment(beta)
      mean=result[0]
  ENDFOR
ENDFOR

final[4,0]=mean
final_t[52,0]=mean

close,1

openr,1, '/pamenar/u1/anap/NDVI/final/right_NDVI_anommai87_c
readf,1, alfa

gama=congrid(alfa,600,480)
beta=gama[50:70,180:200]

tv, beta

FOR i=0,2 do begin
  FOR j=0,2 do begin
      result=moment(beta)
      mean=result[0]
  ENDFOR
ENDFOR

final[5,0]=mean
final_t[64,0]=mean

close,1

openr,1, '/pamenar/u1/anap/NDVI/final/right_NDVI_anommai88_c
readf,1, alfa

gama=congrid(alfa,600,480)
beta=gama[50:70,180:200]

tv, beta

FOR i=0,2 do begin
  FOR j=0,2 do begin
      result=moment(beta)
      mean=result[0]
  ENDFOR
ENDFOR

final[6,0]=mean
final_t[76,0]=mean

close,1

openr,1, '/pamenar/u1/anap/NDVI/final/right_NDVI_anommai89_c
readf,1, alfa
```

```
gama=congrid(alfa,600,480)
beta=gama[50:70,180:200]

tv, beta

FOR i=0,2 do begin
  FOR j=0,2 do begin
      result=moment(beta)
      mean=result[0]
   ENDFOR
ENDFOR

final[7,0]=mean
final_t[88,0]=mean

close,1

openr,1, '/pamenar/u1/anap/NDVI/final/right_NDVI_anommai90_c
readf,1, alfa

gama=congrid(alfa,600,480)
beta=gama[50:70,180:200]

tv, beta

FOR i=0,2 do begin
  FOR j=0,2 do begin
      result=moment(beta)
      mean=result[0]
   ENDFOR
ENDFOR

final[8,0]=mean
final_t[100,0]=mean

print, final


close,1

openw,1, '/pamenar/u1/anap/NDVI/plots/ireland/NDVI_ANOM_mai'
printf,1, final

close, 1

openr,1, '/pamenar/u1/anap/NDVI/final/right_NDVI_anomjun82_c
readf,1, alfa

gama=congrid(alfa,600,480)
beta=gama[50:70,180:200]

tv, beta

FOR i=0,2 do begin
  FOR j=0,2 do begin
      result=moment(beta)
      mean=result[0]
```

```
  ENDFOR
ENDFOR

final[0,0]=mean
final_t[5,0]=mean

close,1

openr,1, '/pamenar/u1/anap/NDVI/final/right_NDVI_anomjun83_c
readf,1, alfa

gama=congrid(alfa,600,480)
beta=gama[50:70,180:200]

tv, beta

FOR i=0,2 do begin
  FOR j=0,2 do begin
      result=moment(beta)
      mean=result[0]
  ENDFOR
ENDFOR

final[1,0]=mean
final_t[17,0]=mean

close,1

openr,1, '/pamenar/u1/anap/NDVI/final/right_NDVI_anomjun84_c
readf,1, alfa

gama=congrid(alfa,600,480)
beta=gama[50:70,180:200]

tv, beta

FOR i=0,2 do begin
  FOR j=0,2 do begin
      result=moment(beta)
      mean=result[0]
  ENDFOR
ENDFOR

final[2,0]=mean
final_t[29,0]=mean

close,1

openr,1, '/pamenar/u1/anap/NDVI/final/right_NDVI_anomjun85_c
readf,1, alfa

gama=congrid(alfa,600,480)
beta=gama[50:70,180:200]

tv, beta

FOR i=0,2 do begin
  FOR j=0,2 do begin
```

```
    result=moment(beta)
    mean=result[0]
  ENDFOR
ENDFOR

final[3,0]=mean
final_t[41,0]=mean

close,1

openr,1, '/pamenar/u1/anap/NDVI/final/right_NDVI_anomjun86_c
readf,1, alfa

gama=congrid(alfa,600,480)
beta=gama[50:70,180:200]

tv, beta

FOR i=0,2 do begin
  FOR j=0,2 do begin
    result=moment(beta)
    mean=result[0]
  ENDFOR
ENDFOR

final[4,0]=mean
final_t[53,0]=mean

close,1

openr,1, '/pamenar/u1/anap/NDVI/final/right_NDVI_anomjun87_c
readf,1, alfa

gama=congrid(alfa,600,480)
beta=gama[50:70,180:200]

tv, beta

FOR i=0,2 do begin
  FOR j=0,2 do begin
    result=moment(beta)
    mean=result[0]
  ENDFOR
ENDFOR

final[5,0]=mean
final_t[65,0]=mean

close,1

openr,1, '/pamenar/u1/anap/NDVI/final/right_NDVI_anomjun88_c
readf,1, alfa

gama=congrid(alfa,600,480)

beta=gama[50:70,180:200]

tv, beta
```

```
FOR i=0,2 do begin
  FOR j=0,2 do begin
      result=moment(beta)
      mean=result[0]
   ENDFOR
ENDFOR

final[6,0]=mean
final_t[77,0]=mean

close,1

openr,1, '/pamenar/u1/anap/NDVI/final/right_NDVI_anomjun89_c
readf,1, alfa

gama=congrid(alfa,600,480)
beta=gama[50:70,180:200]

tv, beta

FOR i=0,2 do begin
  FOR j=0,2 do begin
      result=moment(beta)
      mean=result[0]
   ENDFOR
ENDFOR

final[7,0]=mean
final_t[89,0]=mean

close,1

openr,1, '/pamenar/u1/anap/NDVI/final/right_NDVI_anomjun90_c
readf,1, alfa

gama=congrid(alfa,600,480)
beta=gama[50:70,180:200]

tv, beta

FOR i=0,2 do begin
  FOR j=0,2 do begin
      result=moment(beta)
      mean=result[0]
   ENDFOR
ENDFOR

final[8,0]=mean
final_t[101,0]=mean

print, final

close,1

openw,1, '/pamenar/u1/anap/NDVI/plots/ireland/NDVI_ANOM_jun'
printf,1, final
close, 1
```

```
openr,1, '/pamenar/u1/anap/NDVI/final/right_NDVI_anomjul82_c
readf,1, alfa

gama=congrid(alfa,600,480)
beta=gama[50:70,180:200]

tv, beta

FOR i=0,2 do begin
 FOR j=0,2 do begin
     result=moment(beta)
     mean=result[0]
  ENDFOR
ENDFOR

final[0,0]=mean
final_t[6,0]=mean

close,1

openr,1, '/pamenar/u1/anap/NDVI/final/right_NDVI_anomjul83_c
readf,1, alfa

gama=congrid(alfa,600,480)
beta=gama[50:70,180:200]

tv, beta

FOR i=0,2 do begin
 FOR j=0,2 do begin
     result=moment(beta)
     mean=result[0]
  ENDFOR
ENDFOR

final[1,0]=mean
final_t[18,0]=mean

close,1

openr,1, '/pamenar/u1/anap/NDVI/final/right_NDVI_anomjul84_c
readf,1, alfa

gama=congrid(alfa,600,480)
beta=gama[50:70,180:200]

tv, beta

FOR i=0,2 do begin
 FOR j=0,2 do begin
     result=moment(beta)
     mean=result[0]
  ENDFOR
ENDFOR

final[2,0]=mean
final_t[30,0]=mean
```

```
close,1

openr,1, '/pamenar/u1/anap/NDVI/final/right_NDVI_anomjul85_c
readf,1, alfa

gama=congrid(alfa,600,480)
beta=gama[50:70,180:200]

tv, beta

FOR i=0,2 do begin
  FOR j=0,2 do begin
      result=moment(beta)
      mean=result[0]
   ENDFOR
ENDFOR

final[3,0]=mean
final_t[42,0]=mean

close,1

openr,1, '/pamenar/u1/anap/NDVI/final/right_NDVI_anomjul86_c
readf,1, alfa

gama=congrid(alfa,600,480)
beta=gama[50:70,180:200]

tv, beta

FOR i=0,2 do begin
  FOR j=0,2 do begin
      result=moment(beta)
      mean=result[0]
   ENDFOR
ENDFOR

final[4,0]=mean
final_t[54,0]=mean

close,1

openr,1, '/pamenar/u1/anap/NDVI/final/right_NDVI_anomjul87_c
readf,1, alfa

gama=congrid(alfa,600,480)
beta=gama[50:70,180:200]

tv, beta

FOR i=0,2 do begin
  FOR j=0,2 do begin
      result=moment(beta)
      mean=result[0]
   ENDFOR
ENDFOR
```

```
final[5,0]=mean
final_t[66,0]=mean

close,1

openr,1, '/pamenar/u1/anap/NDVI/final/right_NDVI_anomjul88_c
readf,1, alfa

gama=congrid(alfa,600,480)
beta=gama[50:70,180:200]

tv, beta

FOR i=0,2 do begin
  FOR j=0,2 do begin
      result=moment(beta)
      mean=result[0]
   ENDFOR
ENDFOR

final[6,0]=mean
final_t[78,0]=mean

close,1

openr,1, '/pamenar/u1/anap/NDVI/final/right_NDVI_anomjul89_c
readf,1, alfa

gama=congrid(alfa,600,480)

beta=gama[50:70,180:200]

tv, beta

FOR i=0,2 do begin
  FOR j=0,2 do begin
      result=moment(beta)
      mean=result[0]
   ENDFOR
ENDFOR

final[7,0]=mean
final_t[90,0]=mean

close,1

openr,1, '/pamenar/u1/anap/NDVI/final/right_NDVI_anomjul90_c
readf,1, alfa

gama=congrid(alfa,600,480)
beta=gama[50:70,180:200]

tv, beta

FOR i=0,2 do begin
  FOR j=0,2 do begin
      result=moment(beta)
      mean=result[0]
```

```
  ENDFOR
ENDFOR

final[8,0]=mean
final_t[102,0]=mean

print, final

close,1

openw,1, '/pamenar/u1/anap/NDVI/plots/ireland/NDVI_ANOM_jul'
printf,1, final

close, 1

openr,1, '/pamenar/u1/anap/NDVI/final/right_NDVI_anomago82_c
readf,1, alfa

gama=congrid(alfa,600,480)
beta=gama[50:70,180:200]

tv, beta

FOR i=0,2 do begin
  FOR j=0,2 do begin
      result=moment(beta)
      mean=result[0]
  ENDFOR
ENDFOR

final[0,0]=mean
final_t[7,0]=mean

close,1

openr,1, '/pamenar/u1/anap/NDVI/final/right_NDVI_anomago83_c
readf,1, alfa

gama=congrid(alfa,600,480)
beta=gama[50:70,180:200]

tv, beta

FOR i=0,2 do begin
  FOR j=0,2 do begin
      result=moment(beta)
      mean=result[0]
  ENDFOR
ENDFOR

final[1,0]=mean
final_t[19,0]=mean

close,1

openr,1, '/pamenar/u1/anap/NDVI/final/right_NDVI_anomago84_c
readf,1, alfa
```

```
gama=congrid(alfa,600,480)
beta=gama[50:70,180:200]

tv, beta

FOR i=0,2 do begin
  FOR j=0,2 do begin
      result=moment(beta)
      mean=result[0]
   ENDFOR
ENDFOR

final[2,0]=mean
final_t[31,0]=mean

close,1

openr,1, '/pamenar/u1/anap/NDVI/final/right_NDVI_anomago85_c
readf,1, alfa

gama=congrid(alfa,600,480)

beta=gama[50:70,180:200]

tv, beta

FOR i=0,2 do begin
  FOR j=0,2 do begin
      result=moment(beta)
      mean=result[0]
   ENDFOR
ENDFOR

final[3,0]=mean
final_t[43,0]=mean

close,1

openr,1, '/pamenar/u1/anap/NDVI/final/right_NDVI_anomago86_c
readf,1, alfa

gama=congrid(alfa,600,480)
beta=gama[50:70,180:200]

tv, beta

FOR i=0,2 do begin
  FOR j=0,2 do begin
      result=moment(beta)
      mean=result[0]
   ENDFOR
ENDFOR

final[4,0]=mean
final_t[55,0]=mean

close,1
```

```
openr,1, '/pamenar/u1/anap/NDVI/final/right_NDVI_anomago87_c
readf,1, alfa

gama=congrid(alfa,600,480)
beta=gama[50:70,180:200]

tv, beta

FOR i=0,2 do begin
 FOR j=0,2 do begin
     result=moment(beta)
     mean=result[0]
  ENDFOR
ENDFOR

final[5,0]=mean
final_t[67,0]=mean

close,1

openr,1, '/pamenar/u1/anap/NDVI/final/right_NDVI_anomago88_c
readf,1, alfa

gama=congrid(alfa,600,480)
beta=gama[50:70,180:200]

tv, beta

FOR i=0,2 do begin
 FOR j=0,2 do begin
     result=moment(beta)
     mean=result[0]
  ENDFOR
ENDFOR

final[6,0]=mean
final_t[79,0]=mean

close,1

openr,1, '/pamenar/u1/anap/NDVI/final/right_NDVI_anomago89_c
readf,1, alfa

gama=congrid(alfa,600,480)
beta=gama[50:70,180:200]

tv, beta

FOR i=0,2 do begin
 FOR j=0,2 do begin
     result=moment(beta)
     mean=result[0]
  ENDFOR
ENDFOR

final[7,0]=mean
final_t[91,0]=mean
```

```
close,1

openr,1, '/pamenar/u1/anap/NDVI/final/right_NDVI_anomago90_c
readf,1, alfa

gama=congrid(alfa,600,480)
beta=gama[50:70,180:200]

tv, beta

FOR i=0,2 do begin
  FOR j=0,2 do begin
      result=moment(beta)
      mean=result[0]
   ENDFOR
ENDFOR

final[8,0]=mean
final_t[103,0]=mean

print, final

close,1

openw,1, '/pamenar/u1/anap/NDVI/plots/ireland/NDVI_ANOM_ago'
printf,1, final

close, 1

openr,1, '/pamenar/u1/anap/NDVI/final/right_NDVI_anomsep82_c
readf,1, alfa

gama=congrid(alfa,600,480)
beta=gama[50:70,180:200]

tv, beta

FOR i=0,2 do begin
  FOR j=0,2 do begin
      result=moment(beta)
      mean=result[0]
   ENDFOR
ENDFOR

final[0,0]=mean
final_t[8,0]=mean

close,1

openr,1, '/pamenar/u1/anap/NDVI/final/right_NDVI_anomsep83_c
readf,1, alfa

gama=congrid(alfa,600,480)
beta=gama[50:70,180:200]

tv, beta

FOR i=0,2 do begin
```

```
 FOR j=0,2 do begin
     result=moment(beta)
     mean=result[0]
  ENDFOR
ENDFOR

final[1,0]=mean
final_t[20,0]=mean

close,1

openr,1, '/pamenar/u1/anap/NDVI/final/right_NDVI_anomsep84_c
readf,1, alfa

gama=congrid(alfa,600,480)
beta=gama[50:70,180:200]

tv, beta

FOR i=0,2 do begin
 FOR j=0,2 do begin
     result=moment(beta)
     mean=result[0]
  ENDFOR
ENDFOR

final[2,0]=mean
final_t[32,0]=mean

close,1

openr,1, '/pamenar/u1/anap/NDVI/final/right_NDVI_anomsep85_c
readf,1, alfa

gama=congrid(alfa,600,480)
beta=gama[50:70,180:200]

tv, beta

FOR i=0,2 do begin
 FOR j=0,2 do begin
     result=moment(beta)
     mean=result[0]
  ENDFOR
ENDFOR

final[3,0]=mean
final_t[44,0]=mean

close,1

openr,1, '/pamenar/u1/anap/NDVI/final/right_NDVI_anomsep86_c
readf,1, alfa

gama=congrid(alfa,600,480)
beta=gama[50:70,180:200]

tv, beta
```

```
FOR i=0,2 do begin
 FOR j=0,2 do begin
     result=moment(beta)
     mean=result[0]
  ENDFOR
ENDFOR

final[4,0]=mean
final_t[56,0]=mean

close,1

openr,1, '/pamenar/u1/anap/NDVI/final/right_NDVI_anomsep87_c
readf,1, alfa

gama=congrid(alfa,600,480)
beta=gama[50:70,180:200]

tv, beta

FOR i=0,2 do begin
 FOR j=0,2 do begin
     result=moment(beta)
     mean=result[0]
  ENDFOR
ENDFOR

final[5,0]=mean
final_t[68,0]=mean

close,1

openr,1, '/pamenar/u1/anap/NDVI/final/right_NDVI_anomsep88_c
readf,1, alfa

gama=congrid(alfa,600,480)
beta=gama[50:70,180:200]

tv, beta

FOR i=0,2 do begin
 FOR j=0,2 do begin
     result=moment(beta)
     mean=result[0]
  ENDFOR
ENDFOR

final[6,0]=mean
final_t[80,0]=mean

close,1

openr,1, '/pamenar/u1/anap/NDVI/final/right_NDVI_anomsep89_c
readf,1, alfa

gama=congrid(alfa,600,480)
beta=gama[50:70,180:200]
```

```
tv, beta

FOR i=0,2 do begin
  FOR j=0,2 do begin
      result=moment(beta)
      mean=result[0]
   ENDFOR
ENDFOR

final[7,0]=mean
final_t[92,0]=mean

close,1

openr,1, '/pamenar/u1/anap/NDVI/final/right_NDVI_anomsep90_c
readf,1, alfa

gama=congrid(alfa,600,480)
beta=gama[50:70,180:200]

tv, beta

FOR i=0,2 do begin
  FOR j=0,2 do begin
      result=moment(beta)
      mean=result[0]
   ENDFOR
ENDFOR

final[8,0]=mean
final_t[104,0]=mean

print, final

close,1

openw,1, '/pamenar/u1/anap/NDVI/plots/ireland/NDVI_ANOM_sep'
printf,1, final
close, 1

openr,1, '/pamenar/u1/anap/NDVI/final/right_NDVI_anomout82_c
readf,1, alfa

gama=congrid(alfa,600,480)
beta=gama[50:70,180:200]

tv, beta

FOR i=0,2 do begin
  FOR j=0,2 do begin
      result=moment(beta)
      mean=result[0]
   ENDFOR
ENDFOR

final[0,0]=mean
final_t[9,0]=mean
```

```
close,1

openr,1, '/pamenar/u1/anap/NDVI/final/right_NDVI_anomout83_c
readf,1, alfa

gama=congrid(alfa,600,480)
beta=gama[50:70,180:200]

tv, beta

FOR i=0,2 do begin
 FOR j=0,2 do begin
     result=moment(beta)
     mean=result[0]
  ENDFOR
ENDFOR

final[1,0]=mean
final_t[21,0]=mean

close,1

openr,1, '/pamenar/u1/anap/NDVI/final/right_NDVI_anomout84_c
readf,1, alfa

gama=congrid(alfa,600,480)
beta=gama[50:70,180:200]

tv, beta

FOR i=0,2 do begin
 FOR j=0,2 do begin
     result=moment(beta)
     mean=result[0]
  ENDFOR
ENDFOR

final[2,0]=mean
final_t[33,0]=mean

close,1

openr,1, '/pamenar/u1/anap/NDVI/final/right_NDVI_anomout85_c
readf,1, alfa

gama=congrid(alfa,600,480)
beta=gama[50:70,180:200]

tv, beta

FOR i=0,2 do begin
 FOR j=0,2 do begin
     result=moment(beta)
     mean=result[0]
  ENDFOR
ENDFOR
```

```
final[3,0]=mean
final_t[45,0]=mean

close,1

openr,1, '/pamenar/u1/anap/NDVI/final/right_NDVI_anomout86_c
readf,1, alfa

gama=congrid(alfa,600,480)
beta=gama[50:70,180:200]

tv, beta

FOR i=0,2 do begin
 FOR j=0,2 do begin
     result=moment(beta)
     mean=result[0]
  ENDFOR
ENDFOR

final[4,0]=mean
final_t[57,0]=mean

close,1

openr,1, '/pamenar/u1/anap/NDVI/final/right_NDVI_anomout87_c
readf,1, alfa

gama=congrid(alfa,600,480)
beta=gama[50:70,180:200]

tv, beta

FOR i=0,2 do begin
 FOR j=0,2 do begin
     result=moment(beta)
     mean=result[0]
  ENDFOR
ENDFOR

final[5,0]=mean
final_t[69,0]=mean

close,1

openr,1, '/pamenar/u1/anap/NDVI/final/right_NDVI_anomout88_c
readf,1, alfa

gama=congrid(alfa,600,480)

beta=gama[50:70,180:200]

tv, beta

FOR i=0,2 do begin
 FOR j=0,2 do begin
     result=moment(beta)
     mean=result[0]
```

```
  ENDFOR
ENDFOR

final[6,0]=mean
final_t[81,0]=mean

close,1

openr,1, '/pamenar/u1/anap/NDVI/final/right_NDVI_anomout89_c
readf,1, alfa

gama=congrid(alfa,600,480)
beta=gama[50:70,180:200]

tv, beta

FOR i=0,2 do begin
  FOR j=0,2 do begin
      result=moment(beta)
      mean=result[0]
  ENDFOR
ENDFOR

final[7,0]=mean
final_t[93,0]=mean

close,1

openr,1, '/pamenar/u1/anap/NDVI/final/right_NDVI_anomout90_c
readf,1, alfa

gama=congrid(alfa,600,480)
beta=gama[50:70,180:200]

tv, beta

FOR i=0,2 do begin
  FOR j=0,2 do begin
      result=moment(beta)
      mean=result[0]
  ENDFOR
ENDFOR

final[8,0]=mean
final_t[105,0]=mean

print, final

close,1

openw,1, '/pamenar/u1/anap/NDVI/plots/ireland/NDVI_ANOM_out'
printf,1, final

close, 1

openr,1, '/pamenar/u1/anap/NDVI/final/right_NDVI_anomnov82_c
readf,1, alfa
```

```
gama=congrid(alfa,600,480)
beta=gama[50:70,180:200]

tv, beta

FOR i=0,2 do begin
 FOR j=0,2 do begin
     result=moment(beta)
     mean=result[0]
  ENDFOR
ENDFOR

final[0,0]=mean
final_t[10,0]=mean

close,1

openr,1, '/pamenar/u1/anap/NDVI/final/right_NDVI_anomnov83_c
readf,1, alfa

gama=congrid(alfa,600,480)
beta=gama[50:70,180:200]

tv, beta

FOR i=0,2 do begin
 FOR j=0,2 do begin
     result=moment(beta)
     mean=result[0]
  ENDFOR
ENDFOR

final[1,0]=mean
final_t[22,0]=mean

close,1

openr,1, '/pamenar/u1/anap/NDVI/final/right_NDVI_anomnov84_c
readf,1, alfa

gama=congrid(alfa,600,480)
beta=gama[50:70,180:200]

tv, beta

FOR i=0,2 do begin
 FOR j=0,2 do begin
     result=moment(beta)
     mean=result[0]
  ENDFOR
ENDFOR

final[2,0]=mean
final_t[34,0]=mean

close,1

openr,1, '/pamenar/u1/anap/NDVI/final/right_NDVI_anomnov85_c
```

```
readf,1, alfa

gama=congrid(alfa,600,480)
beta=gama[50:70,180:200]

tv, beta

FOR i=0,2 do begin
 FOR j=0,2 do begin
     result=moment(beta)
     mean=result[0]
  ENDFOR
ENDFOR

final[3,0]=mean
final_t[46,0]=mean

close,1

openr,1, '/pamenar/u1/anap/NDVI/final/right_NDVI_anomnov86_c
readf,1, alfa

gama=congrid(alfa,600,480)
beta=gama[50:70,180:200]

tv, beta

FOR i=0,2 do begin
 FOR j=0,2 do begin
     result=moment(beta)
     mean=result[0]
  ENDFOR
ENDFOR

final[4,0]=mean
final_t[58,0]=mean

close,1

openr,1, '/pamenar/u1/anap/NDVI/final/right_NDVI_anomnov87_c
readf,1, alfa

gama=congrid(alfa,600,480)
beta=gama[50:70,180:200]

tv, beta

FOR i=0,2 do begin
 FOR j=0,2 do begin
     result=moment(beta)
     mean=result[0]
  ENDFOR
ENDFOR

final[5,0]=mean
final_t[70,0]=mean

close,1
```

```
openr,1, '/pamenar/u1/anap/NDVI/final/right_NDVI_anomnov88_c
readf,1, alfa

gama=congrid(alfa,600,480)
beta=gama[50:70,180:200]

tv, beta

FOR i=0,2 do begin
 FOR j=0,2 do begin
     result=moment(beta)
     mean=result[0]
  ENDFOR
ENDFOR

final[6,0]=mean
final_t[82,0]=mean

close,1

openr,1, '/pamenar/u1/anap/NDVI/final/right_NDVI_anomnov89_c
readf,1, alfa

gama=congrid(alfa,600,480)

beta=gama[50:70,180:200]

tv, beta

FOR i=0,2 do begin
 FOR j=0,2 do begin
     result=moment(beta)
     mean=result[0]
  ENDFOR
ENDFOR

final[7,0]=mean
final_t[94,0]=mean

close,1

openr,1, '/pamenar/u1/anap/NDVI/final/right_NDVI_anomnov90_c
readf,1, alfa

gama=congrid(alfa,600,480)
beta=gama[50:70,180:200]

tv, beta

FOR i=0,2 do begin
 FOR j=0,2 do begin
     result=moment(beta)
     mean=result[0]
  ENDFOR
ENDFOR

final[8,0]=mean
```

```
final_t[106,0]=mean

print, final

close,1

openw,1, '/pamenar/u1/anap/NDVI/plots/ireland/NDVI_ANOM_nov'
printf,1, final

close, 1

openr,1, '/pamenar/u1/anap/NDVI/final/right_NDVI_anomdec82_c
readf,1, alfa

gama=congrid(alfa,600,480)
beta=gama[50:70,180:200]

tv, beta

FOR i=0,2 do begin
  FOR j=0,2 do begin
      result=moment(beta)
      mean=result[0]
   ENDFOR
ENDFOR

final[0,0]=mean
final_t[11,0]=mean

close,1

openr,1, '/pamenar/u1/anap/NDVI/final/right_NDVI_anomdec83_c
readf,1, alfa

gama=congrid(alfa,600,480)
beta=gama[50:70,180:200]

tv, beta

FOR i=0,2 do begin
  FOR j=0,2 do begin
      result=moment(beta)
      mean=result[0]
   ENDFOR
ENDFOR

final[1,0]=mean
final_t[23,0]=mean

close,1

openr,1, '/pamenar/u1/anap/NDVI/final/right_NDVI_anomdec84_c
readf,1, alfa

gama=congrid(alfa,600,480)
beta=gama[50:70,180:200]

tv, beta
```

```
FOR i=0,2 do begin
  FOR j=0,2 do begin
      result=moment(beta)
      mean=result[0]
   ENDFOR
ENDFOR

final[2,0]=mean
final_t[35,0]=mean

close,1

openr,1, '/pamenar/u1/anap/NDVI/final/right_NDVI_anomdec85_c
readf,1, alfa

gama=congrid(alfa,600,480)

beta=gama[50:70,180:200]

tv, beta

FOR i=0,2 do begin
  FOR j=0,2 do begin
      result=moment(beta)
      mean=result[0]
   ENDFOR
ENDFOR

final[3,0]=mean
final_t[47,0]=mean

close,1

openr,1, '/pamenar/u1/anap/NDVI/final/right_NDVI_anomdec86_c
readf,1, alfa

gama=congrid(alfa,600,480)
beta=gama[50:70,180:200]

tv, beta

FOR i=0,2 do begin
  FOR j=0,2 do begin
      result=moment(beta)
      mean=result[0]
   ENDFOR
ENDFOR

final[4,0]=mean
final_t[59,0]=mean

close,1

openr,1, '/pamenar/u1/anap/NDVI/final/right_NDVI_anomdec87_c
readf,1, alfa

gama=congrid(alfa,600,480)
```

```
beta=gama[50:70,180:200]

tv, beta

FOR i=0,2 do begin
  FOR j=0,2 do begin
      result=moment(beta)
      mean=result[0]
  ENDFOR
ENDFOR

final[5,0]=mean
final_t[71,0]=mean

close,1

openr,1, '/pamenar/u1/anap/NDVI/final/right_NDVI_anomdec88_c
readf,1, alfa

gama=congrid(alfa,600,480)
beta=gama[50:70,180:200]

tv, beta

FOR i=0,2 do begin
  FOR j=0,2 do begin
      result=moment(beta)
      mean=result[0]
  ENDFOR
ENDFOR

final[6,0]=mean
final_t[83,0]=mean

close,1

openr,1, '/pamenar/u1/anap/NDVI/final/right_NDVI_anomdec89_c
readf,1, alfa

gama=congrid(alfa,600,480)
beta=gama[50:70,180:200]

tv, beta

FOR i=0,2 do begin
  FOR j=0,2 do begin
      result=moment(beta)
      mean=result[0]
  ENDFOR
ENDFOR

final[7,0]=mean
final_t[95,0]=mean

close,1

openr,1, '/pamenar/u1/anap/NDVI/final/right_NDVI_anomdec90_c
readf,1, alfa
```

```
gama=congrid(alfa,600,480)
beta=gama[50:70,180:200]

tv, beta

FOR i=0,2 do begin
 FOR j=0,2 do begin
     result=moment(beta)
     mean=result[0]
  ENDFOR
ENDFOR

final[8,0]=mean
final_t[107,0]=mean

print, final
close,1

openw,1, '/pamenar/u1/anap/NDVI/plots/ireland/NDVI_ANOM_dec'
printf,1, final

close, 1

openw,1, '/pamenar/u1/anap/NDVI/plots/ireland/NDVI_ANOM_total'
printf,1, final_t

close, 1
 print, final_t

end
```

- **IDL routine to correlate, pixel-by-pixel, NDVI, soil wetness and precipitation averaged over the growing season**

Note: Similar routine was applied to NDVI and soil wetness data.

```
PRO corrgrowingseason

alfa=fltarr(75,60,9)
beta=fltarr(75,60,9)
gama=fltarr(75,60,9)

openr, 1, '/pamenar/u1/anap/NDVI/plots/growingseasonNDVI'
readf,1, alfa

openr, 2, '/pamenar/u1/anap/hydrology/Hydrology/plots/growingseasonSOIL'
readf,2, beta

openr, 3, '/pamenar/u1/anap/hydrology/precipitation/plots/growingseasonPREC'
readf,3, gama

temp=fltarr(9,1)
temp2=fltarr(9,1)
```

```
temp3=fltarr(9,1)
corndvisoil=fltarr(75,60)
corndviprec=fltarr(75,60)

FOR i=0,74 do for j=0,59 do begin
        temp[0,0]=alfa[i,j,0]
        temp[1,0]=alfa[i,j,1]
        temp[2,0]=alfa[i,j,2]
        temp[3,0]=alfa[i,j,3]
        temp[4,0]=alfa[i,j,4]
        temp[5,0]=alfa[i,j,5]
        temp[6,0]=alfa[i,j,6]
        temp[7,0]=alfa[i,j,7]
        temp[7,0]=alfa[i,j,8]
        temp2[0,0]=beta[i,j,0]
        temp2[1,0]=beta[i,j,1]
        temp2[2,0]=beta[i,j,2]
        temp2[3,0]=beta[i,j,3]
        temp2[4,0]=beta[i,j,4]
        temp2[5,0]=beta[i,j,5]
        temp2[6,0]=beta[i,j,6]
        temp2[7,0]=beta[i,j,7]
        temp2[8,0]=beta[i,j,8]
        temp3[0,0]=gama[i,j,0]
        temp3[1,0]=gama[i,j,1]
        temp3[2,0]=gama[i,j,2]
        temp3[3,0]=gama[i,j,3]
        temp3[4,0]=gama[i,j,4]
        temp3[5,0]=gama[i,j,5]
        temp3[6,0]=gama[i,j,6]
        temp3[7,0]=gama[i,j,7]
        temp3[8,0]=gama[i,j,8]

        corsoil=correlate(temp,temp2)
        corprec=correlate(temp,temp3)
        corndvisoil[i,j]=corsoil
        corndviprec[i,j]=corprec

        IF (corndvisoil[i,j] GT 0) OR (corndvisoil[i,j] LE 0) OR (corndvisoil[i,j] EQ 0) THEN begin
corndvisoil[i,j]=corndvisoil[i,j]
                ENDIF ELSE begin
                corndvisoil[i,j]=0
                ENDELSE
        IF (corndviprec[i,j] GT 0) OR (corndviprec[i,j] LE 0) OR (corndviprec[i,j] EQ 0) THEN begin
corndviprec[i,j]=corndviprec[i,j]
                ENDIF ELSE begin
                corndviprec[i,j]=0
                ENDELSE
ENDFOR

print, corndvisoil
print, corndviprec

help, corndvisoil
help,corndviprec

openw,4,'/pamenar/u1/anap/NDVI/plots/CORRgrowingseasonNDVISOIL
printf,4,corndvisoil
```

```
openw,5,'/pamenar/u1/anap/NDVI/plots/CORRgrowingseasonNDVIPREC
printf,5,corndviprec

print, corndvisoil

close, 1
close, 2
close, 3
close, 4
close, 5


end
```

- **IDL routine to plot NDVI data versus soil wetness and precipitation data in Ireland and save it as .ps image.**

Note: Similar routine was applied to 'South Portugal', 'South Spain', 'South England', and 'North Spain'.

```
PRO plotireland

alfa=fltarr(108,1)
beta=fltarr(108,1)
gama=fltarr(108,1)
psy=fltarr(75,60)

openr, 1, '/pamenar/u1/anap/hydrology/Hydrology/plots/ireland/SOIL_total
openr, 2, '/pamenar/u1/anap/hydrology/precipitation/plots/ireland/PREC_total
openr, 3, '/pamenar/u1/anap/NDVI/plots/ireland/NDVI_total

readf,1, alfa
readf,2, beta
readf,3, gama

FOR i=0,107 DO BEGIN
if beta[i,0] LT 0 THEN beta[i,0]=-999
if alfa[i,0] LT 0 THEN alfa[i,0]=-999
ENDFOR

print, alfa
psy2=gama/1000
psy=gama/100

!P.MULTI=[0,1,2]

set_plot,'ps'
device, filename='/pamenar/u1/anap/images/irelandsoilprec.ps'

plot, psy2, PSYM=1, title='NDVI, SOIL WETNESS DATA IN IRELAND', xtitle=Years, ytitle='NDVI,SOIL
WETNESS', yrange=[0.4,1.2]
oplot, alfa
```

```
plot, psy, PSYM=1, title='NDVI AND PRECIPITATION DATA IN IRELAND', xtitle=Years,
ytitle='NDVI,PRECIPITATION', yrange=[0,10]
oplot, beta

device,/close
set_plot, 'x'

plot, psy2, PSYM=1, title='NDVI, SOIL WETNESS DATA IN IRELAND', xtitle=Years, ytitle='NDVI,SOIL
WETNESS', yrange=[0.4,1.2]
oplot, alfa

plot, psy, PSYM=1, title='NDVI AND PRECIPITATION DATA IN IRELAND', xtitle=Years,
ytitle='NDVI,PRECIPITATION', yrange=[0,10]
oplot, beta

close, 1
close,2
close,3

end
```

- **IDL routine to create a color range in NDVI data and save image as a .ps**

Note: Same routine was applied to soil wetness and precipitation data.

```
PRO rangeNDVI

alfa=fltarr(75,60)
beta=fltarr(75,60)
ana=fltarr(300,240)
ana2=fltarr(300,240)

openr, 1, '/pamenar/u1/anap/NDVI/final/right_fasir_eur82_1
readf,1, alfa

openr, 2, '/pamenar/u1/anap/NDVI/final/right_NDVI_anomdec82_c
readf,2, beta

close,1
close,2

FOR i=0,74 do FOR j=0,59 DO BEGIN

        IF alfa[i,j] EQ 200 THEN alfa[i,j]=39

        IF alfa[i,j] GT 0 AND alfa[i,j] LT 100 THEN alfa[i,j]=111

        IF alfa[i,j] GT 100 AND alfa[i,j] LT 200 THEN alfa[i,j]=127

        IF alfa[i,j] GT 200 AND alfa[i,j] LT 300 THEN alfa[i,j]=143

        IF alfa[i,j] GT 300 AND alfa[i,j] LT 400 THEN alfa[i,j]=159

        IF alfa[i,j] GT 400 AND alfa[i,j] LT 500 THEN alfa[i,j]=175
```

```
        IF alfa[i,j] GT 500 AND alfa[i,j] LT 600 THEN alfa[i,j]=191

        IF alfa[i,j] GT 600 AND alfa[i,j] LT 700 THEN alfa[i,j]=207

        IF alfa[i,j] GT 700 AND alfa[i,j] LT 800 THEN alfa[i,j]=63

        IF alfa[i,j] GT 800 AND alfa[i,j] LT 900 THEN alfa[i,j]=79

        IF alfa[i,j] GT 900 AND alfa[i,j] LT 1000 THEN alfa[i,j]=95

ENDFOR

print, beta

FOR i=0,74 do FOR j=0,59 DO BEGIN

        IF beta[i,j] EQ 200 THEN beta[i,j]=39

        IF beta[i,j] GT -4 AND beta[i,j] LT -2.5 THEN beta[i,j]=111

        IF beta[i,j] GT -2.5 AND beta[i,j] LT -2 THEN beta[i,j]=127

        IF beta[i,j] GT -2 AND beta[i,j] LT -1.5 THEN beta[i,j]=143

        IF beta[i,j] GT -1.5 AND beta[i,j] LT -1 THEN beta[i,j]=159

        IF beta[i,j] GT -1 AND beta[i,j] LT -0.5 THEN beta[i,j]=175

        IF beta[i,j] GT 500 AND beta[i,j] LT 600 THEN beta[i,j]=191

        IF beta[i,j] GT 600 AND beta[i,j] LT 700 THEN beta[i,j]=207

        IF beta[i,j] GT 700 AND beta[i,j] LT 800 THEN beta[i,j]=63

        IF beta[i,j] GT 800 AND beta[i,j] LT 900 THEN beta[i,j]=79

        IF beta[i,j] GT 900 AND beta[i,j] LT 1000 THEN beta[i,j]=95

ENDFOR

close, 2

ana=congrid(alfa,300,240)
ana2=congrid(beta,300,240)

set_plot,'ps'
device,filename='/pamenar/u1/anap/images/NDVI82Jan-mar.ps'
!order=1

tv, alfa, 487,284
cbar,vmin=min(alfa), vmax=max(alfa), title='NDVI',/vertical, pos=[0.9,0.2,0.95,0.8]

tv, beta, 16,196
cbar,vmin=min(beta), vmax=max(beta), title='NDVI !CAnomalies',/vertical, pos=[0.9,0.2,0.95,0.8], 16,196

device,/close
set_plot,'x'
```

```
tv, ana, 487,284
cbar,vmin=min(alfa), vmax=max(alfa), title='NDVI',/vertical, pos=[0.9,0.2,0.95,0.8]

tv, ana2, 16,196
cbar,vmin=min(beta), vmax=max(beta), title='NDVI !CAnomalies',/vertical, pos=[0.9,0.2,0.95,0.8]


end
```

- **IDL routine to correlate, pixel-by-pixel, NDVI, soil wetness and precipitation anomalies averaged over the growing season**

```
PRO corrgrowingseasonANOM

alfa=fltarr(75,60,9)
beta=fltarr(75,60,9)
gama=fltarr(75,60,9)

openr, 1, '/pamenar/u1/anap/NDVI/final/growingseasonNDVIANOM'
readf,1, alfa

openr, 2, '/pamenar/u1/anap/hydrology/Hydrology/growingseasonSOILANOM'
readf,2, beta

openr, 3, '/pamenar/u1/anap/hydrology/precipitation/growingseasonPRECANOM'
readf,3, gama

temp=fltarr(9,1)
temp2=fltarr(9,1)
temp3=fltarr(9,1)
corndvisoil=fltarr(75,60)
corndviprec=fltarr(75,60)

FOR i=0,74 do for j=0,59 do begin
        temp[0,0]=alfa[i,j,0]
        temp[1,0]=alfa[i,j,1]
        temp[2,0]=alfa[i,j,2]
        temp[3,0]=alfa[i,j,3]
        temp[4,0]=alfa[i,j,4]
        temp[5,0]=alfa[i,j,5]
        temp[6,0]=alfa[i,j,6]
        temp[7,0]=alfa[i,j,7]
        temp[8,0]=alfa[i,j,8]
        temp2[0,0]=beta[i,j,0]
        temp2[1,0]=beta[i,j,1]
        temp2[2,0]=beta[i,j,2]
        temp2[3,0]=beta[i,j,3]
        temp2[4,0]=beta[i,j,4]
        temp2[5,0]=beta[i,j,5]
        temp2[6,0]=beta[i,j,6]
        temp2[7,0]=beta[i,j,7]
        temp2[8,0]=beta[i,j,8]
```

```
        temp3[0,0]=gama[i,j,0]
        temp3[1,0]=gama[i,j,1]
        temp3[2,0]=gama[i,j,2]
        temp3[3,0]=gama[i,j,3]
        temp3[4,0]=gama[i,j,4]
        temp3[5,0]=gama[i,j,5]
        temp3[6,0]=gama[i,j,6]
        temp3[7,0]=gama[i,j,7]
        temp3[8,0]=gama[i,j,8]
        corsoil=correlate(temp,temp2)
        corprec=correlate(temp,temp3)
        corndvisoil[i,j]=corsoil
        corndviprec[i,j]=corprec

        IF (corndvisoil[i,j] GT 0) OR (corndvisoil[i,j] LE 0) OR (corndvisoil[i,j] EQ 0) THEN begin
corndvisoil[i,j]=corndvisoil[i,j]
                ENDIF ELSE begin
                corndvisoil[i,j]=0
                ENDELSE
        IF (corndviprec[i,j] GT 0) OR (corndviprec[i,j] LE 0) OR (corndviprec[i,j] EQ 0) THEN begin
corndviprec[i,j]=corndviprec[i,j]
                ENDIF ELSE begin
                corndviprec[i,j]=0
                ENDELSE
ENDFOR

print, corndvisoil
print, corndviprec

help, corndvisoil
help,corndviprec

openw,4,'/pamenar/u1/anap/NDVI/plots/CORRgrowingseasonNDVISOILANOM
printf,4,corndvisoil

openw,5,'/pamenar/u1/anap/NDVI/plots/CORRgrowingseasonNDVIPRECANOM
printf,5,corndviprec

print, corndvisoil

close, 1
close, 2
close, 3
close, 4
close, 5


end
```

- **IDL routine to create color range and produce .ps image with pixel-by-pixel correlations between NDVI, soil wetness and precipitation**

```
PRO corrIMAGES
```

```
alfa=fltarr(75,60)
beta=fltarr(75,60)
gama=fltarr(75,60)
delta=fltarr(75,60)

alfa2=fltarr(75,60)
beta2=fltarr(75,60)
gama2=fltarr(75,60)
delta2=fltarr(75,60)

openr,1,'/pamenar/u1/anap/NDVI/plots/CORRgrowingseasonNDVISOILANOM
readf,1,alfa

openr,2,'/pamenar/u1/anap/NDVI/plots/CORRgrowingseasonNDVIPRECANOM
readf,2,beta

a=max(alfa)
b=max(beta)
c=min(alfa)
d=min(beta)
print, a
print, b
print, c
print, d

gama=alfa
delta=beta

FOR i=0,74 DO FOR j=0,59 DO BEGIN
        IF alfa[i,j] GT -1 AND alfa[i,j] LT -0.80 THEN gama[i,j]=160
        IF alfa[i,j] GT -0.8 AND alfa[i,j] LT -0.60 THEN gama[i,j]=144
        IF alfa[i,j] GT -0.6 AND alfa[i,j] LT -0.40 THEN gama[i,j]=120
        IF alfa[i,j] GT -0.4 AND alfa[i,j] LT -0.20 THEN gama[i,j]=112
        IF alfa[i,j] GT -0.2 AND alfa[i,j] LT 0 THEN gama[i,j]=96
        IF alfa[i,j] EQ 0 THEN gama[i,j]=192
        IF alfa[i,j] GT 0 AND alfa[i,j] LT 0.20 THEN gama[i,j]=64
        IF alfa[i,j] GT 0.2 AND alfa[i,j] LT 0.40 THEN gama[i,j]=48
        IF alfa[i,j] GT 0.4 AND alfa[i,j] LT 0.60 THEN gama[i,j]=32
        IF alfa[i,j] GT 0.6 AND alfa[i,j] LT 0.80 THEN gama[i,j]=16
        IF alfa[i,j] GT 0.8 AND alfa[i,j] LT 1.0 THEN gama[i,j]=0
ENDFOR

FOR i=0,74 DO FOR j=0,59 DO BEGIN
        IF beta[i,j] GT -1 AND beta[i,j] LT -0.80 THEN delta[i,j]=160
        IF beta[i,j] GT -0.8 AND beta[i,j] LT -0.60 THEN delta[i,j]=144
        IF beta[i,j] GT -0.6 AND beta[i,j] LT -0.40 THEN delta[i,j]=120
        IF beta[i,j] GT -0.4 AND beta[i,j] LT -0.20 THEN delta[i,j]=112
        IF beta[i,j] GT -0.2 AND beta[i,j] LT 0 THEN delta[i,j]=96
        IF beta[i,j] EQ 0 THEN delta[i,j]=192
        IF beta[i,j] GT 0 AND beta[i,j] LT 0.20 THEN delta[i,j]=64
        IF beta[i,j] GT 0.2 AND beta[i,j] LT 0.40 THEN delta[i,j]=48
        IF beta[i,j] GT 0.4 AND beta[i,j] LT 0.60 THEN delta[i,j]=32
        IF beta[i,j] GT 0.6 AND beta[i,j] LT 0.80 THEN delta[i,j]=16
        IF beta[i,j] GT 0.8 AND beta[i,j] LT 1.0 THEN delta[i,j]=0
ENDFOR

close,1
```

```
close,2

alfa2=rotate(delta,3)
alfa3=transpose(alfa2)
alfa4=rotate(alfa3,2)

beta2=rotate(delta,3)
beta3=transpose(beta2)
beta4=rotate(beta3,2)

set_plot,'ps'
device,filename='/pamenar/u1/anap/images/correlationSOILANOMgrowingseason.ps',/color,BITS=8

cbar,vmin= min(alfa), vmax=max(alfa), title='r',/vertical, pos=[0.9,0.2,0.95,0.8]
tv, alfa4

device,/close
set_plot,'x'

set_plot,'ps'
device,filename='/pamenar/u1/anap/images/correlationPRECANOMgrowingseason.ps',/color,BITS=8

cbar,vmin=min(beta), vmax=max(beta), title='r',/vertical, pos=[0.9,0.2,0.95,0.8]
tv, beta4

device,/close
set_plot,'x'

tv, alfa4
cbar,vmin= min(alfa), vmax=max(alfa), title='r',/vertical, pos=[0.9,0.2,0.95,0.8]

print, gama

end
```

- **IDL routine to average NDVI data over Ireland.**

Note1: Same routine was applied to 'South Portugal', 'South Spain', 'South England', and 'North Spain'.
Note2: Similar routine was used for all months of the year.

```
PRO irelandNDVI

alfa=fltarr(75,60)
ana=fltarr(600,480)
beta=fltarr(3,3)
mean=fltarr(1,1)

final=fltarr(9,1)
final_t=fltarr(108,1)

openr, 1, '/pamenar/u1/anap/NDVI/final/right_fasir_eur82_1'
readf,1, alfa

ana=congrid(alfa,600,480)
beta=ana[50:70,180:200]
```

```
tv, beta

FOR i=0,2 do begin
  FOR j=0,2 do begin
      result=moment(beta)
      mean=result[0]
  ENDFOR
ENDFOR

final[0,0]=mean
final_t[0,0]=mean

close,1

openr,1, '/pamenar/u1/anap/NDVI/final/right_fasir_eur83_1
readf,1, alfa

ana=congrid(alfa,600,480)
beta=ana[50:70,180:200]

tv, beta

FOR i=0,2 do begin
  FOR j=0,2 do begin
      result=moment(beta)
      mean=result[0]
  ENDFOR
ENDFOR

final[1,0]=mean
final_t[12,0]=mean

close,1

openr,1, '/pamenar/u1/anap/NDVI/final/right_fasir_eur84_1
readf,1, alfa

ana=congrid(alfa,600,480)
beta=ana[50:70,180:200]

tv, beta

FOR i=0,2 do begin
  FOR j=0,2 do begin
      result=moment(beta)
      mean=result[0]
  ENDFOR
ENDFOR

final[2,0]=mean
final_t[24,0]=mean

close,1

openr,1, '/pamenar/u1/anap/NDVI/final/right_fasir_eur85_1
readf,1, alfa

ana=congrid(alfa,600,480)
```

```
beta=ana[50:70,180:200]

tv, beta

FOR i=0,2 do begin
  FOR j=0,2 do begin
      result=moment(beta)
      mean=result[0]
   ENDFOR
ENDFOR

final[3,0]=mean
final_t[36,0]=mean

close,1

openr,1, '/pamenar/u1/anap/NDVI/final/right_fasir_eur86_1
readf,1, alfa

ana=congrid(alfa,600,480)
beta=ana[50:70,180:200]

tv, beta

FOR i=0,2 do begin
  FOR j=0,2 do begin
      result=moment(beta)
      mean=result[0]
   ENDFOR
ENDFOR

final[4,0]=mean
final_t[48,0]=mean

close,1

openr,1, '/pamenar/u1/anap/NDVI/final/right_fasir_eur87_1
readf,1, alfa

ana=congrid(alfa,600,480)
beta=ana[50:70,180:200]

tv, beta

FOR i=0,2 do begin
  FOR j=0,2 do begin
      result=moment(beta)
      mean=result[0]
   ENDFOR
ENDFOR

final[5,0]=mean
final_t[60,0]=mean

close,1

openr,1, '/pamenar/u1/anap/NDVI/final/right_fasir_eur88_1
readf,1, alfa
```

```
ana=congrid(alfa,600,480)
beta=ana[50:70,180:200]

tv, beta

FOR i=0,2 do begin
 FOR j=0,2 do begin
     result=moment(beta)
     mean=result[0]
  ENDFOR
ENDFOR

final[6,0]=mean
final_t[72,0]=mean

close,1

openr,1, '/pamenar/u1/anap/NDVI/final/right_fasir_eur89_1
readf,1, alfa

ana=congrid(alfa,600,480)
beta=ana[50:70,180:200]

tv, beta

FOR i=0,2 do begin
 FOR j=0,2 do begin
     result=moment(beta)
     mean=result[0]
  ENDFOR
ENDFOR

final[7,0]=mean
final_t[84,0]=mean

close,1

openr,1, '/pamenar/u1/anap/NDVI/final/right_fasir_eur90_1
readf,1, alfa

ana=congrid(alfa,600,480)
beta=ana[50:70,180:200]

tv, beta

FOR i=0,2 do begin
 FOR j=0,2 do begin
     result=moment(beta)
     mean=result[0]
  ENDFOR
ENDFOR

final[8,0]=mean
final_t[96,0]=mean

print, final
```

```
close,1

openw,1, '/pamenar/u1/anap/NDVI/plots/ireland/NDVI_jan'
printf,1, final

close, 1
```